# ELECTROCHEMICAL STUDIES ON CORROSION-RESISTANT STEEL BARS

BY

**ADESHINA ADEWALE ADEWUMI**

A Thesis Presented to the

DEANSHIP OF GRADUATE STUDIES

**KING FAHD UNIVERSITY OF PETROLEUM & MINERALS**

DHAHRAN, SAUDI ARABIA

In Partial Fulfillment of the
Requirements for the Degree of

## MASTER OF SCIENCE

In

**CIVIL ENGINEERING**

**MAY 2015**

KING FAHD UNIVERSITY OF PETROLEUM & MINERALS

DHAHRAN- 31261, SAUDI ARABIA

**DEANSHIP OF GRADUATE STUDIES**

This thesis, written by **ADESHINA ADEWALE ADEWUMI** under the direction of his thesis advisor and approved by his thesis committee, has been presented and accepted by the Dean of Graduate Studies, in partial fulfillment of the requirements for the degree of MASTER OF SCIENCE IN CIVIL ENGINEERING.

Dr. Salah U. Al-Dulaijan
(Advisor)

Dr. Omar Abdullah Al-Swailem
Department Chairman (A)

Dr. Mohammed Maslehuddin
(Member)

Dr. Salam A. Zummo
Dean of Graduate Studies

Dr. Shamshad Ahmad
(Member)

10/6/15

Date

***In the Name of Allah, Most Gracious, Most Merciful.***

*Dedicated to:*

*My beloved parents, wife, family and friends*

*for their supports, love, sacrifices and prayers*

# ACKNOWLEDGMENTS

All praises and thanks is due to Allah (subhana wa taala) for bestowing me with sound health, knowledge and patience to complete this research work. May the peace and blessings of Allah be upon the noblest of mankind, Prophet Muhammad (PBUH), his family and his companions. Thereafter, I acknowledged the ministry of higher education through KFUPM, for the support given to this research through its tremendous facilities and for granting me the opportunity to pursue my graduate studies with financial support.

I acknowledged, with deep gratitude and appreciation the encouragement, the inspiration, valuable time and guidance given to me by my Advisor, Dr. Salah U. Al-Dulaijan. Also, my deep gratitude and appreciations go to Dr. Mohammed Maslehuddin, for the encouragement, inspiration, valuable time and guidance given to me and the fatherly role he played during my stay here in KFUPM and to Dr. Shamshad Ahmad for his continuous encouragement, moral support, valuable time and guidance during my studies at KFUPM.

My appreciation also goes to the Department of Civil and Environmental Engineering particularly the immediate former chairman, Prof. Nedal T. Ratrout, and the other faculty members for their supports and encouragements. Many thanks to the Center of Engineering researchers: Eng. Mohammed Shameem (My boss) for facilitating the success of this research, Eng. Mohammed Bari, Eng. Mohammed Ibrahim, and Eng. Mohammad Rizwan, for their sincere and untiring efforts and provision of the necessary materials for this research work. Special thanks also go to the laboratory personnels; Eng.

Mukaram (retired), Eng. Imran, Mr. Mohammed Shuwaikhat, Mr. Hussain, and Mr. Alam who assisted me in the experimental work.

Finally, my heartfelt gratitude goes to my parents, beloved wife, and my friends Engr. Azeez Mukhtar, Engr. Saheed Adekunle, Engr. Moruf Olalekan, Engr. Babatunde Salami, Engr. Lukman Adewunmi, Engr. Alabi Wahab, Engr. Rasaz Kehinde and Mr. Tope Dada for all their supports, love, encouragement and constant prayers. I would like to thank all my friends in KFUPM and the Nigeria Muslim community in KFUPM under the able leadership of Dr. Balarabe.

# TABLE OF CONTENTS

# LIST OF FIGURES

# LIST OF TABLES

# LIST OF ABBREVIATIONS

| | | |
|---|---|---|
| LPRM | : | Linear polarization resistance method |
| SCPS | : | Simulated concrete pore solution |
| $E_{corr}$ | : | Corrosion potential (V) |
| $I_{corr}$ | : | Corrosion current density ($\mu A/cm^2$) |
| SEM | : | Scanning electron microscopy |
| *R*p | : | Polarization resistance |
| SCPS | : | Simulated concrete pore solution |
| PDP | : | Potentiodynamic polarization |
| EDS | : | Electric dispersive spectroscopy |
| SCE | : | Saturated calomel electrode |
| BB | : | Black bar or Carbon steel bar |
| MMFX | : | Microcomposite steel bar |
| SCS | : | Stainless Clad Bar |
| SS | : | Stainless steel bar |

# THESIS ABSTRACT

**Name: ADESHINA ADEWALE ADEWUMI**

**Thesis Title: ELECTROCHEMICAL STUDIES ON CORROSION-RESISTANT STEEL BARS**

**Major Field: CIVIL ENGINEERING (STRUCTURES)**

**Date of Degree: MAY, 2015**

Corrosion of reinforcing steel is a major and most costly form of durability problem that currently threatens the performance of reinforced concrete (RC) structures, especially environments characterized by severe environmental factors, such as in the marine environment. Corrosion of reinforcing steel usually results in cracking and spalling of the concrete cover. This shortens the life-span of RC structures. This normally results in repair or replacement of the RC structures which consumes billions of dollars. Corrosion-resistant steel reinforcing bars can be a means for prolonging the service life of reinforced concrete structures in aggressive environments.

This research work investigated the effect of chloride, sulfate and temperature on the chloride-induced corrosion of carbon steel or black bar (BB), micro-composite steel (MMFX), stainless-clad steel (SCS), and stainless steel (SS) rebars. This research program was divided into two parts. The first part consisted of preparing a set of steel specimens immersed in simulated concrete pore solution and varying the three key exposure parameters (chloride and/or sulfate concentration, and exposure temperature)

using potentiodynamic polarization and linear polarization techniques. In the second part of this research, concrete specimens were prepared to evaluate the macro currents of the steel bars according to ASTM G 109 test.

Corrosion current density was used to evaluate the performance of the steel specimens with the polarization test, while the macro current was used to evaluate the performance of the steel bars in the concrete ponded with various aggressive species.

The results from PDP and LPR showed that, an increase in temperature significantly increases the corrosion rate of the black steel, while for the MMFX, stainless-clad steel and stainless steel bars an increase in temperature has a marginal effect on corrosion.

Also, the black steel bars specimens placed in (SCPS) and contaminated with 2000ppm chloride concentration and temperatures of 25 $^{0}$C exhibited general corrosion. However, when the temperature of the SCPS was increased to 55 °C, pitting corrosion was observed. Stainless-clad steel exhibited little pitting corrosion for the two exposure temperatures. Pitting was also noted in MMFX and stainless-steel bars.

Furthermore, reinforcement corrosion was accelerated due to the concomitant presence of chloride and sulfate ions, compared to specimens contaminated with only chloride ions for all the tested steel bars. However, the effect of chloride plus sulfate was more in the black bars compared to the specialty steel bars. The stainless steel exhibited the highest corrosion resistance, while MMFX and stainless steel clad bars also show significant corrosion resistance.

From the ASTM G109 experimental result, none of the bars exhibited any signs of active corrosion for concrete specimens ponded with 3% NaCl, 3% NaCl and 0.5% sulphate solution, with 3% NaCl and 3% sulphate solution even after one year due to the high quality concrete used for this research. Corrosion initiation was noted in the black bar in the concrete ponded with sabkha solution after six weeks of wet and dry cycle. However, corrosion was not noted in the specialty steel bars even after one year of exposure to the sabkha solution.

In all, specialty steel bars should be used in aggressive environments characterized with high chloride and sulfate concentration couple with high temperature such as in the Arabian Gulf. Also, MMFX and stainless clad bars may be used instead of stainless steel bars since they are cheaper in the market and provide corrosion resistance almost equivalent to that of the stainless steel bars which are very costly in the market.

# ملخص الرسالة

**الاسم الكامل: أديشنا أديويل أدوومي**

**عنوان الرسالة: دراسات كهروكيميائية على مقاومة اسياخ الحديد للتآكل**

**التخصص: هندسة مدنية (انشاءات)**

**تاريخ الدرجة العلمية: شعبان 1436هـ**

تعتبر مشكلة تآكل حديد التسليح من المشاكل الرئيسية والأكثر تكلفة التي تواجه ديمومة الخرسانة المسلحة وفعاليتها خصوصا الناتجة عن العوامل البيئية القاسية مثل البيئة البحرية. تآكل حديد التسليح ينتج عادة عن تشقق و فقدان غطاء الخرسانة حيث يؤدي الى قصر حياة المنشآت الخرسانية، مما يؤدي الى الحاجة الى عمليات الاصلاح والاستبدال التي تكلف مليارات الدولارات. أسياخ الحديد المقاومة للتآكل يمكن اعتبارها أحد الحلول لاطالة عمر المنشأت الخرسانية المسلحة في ظروف بيئية صعبة.

في هذا البحث تم فحص تاثير الكلورات، السلفات، والحرارة على التآكل الناجم عن الكلوريد على الحديد الصلب او الاسياخ السوداء، مركبات الحديد الصغيرة، الحديد المقاوم للصدأ، اسياخ الحديد المقاومة للصدأ. برنامج هذا البحث ينقسم الي قسمين: في القسم الاول تم تحضير عينات من الحديد المغمورة في الخرسانة مغ تغغير ثلاث عوامل ( تركيز الكلوريد والسلفات بالاضافة للحرارة) باستخدام الاستقطاب عند الجهد و تقنية الاستقطاب الخطي. في القسم الثاني من هذا البحث تم تحضر العينات لقياس التيارات الكلية في لاسياخ الحديد بناء" على المواصفات ASTM G 109.

تم استخدام كثافة تيارات التآكل مع اختبار الاستقطاب لقياس فعالية عينات الحديد بينما اختبار الكثافات الكلية استخدم لقياس فعالية اسياخ الحديد داخل الخرسانة مع انواع مختلفة من الظروف البيئية.

اظهرت نتائج فحوصات الاستقطاب عند الجهد والاستقطاب الخطي ان زيادة درجة الحرارة بشكل كبير ئؤدي الى زيادة معدل التآكل للاسياخ السوداء بينما تآكل مركبات الحديد الصغيرة، الحديد المغلف المقاوم للصدأ، اسياخ الحديد المقاومة للصدأ كان هامشيا بسبب زيادة درجة الحرارة.

ايضا عند وضع عينات الاسياخ السوداء في SCPS حيث يحتوي على كلوريد بتركيز 2000 جزء بالمليون ودرجة حرارة 25 درجة مئوية تعرضت هذه الاسياخ الى تآكل عام. لكن عند زيادة درجة حرارة المحلول الى 55 درجة مئوية لوحظ حصول نتوءات تآكل بصورة اكبر. الحديد المقاوم للصدأ أظهر تآكل اقل على درجتي الحرارة. ايضا لوحظ حول نتوءات في اسياخ الحديد المقاومة للصدأ ومركبات الحديد الصغيرة.

علاوة على ذلك، وجود ايونا الكلوريد والسلفات ادت الى تسارع تآكل حديد التسليح مقارنة مع العيانت التي تعرضت لايونات الكلوريد فقط لجديع العينات. لكن تأثير الكلوريد مع السلفات كان اكثر على الاسياخ السوداء مقارنة مع اسياخ الحديد. الحديد المقاوم للصدأ أبدى مقاومة اعلى للتآكل بينما مركبات الحديد الصغيرة والحديد المغلف المقاوم للصدأ أبدى مقاومة شديدة للتآكل.

بتاء" على نتائج ASTM G 109، كل الاسياخ لم تظهر اي تآكل لعينات الخرسانة التي تحتوي على 3% من كلوريد الصوديوم، و0.5% من محلول السلفات، او تحتوي على 3% من كلوريد الصوديوم 3% من محلول السلفات حتى بعد عام بسبب الجودة العالية للخرسانة التي تم استخدامها

في هذا البحث. بداية التآكل في الاسياخ السوداء في الخرسانة المغمورة في محلول السبخا ظهرت بعد ستة اسابيع من دورات الرطب والجاف. لكن اسياخ الحديد لم يظهر عليها التآكل بعد عام من تعرظها لمحلول السبخا.

اسياخ الحديد الخاصة يجب استخدامها في الظروف البيئية الصعبة التي تتمثل في تركير عالي من الكلوريد والسلفات مع درجة حرارة عالية مثل منطقة الخليج العربي. ايضا مركبات الحديد الصغيرة والحديد المغلف المقاوم للصدأ يمكن استخدامه بدا من الاسياخ المقاومة للصدأ لأنها ارخص وتعطي مقاومة للتآكل تقريبا تكافئ مقامة الاسياخ المقامة للصدأ التي تعتبر باهظة الثمن في الاسواق.

# CHAPTER 1

# INTRODUCTION

## 1.1 Durability of Reinforced Concrete Structures

Portland cement concrete is the most widely used material in the construction industry. This wide use of concrete is attributed to it four specific characteristics. Firstly, Portland cement concrete provides both chemical and physical protection to the reinforcing steel. The chemical protection is provided by the highly alkaline nature of the pore solution (pH > 13), The physical protection to steel is provided by the dense and impermeable structure of concrete that retards the diffusion of aggressive species, like chlorides, carbon dioxide, oxygen, and moisture, to the steel-concrete interface. Secondly, concrete can be molded into different sizes and shapes either in a precast concrete plant or on the site and thirdly, is because of its low-cost. Fourthly is the easy availability of its constituent materials. Furthermore, concrete has good fire-resistance, excellent compressive strength, low maintenance requirements, long service-life, and high water resistance. Due to all these advantages, concrete has established itself as a major construction material.

Concrete is characterized with low tensile strength; the typical tensile strength of concrete is 8% to 15% of its compressive strength, which is low compared to its compressive strength [1]. This weakness of the concrete has been overcome by the addition of reinforcing steel bars, so that reinforcement bars resist shear and tensile stresses and

concrete primarily resists compressive stresses. The reinforcing steels normally face corrosion problem due to ingress of aggressive ions.

Corrosion of steel reinforcements is a major and most costly form of durability problem that currently threatens the performance of reinforced concrete (RC) structures, especially in an environment characterized by severe environmental factors such as in the Arabian Gulf. Corrosion of reinforcing steel usually leads to cracking and spalling of the concrete cover which shortens the life-span of the structures. This type of deterioration is principally attributed to the chloride ions that may be contributed by the mix ingredients or by the ingress of these chloride ions into the hardened concrete from the service environment. The extreme climatic conditions and the marginal quality of the aggregates accelerate the concrete deterioration processes [1-3].

Deterioration of reinforced concrete in the coastal areas of the Arabian Gulf is often noted within a short span of 5 to 10 years. Field studies indicate that the deterioration of structures in this region is mainly attributed to: (i) inappropriate materials specifications, (ii) inadequate construction practices, and (iii) severe environment and geomorphic conditions. The environmental conditions of Saudi Arabia are characterized by a large variation in the daily and seasonal temperature. The ambient temperature in the summer is as high as 45 to 55 °C and the relative humidity ranges between 40 to 95% over a period of 24 hours [3].

The variation in the day to night temperature may be as much as 20 °C. This high variation in the day and night temperature leads to the formation of micro-cracks in the concrete that

accelerate the diffusion of aggressive species, such as oxygen, chlorides, moisture, and carbon dioxide, to the steel surface thereby promoting corrosion of reinforcing steel.

## 1.2 Improvement of Concrete Durability

Eliminating or slowing the deterioration of RC structures due to the corrosion of steel reinforcement requires the use of innovative methodologies, which involves slowing the deterioration through methods that lengthen the time it takes the chloride ions to reach the steel reinforcement and the time between initiation of corrosion and the end of service life [4]. Some of the precautionary measures include: use of dense and impermeable concrete, use of FBEC bars or chemical inhibitors.

FBEC steel bars have been used worldwide for more than two decades to enhance the useful service-life of reinforced concrete structures serving in aggressive environments [4-6]. However, they also have a limited life, particularly in severe environments, due to the surface damage to the coating. Furthermore, it is believed that as a steel reinforced concrete ages, epoxy coatings may become brittle and eventually, under exposure to high chloride concentrations, delaminate from the steel reinforcement [7].

The use of alternative reinforcement, such as fiber reinforced plastic, is also becoming more common these days due to the increasing number of cases of concrete deterioration. Each of the aforesaid protective measures has drawbacks and advantages. While special design procedures are necessary for the fiber reinforced plastic bars, conventional design methods could be utilized for steel bars protected by metallic coatings. The cost of a structure and the designed service-life are other parameters that govern the selection of a

protective methodology. Stainless steel bar, micro-composite steel bar (MMFX) and stainless clad bars have the advantage of being utilized as normal reinforcement and additional precautions during transportation and bending are not required. As such, they could be utilized in structures exposed to aggressive service conditions. Another possible scenario is the use of these steel bars in the parts of the structure that are exposed to aggressive environments while the other parts of the structure that are not exposed to severe conditions may be reinforced with normal steel.

## 1.3 Research Objectives

The general objective of this study is to assess the corrosion protection provided by specialty bars in concrete. The specific objectives are the following:

1. Examine the effect of chloride and sulfate concentration, and temperature on corrosion behavior of different specialty steel bars,
2. Evaluate the corrosion protection provided by the different specialty steel bars in minimizing chloride-induced reinforcement corrosion in concrete and
3. Provide recommendations for avenues of utilizing different specialty steel bars based on the data developed in this study.

.

# CHAPTER 2

# LITERATURE REVIEW

According to the report of Federal Highway Administration (FHWA) in 2001 the cost of corrosion for United States (US) industry and government agencies is estimated to be $276 billion per year [8].The average annual direct cost of corrosion for highway bridges is estimated to be $8.29 billion including the replacement of structurally deficient bridges, maintenance of substructure, superstructure, decks of bridges, and painting cost of steel bridges. Because of this enormous cost, many production and manufacturing companies, state and federal highway agencies, public utilities, and infrastructure developers are aggressively pursuing corrosion protection methods for reinforced concrete structures.

Different corrosion protection methods include increased cover depths, lower permeability concrete (lower water-cement ratio and mineral admixtures), corrosion inhibitors, pre-treating sealers, and corrosion resistant reinforcement. Corrosion resistant reinforcements in the market include epoxy coated steel, stainless steel, stainless steel clad reinforcement, galvanized steel, micro composite steel, steels with multiple coatings, and others. Different corrosion protection methods are also being used for existing structures, such as cathodic protection, re-alkalization, and electrochemical removal of chlorides [9].

## 2.1 Mechanism of Reinforcement Corrosion

Corrosion, in general terms, means destruction or deterioration of a material due to a reaction with its environment [10]. Also, metallic corrosion can be defined as a chemical

reaction that returns the metal to compounds which are similar to the minerals from which it was extracted [11]. A refined metal, such as steel or iron, has a natural tendency to return to its stable state (iron oxide, $Fe_2 O_3$) that exists in nature by corroding. The rate of steel corrosion depends on grain structure, the presence of entrained stress from fabrication and its composition. It also depends on the nature of the surrounding environment, such as oxygen, pH, the availability of water, ionic species, and temperature [11].

Concrete normally provides a high alkalinity (pH > 13.5) which increases the reinforcing steel protection against corrosion. Under high alkalinity, steel remains passivated. Also, concrete with a low w/c ratio, well consolidated and well cured, has a low permeability that decreases the penetration of corrosion-inducing agents, for example carbon dioxide, chloride, moisture, etc., to the steel surface. In addition, the high electrical resistivity of concrete restricts corrosion rate by reducing the flow of electrical current from the anodic to the cathode electrode [11].

The presence of alkali elements, such as calcium hydroxide, sodium hydroxide, and potassium hydroxide, increase the alkalinity of the concrete pore solution (pH> 13). This high value of alkalinity results in the formation of a sub-microscopic surface layer on the embedded steel. As long as this layer is not disturbed, it keeps the steel in a passive condition and protects from corrosion.

Reinforcement corrosion is caused either by the carbonation of concrete or diffusion of chloride ions or both of them combined together. Both of these species are able to destroy the chemical protection provided by the concrete to the reinforcing steel. The ingress of

chloride ions to the steel-concrete interface or carbonation leads to the depassivation of steel.

### 2.1.1 Basic Principles of Corrosion

Corrosion of reinforcing steel embedded in concrete is an electrochemical process that requires an anode, a cathode, an electrolyte, and an electrical connection between the anode and cathode for the transfer of electrons. Coupled anodic and cathodic reactions take place on the surface of the reinforcing steel; the most common form of reinforcement corrosion in aqueous medium is of an electrochemical nature in which the corroding metal behaves like a small electrochemical cell. It requires an anode (where oxidation takes place), a cathode (where reduction occurs), an electrical conductor (steel reinforcement), and an electrolyte (concrete). At the anode, oxidation is the principal reaction (loss of electron) [12]. Corrosion starts at the anode when the electrochemical process is initiated by the oxidation of the iron (i.e. loss of electrons). Oxidation is the process when an oxidizing agent (oxygen in this case) takes electrons from the iron atoms transitioning them into soluble ions that enter the solution as shown in Equation 2.1.

$$\boldsymbol{Fe \rightarrow Fe^{++} + e^{-2}} \qquad (\textbf{Oxidation}) \qquad (\mathbf{2.1})$$

At the cathode, reduction is the principal reaction whereby the dissolved oxygen in the electrolyte is reduced by the electrons supplied by the anodic reaction to form hydroxyl ions:

$$\boldsymbol{\frac{1}{2}\,O_2 + H_2O + 2e^- \rightarrow 2OH} \qquad (\textbf{Oxygen reduction}) \qquad (\mathbf{2.2})$$

This $OH^-$ flows back to the anode through the concrete to complete the circuit. The transfer rate of $OH^-$ depends on moisture content, electrical resistivity of concrete, temperature, and ionic concentration. Then, $OH^-$ ions at the anode combine with the $Fe^{++}$, as shown in Equation 2.3, to form a fairly soluble ferrous hydroxide, $Fe(OH)_2$ [12]. Figure 2.1 schematically represents the mechanisms of reinforcement corrosion.

$$\mathbf{Fe^{++} + 2OH^- \rightarrow Fe(OH)_2} \qquad \text{Rust formation} \qquad (\mathbf{2.3})$$

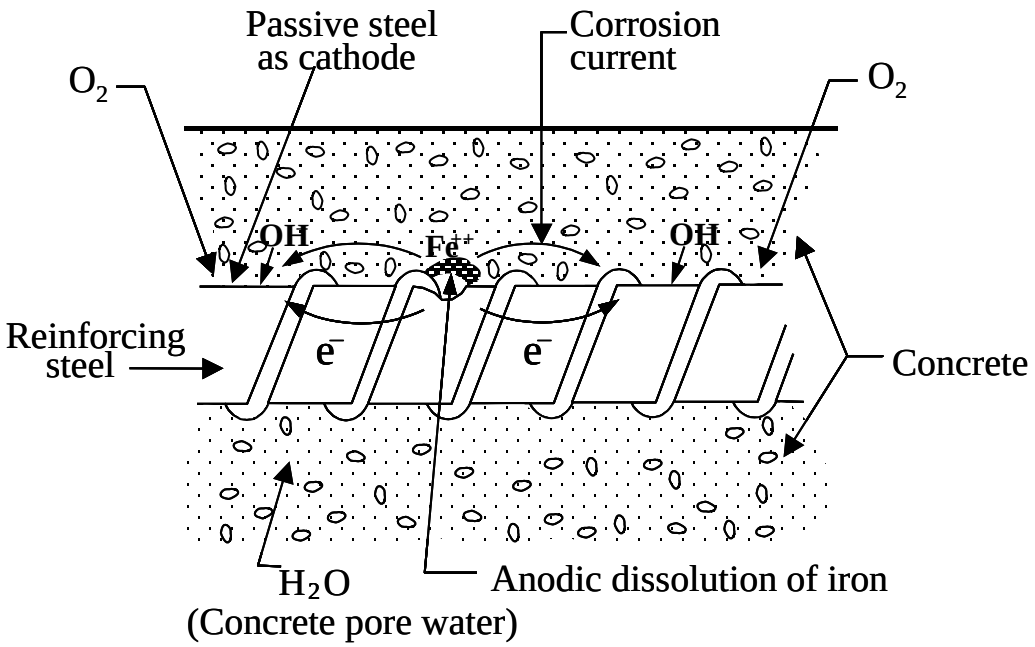


Figure 2.1: Schematic Representation of Mechanism of Reinforcement Corrosion [12].

If there is sufficient oxygen available, this product can further be more oxidized to form insoluble hydrated red rust. The rust thus developed can have a volume 2 to 10 times of the parent iron from which it is formed, depending on the type of oxide formed, as shown in Figure 2.2 [12]. This rust product can exert tensile stresses which is roughly equal to 10

times the tensile strength of concrete. This excessive tensile pressure causes the concrete cover to crack. This leads to eventual spalling off the cover concrete at an advanced stage of the corrosion process, and it may be lead to a reduction in the cross-sectional area of the structural member [12].

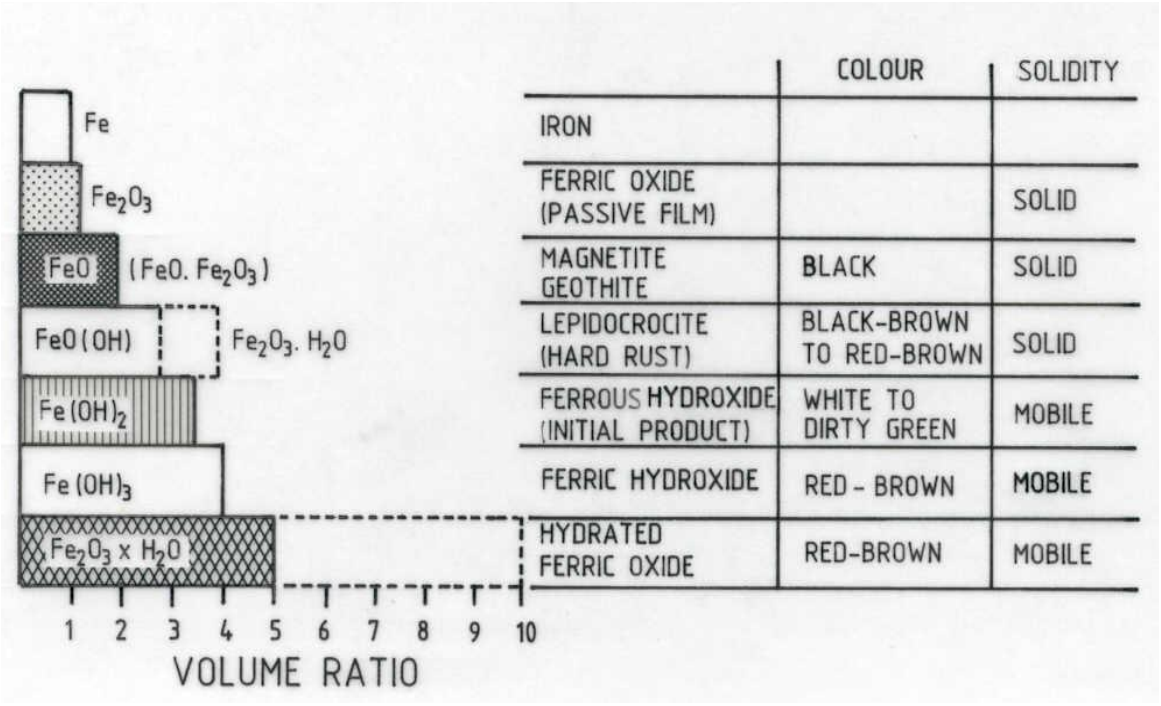


Figure 2.2: Volume of Various Oxides Formed due to Corrosion of Iron [12]

### 2.1.2 Effect of Chloride on Reinforcement Corrosion

Chloride ions in concrete can be contributed from different sources including: contaminated aggregates, salts in chemicals that are applied to the concrete surface, air born salts, salts in ground water, mixing water, and chloride containing admixtures which are used to accelerate curing. The chloride ions from these sources slowly attack the concrete through the pores in the hydrated cement paste till they eventually reach the steel

bars. At certain level of concentration, the protective film will be destroyed and the steel will start to corrode when sufficient moisture and oxygen are present at the steel-concrete interface.

The chloride ions initiate corrosion of steel reinforcement by destroying the natural submicroscopic oxide film on the steel surface, allowing the iron to dissolve into solution. Once chloride ions reach the steel surface, they oxidize iron, as shown in Equation 2.4, to form $FeCl_3$. At the cathode, reduction is the principal reaction; dissolved oxygen in the electrolyte is reduced by the electrons supplied by the anodic reaction to form hydroxyl ions, as shown in Equation 2.5. Thereafter, $FeCl_3$ drags its unstable ferrous ions into solution, where they react with the available hydroxyl ions to form $Fe(OH)_2$. This reaction releases $Cl^-$ ions into the solution and consumes the hydroxyl ions, as shown in Equation 2.6.

$$\mathbf{2Fe + 6Cl^- \rightarrow 2FeCl_3^- + 4e^-} \qquad (\mathbf{2.4})$$

$$\mathbf{2H_2 + O_2 + 4\,e^- \rightarrow 4OH^-} \qquad (\mathbf{2.5})$$

$$\mathbf{FeCl_3^- + 2OH^- \rightarrow Fe(OH)_2 + 3Cl^-} \qquad (\mathbf{2.6})$$

During the oxidation reaction, electrons are released then flow through the steel bar to the cathode. This process results in an increase in the concentration of the chloride ions and a reduction of the pH at the points of corrosion initiation, which may probably lead to the process of pitting corrosion.

"The chloride ions play a dominant role in the initiation of reinforcement corrosion. From this perspective, ACI 318 limits the water-soluble chlorides to 0.15% by weight of cement. ACI Committee 224, adopting a more conservative approach, has suggested that the acid-soluble chloride content should not be more than 0.2% by weight of cement. The British Standard, (BS 8110) allows a maximum total chloride content of 0.4%" [12]. Hausmann [13] suggested that the critical $Cl^-/OH^-$ ratio is about 0.6. Amoudi et al. [14] reported that minimal reinforcement corrosion in blast furnace slag and silica fume cement mortar specimens placed in aggressive environment of sabkha has been observed even at $Cl^-/OH^-$ ratios of 6.5 and 3.3, respectively.

### 2.1.3 Effect of Sulfate Ions on Reinforcement Corrosion

In sabkha soils and marine environment, sulfates and chlorides are present together and they considerably affect the durability of concrete. Studies conducted by Holden et al. [15] on the pore solution composition of pastes prepared with fixed quantities of sulfates and chlorides indicate an increase in the $OH^-$ concentration due to the addition of sulfates as compared to the alkalinity of pore solution of cement contaminated with similar quantities of chloride salts alone. These results showed the tendency of sulfates ion to reacts preferentially with the $C_3A$ in cement. Hence, corrosion risk is probably to be significantly increased in environments where concrete is subjected to both chloride and sulfate salts [15].

Al-Amoudi and Maslehuddin [16] investigated reinforcement corrosion in cement paste specimens immersed in sulfate, chloride, and sulfate plus chloride environments. It

was reported that while the sulfate ions alone were not able to induce reinforcement corrosion while substantial corrosion activity was observed in the specimens immersed in sulfate plus chloride solution.

### 2.1.4 Effect of Temperature on Reinforcement Corrosion

Most regions in the Kingdom of Saudi Arabia are exposed to relatively high temperature of 40 to 50 ºC especially in the summer. The temperature of concrete surface reaches 70 to 75 ºC due to solar radiation. Mehta and Gerwica[17] reported that an increase in temperature increases the kinetics of corrosion reaction and respective factors such as corrosion rate and corrosion current density. They investigated the concrete with high quantity of cement 375 kg/m$^3$ and w/c ratio of 0.45 which was used in beams of San Mateo Bridge. All beams were exposed to the same environment, however, after 17 years; the steam-cured beams were damaged due to corrosion impact and needed to be repaired. However, the naturally-cured beams showed no corrosion damage. They reported that the micro-cracking in the steam cured beams due to temperature gradients made them more permeable to oxygen and chloride, thus accelerating the corrosion process.

The data available for the performance of concrete under high temperature is very little. It was reported that the initiation time for the corrosion of reinforcement at 10 ºC is approximately three times lower than that at 30º C [18].

## 2.2 Concrete Deterioration and Its Protection

Instances of concrete deterioration, due to its interaction with the service-environment, have been reported from several parts of the world. Concrete deterioration in countries with a cold climate has been mostly due to freeze-thaw action or reinforcement corrosion due to the use of deicer salts. In the hot weather conditions of the Arabian Gulf, premature deterioration of concrete has been attributed to accelerated reinforcement corrosion. Other forms of concrete deterioration, such as sulfate attack, salt weathering and cracking due to plastic and drying shrinkage, are also reported. However, the extent of deterioration due to reinforcement corrosion outweighs that due to the other causes.

The preventive measures that can be utilized to protect the reinforcing steel from corrosion are:(i) production of dense and impermeable concrete, using appropriate design and construction practices and incorporating supplementary cementing materials, (ii) enhancing the performance of concrete through the application of surface coatings, or (iii) protection of steel through metallic or non-metallic coatings or the use of chemical inhibitors.

Several studies have been conducted at King Fahd University of Petroleum and Minerals (KFUPM) to evaluate the effectiveness of the aforesaid preventive techniques in improving concrete durability. One of the measures that is being actively utilized is coating the steel with a fusion bonded epoxy coating. FBEC steel bars have been used worldwide for more than three decades to enhance the useful service-life of reinforced concrete structures serving in aggressive environments. However, the effect of pin holes

and/or surface damage on the performance of FBEC bars is of concern, particularly if the structures are serving in a very aggressive environment. Several case studies of failure of FBEC bars in the marine structures in Key West Florida and other parts of the world has lead to an apprehension on the use of FBEC bars. Consequently, there is a trend towards utilizing steel bars with metal coatings in aggressive environments. Since these bars have mechanical properties similar to mild steel, the concern with regard to their compatibility with concrete may not be of concern as in the case of non-metallic bars.

## 2.3 Stainless Steel Bars

According to the report of the U.S FHWA "Stainless steels are bars with low content of carbon steels normally less than one percent and also contain at least 10.% chromium by weight. The chromium content allows an invisible chromium oxide film to form on the bar surface, which makes the material "passive" or corrosion resistant, i.e. stainless. This oxide film is self-healing when damaged, even when very small amount of oxygen is present. The corrosion resistance and other useful properties of stainless steels are enhanced through the addition of more chromium, molybdenum, nickel, and nitrogen" [18]. Stainless steel bars are 800 to 1,500 times more corrosion-resistant than carbon steel bar. They can be bent, cut, and welded in the field, and have chloride thresholds 15 to 24 times higher than carbon steel bar.

Stainless steel is produced using recycled stainless scraps and various chromium alloys in an electric arc furnace. Nickel, molybdenum, and other alloys contents are added as per the specified standard requirements. Final annealing will be done on the stainless steel and a

heat treatment to soften the structure will be carried out. Then follow by pickling and an acid wash for the removal of the furnace scale resulting from the annealing process, which helps to promote development of the passive oxide surface film [18].

The chemical composition and production steps determine the alloy's metallurgical structure. They can be enhanced by further alloy modifications to meet different corrosion conditions, temperature ranges, strength requirements, or to achieve improved weldability, machinability, work hardening and formability. The five alloy groups or classes are martensitic, ferritic, austenitic, duplex (ferritic-austenitic), and precipitation hardening. Austenitic and duplex alloys are used the most for rebar applications. The alloy is selected based on mechanical properties and the expected exposure or corrosivity of the service environment, i.e. the level of corrosion resistance required. Both solid stainless steel and stainless steel clad bars are available [18].

According to the report of the U.S FHWA [19], “Austenitic stainless steels have the best corrosion resistance. They are made by adding nickel (from 8 to 25%) and increasing the chromium level (from 17 to 25%). Molybdenum can also be added (up to 7 percent) to increase the corrosion resistance. These stainless steels are not magnetic. They cannot be hardened by "heat treatment" but can be hardened by cold working. They also develop high strength by cold working. They can be easily welded. Austenitics have exceptional resistance to high and low temperatures. Some common grades are 304 (used the most), 310 (used for high temperatures), 316 (has better corrosion resistance), and 317 (has the best corrosion resistance). However, austenitic stainless steels have some limitations on

their use. Exposure to very high levels of halide ions, especially chloride ions, can break down the passive oxide film"[18].

Duplex stainless steels have a metallurgical structure that is a combination of both ferritic and austenitic. They have high chromium content (from 18 to 26%) and low nickel content (from 4 to 7%). Most grades also contain some molybdenum (from 2 to 3 percent). They have a higher resistance to stress corrosion cracking than austenitic stainless and increased resistance to chloride ion attack. They are tougher than fully ferritic alloys. They are very weldable. They also have higher tensile and yield strengths than austenitic or ferritic stainless steels. A common grade is 2205 [18, 9].

There is considerable published literature (with field and laboratory data) that has shown that solid stainless steel rebars are capable of maintaining excellent corrosion resistance in severe chloride environments.

## 2.4 MMFX Steel bar

MMFX, microcomposite steel reinforcement is a steel alloy containing 9% chromium, it was introduced to the market by MMFX Steel Corporation in 1998 publicized as a proprietary chemical composition material and advertised as having a unique microstructure with enhanced corrosion resistance characteristics and higher mechanical properties (yield and tensile strengths) than conventional ASTM A 615 steel. The manufacturer claims that this type of steel has corrosion resistance that approaches that of stainless steel with much lower cost due to the use of a new production technology that minimizes the formation of the micro-galvanic cells in the steel structure (MMFX

Technologies Corp., Irvine, CA, web page). Since its production, a number of studies have been conducted to study the corrosion resistance of this new type of reinforcement some contradictions were observed [21].

## 2.5 Stainless Steel Clad

Stainless steel clad reinforcing bars have the advantages of stainless steels at a lower cost than their solid stainless steel. Clad reinforcing bars do not need to be cold worked like austenitic stainless steels because of the higher tensile strength carbon steel core. The stainless steel cladding is much thicker and tougher than other metallic and non-metallic coatings. However, cut bar ends must be protected. ASTM is developing a standard specification for deformed and plain stainless steel clad carbon steel bars for concrete reinforcement [8].

To achieve the service-life of 100 years for major reinforced concrete structures, reinforcing bars made of intrinsically corrosion-resistant materials are needed. Bars with a realistic prospect of immediate application are those made of stainless steel. Unfortunately, their cost is very high and has been the major obstacle to their widespread acceptance by transportation and construction agencies [23]. Economically viable alternatives to solid stainless steel bars are bars made of a carbon steel core protected by a cladding made of a stainless steel. Since the stainless steel cladding is tough, it does not have the inherent weakness of the organic coating used on the epoxy-coated bars. Stainless steel clad bars provide enhanced corrosion protection of reinforcing steel bars and are economically viable products. They combine the cost effective attributes of commonly specified ASTM

A615 carbon steel as the core with a metallurgically bonded outside layer of stainless steel widely recognized for its superior corrosion protection.

The physical and mechanical properties of the clad bar is determined by the carbon steel core. It can meet the strength levels as required for the American and the British specifications. Depending on the composition of the inner carbon core and the production conditions the final product meets the minimum yield levels as per ASTM A615/A615M specification for any of the grades designated as Grade 40 (40 ksi, 300 MPa), Grade 60

(60 ksi, 420 MPa) or Grade 75 (75 ksi, 520 MPa). The carbon steel core can also be produced according to ASTM A706. The outer stainless steel layer meets the ASTM specification A276. Alternative stainless steels cladding can be produced depending on the demand. The clad bars are available in rebar sizes #4 (13mm) through #18 (57 mm). They are also available as stock rounds in 1-1/4" (25.4 – 6.35 mm) and 1-1/2" (25.4 – 12.7 mm) diameters primarily used for concrete paving dowels.

Generally, the investigations in stainless steel bars have taken two directions, clad stainless steel over a carbon steel substrate and solid stainless steel bar. Clad bars were found to have almost similar corrosion resistance to solid stainless steel bars provided adequate attention is paid to the following concerns. The primary concerns of cladding are: (1) adherence to bar substrate, (2) defects formed after bending, (3) uniform cladding thickness [a typical cladding for stainless steel is 0.5 mm (0.020-in) thick], and (4) metallurgical changes due to the cladding process that may affect the corrosion resistance. It should be appreciated that the chloride threshold for pitting in a non-aqueous and non-

homogeneous environment of concrete can be significantly less than for the same aqueous environment. Therefore, any research must utilize actual concrete environments. Pitting in reinforced-concrete structures may not be as significant a concern as decreasing the average corrosion rate.

## 2.6 Previous Studies on Corrosion resistant steel bars

A five-year study [19] sponsored by FHWA, included 11 different bar types, showed that 316 stainless steel bars have the best corrosion resistance, even when used in pre-cracked concrete. The results also demonstrated that 316 stainless steel bars were significantly more corrosion-resistant than the fusion-bonded, epoxy-coated reinforcement and estimates showed that these bars could easily provide "corrosion-free design life 75 to 100 years when exposed to adverse environments."

Because of the superior corrosion resistance of stainless steel, it has a long service life compared to mild steel. Even though stainless steel has a higher initial cost, the life cycle cost is estimated to be lower because the frequency and cost of future maintenance and replacement work are reduced [18].

Yamaji et al. [26] investigated the corrosion of stainless steel bars in concrete using sound and pre-cracked concrete specimens. Three types of stainless steel were investigated, such as 18Cr, 18Cr-8Ni and 18Cr-12Ni-2.5Mo. Concrete specimens were exposed to two environments, where wetting and drying was alternately repeated. One was in the outdoor with atmospheric temperature, and the other was in a controlled chamber, where the temperature was 60 °C during wetting and 15 °C during drying. The detail investigation

was carried out after two years. No corrosion was observed on stainless steel bar in both sound and pre-cracked concrete exposed to outdoor. The maximum chloride ion concentration was 7.0 kg/$m^3$ for 18Cr-8Ni, 8.0 kg/$m^3$ for 18Cr-12Ni-2.5Mo and 6.0 kg/$m^3$ for 18Cr at the crack region of concrete. The results indicated that the chloride ion threshold level for stainless steel was larger than these values under marine environment with atmospheric temperature. No corrosion was observed on both 18Cr-12M-2.Wo and 18Cr in both sound and pre-cracked concrete exposed to controlled chamber. However, corrosion was observed only for 18Cr-8Ni at the crack region, even when the chloride ion concentration at the crack region was 6.0 kg/$m^3$.

Radhakrishna et al. [11] evaluated the influence of the steel reinforcement surface condition on the corrosion performance, by determining the critical chloride threshold values of five uncoated steel reinforcement types (ASTM A 706, ASTM A 615, micro-composite, stainless steel 304, and stainless steel 316LN) with as-received and polished surface conditions using the accelerated chloride threshold (ACT) test procedure. Micrographs of the surfaces for all steel reinforcement types were obtained using both optical and scanning electron microscopy (SEM). This qualitative assessment was correlated with critical chloride threshold values. This study indicated that the mean critical chloride threshold values increased with the complete removal of the as-received surface and with surface polishing for the ASTM A 706, micro-composite, and stainless steel 304 reinforcements and decreased with the complete removal of the as-received surface and with surface polishing of the ASTM A 615 and SS316LN steels.

Tula and Helene [12] utilized the potentiodynamic polarization curves to study electrochemical behavior of ASTM 316L stainless steel reinforcement. Common carbon steel rebars were included for comparison. The bars were studied in non-carbonated concretes with different chloride contents. Other part of the study also included the mechanical consequences of the corrosion development process: the bond (by pull-out) and tensile strength reduction. Integrating both parts of the study made it possible to develop an approach to the service-life prediction of structures reinforced with stainless steel bars.

Gong et al. 2004 [29] concluded that using MMFX-2 is not cost effective compared to the use of epoxy-coated steel; this conclusion was supported by Jing [30]. While Kahl 2007 [31], on the other hand, estimated that using MMFX-2 is more cost effective than epoxy-coated steel and that it can extend the structure's life by 12 years more than the epoxy-coated steel. Only Hurley 2007 [32] studied the corrosion behavior of micro-composite steel in saturated Ca $(OH)_2$ solution. He found that it has a chloride threshold value Cl-/OH- ranging from 0.1 to 4.9, depending on the technique used as well as the test setup and surface condition

With no published study available concerning MMFX reinforcement performance, the University Of Kansas Center for Research conducted a study to evaluate the performance of MMFX reinforcement, with a major emphasis placed on comparing the corrosion resistance of MMFX, epoxy-coated reinforcement, and uncoated reinforcement [33]. The results of the laboratory evaluation were supplemented with construction and maintenance

experience in South Dakota and other states to evaluate the impact of implementing MMFX on the life expectancy and cost effectiveness of concrete bridge decks. From laboratory corrosion testing, epoxy-coated reinforcement was found to be more effective in corrosion resistance than the MMFX steel. Overall, the report concluded that using MMFX reinforcing steel in bridge decks did not appear to be cost effective compared to using epoxy-coated.

The data from a recent limited investigation of clad bars funded by the Federal Highway Administration in the USA as part of a major investigation of many types of reinforcing bars, have suggested that stainless clad bars could be as resistant to chloride attack as solid stainless steel bars [34]. Costing slightly more than twice the cost of carbon steel, this material is extremely attractive.

Initial laboratory tests indicate that stainless steel clad bars will perform up to 75 years or more in severely corrosive environments [35]. The clad bars are especially suited for environments where de-icing salts are used on pavements and bridge decks and also in marine environments. In fact, in marine substructures where the harsh chloride environments are known to cause premature failures in existing bars, the stainless steel clad bars would give considerable corrosion protection.

## 2.7 Significance of this Research

Corrosion of reinforcing steel induces high tensile stress to the concrete leading to cracking and spalling of the concrete cover and billions of dollars are spent every year on repairing such damaged structures. Specialty bars have been developed to avoid these

high-cost of repairs on a long term. Thus, it is important to study the corrosion behavior of specialty steel and compare them to the traditional carbon steel reinforcements under the influence of chloride and sulfate ions couple with increase in temperature.

There is a limited and conflicting information on the use of these special steel bars, also several aspects, such as the high exposure temperature and the combined presence of chloride and sulfate ions, on the effectiveness of these special bars has not been studied. Therefore, there is an urgent need for a more detailed study to evaluate the effectiveness of special steel bars under the combined effect of different chloride and sulfate concentration and temperature.

# CHAPTER 3

# METHODOLOGY OF RESEARCH

This chapter outlines the materials and the test methods utilized to fulfill the objectives of the present study. In this study, the corrosion behavior of the corrosion resistant steel bars under varying exposure conditions in terms of temperature, chloride and sulfate concentration was evaluated. Also, the mechanisms of corrosion resistant bars were evaluated by measuring the corrosion rate using potentiodynamic scanning and linear polarization resistance techniques on steel specimens immersed in simulated concrete pore solution (SCPS). Furthermore, macro-cell current, corrosion potential and total corrosion of the steel bars in different aggressive chemical environments using ASTM G 109 were evaluated. In order to fulfill all the above-mentioned tasks, the following sections describe the materials and various techniques.

## 3.1 Materials

The materials that were used for this research are detailed in the following sub-sections.

### 3.1.1 Types of reinforcing steel bars

The following types of steel bars were utilized.

1. Carbon steel
2. Stainless steel
3. Stainless-Clad steel
4. MMFX steel

The chemical composition of the studied steel bars is shown in Table 3.1.

Table 3.1:The chemical composition of the Studied Steel Bars

| Element | Chemical composition (%) | | | |
|---|---|---|---|---|
| | Black bar | Stainless steel | Stainless-clad | MMFX |
| C | 0.2790 | 0.0607 | 0.2450 | 0.0896 |
| Al | 0.0255 | 0.0351 | 0.0197 | 0.0165 |
| Si | 0.2233 | 0.4387 | 0.3350 | 0.1280 |
| P | 0.0264 | 0.0410 | 0.0360 | 0.0205 |
| S | 0.0253 | 0.0263 | 0.0305 | 0.0255 |
| Ti | 0.0925 | 0.0079 | 0.0063 | 0.0080 |
| V | 0.0086 | 0.0787 | 0.0211 | 0.0171 |
| Cr | 0.0163 | 17.4966 | 0.6181 | 9.3661 |
| Mn | 0.6802 | 1.3828 | 0.9625 | 0.5645 |
| Ni | 0.0295 | 10.3647 | 0.2157 | 0.0811 |
| Cu | 0.0803 | 0.1156 | 0.1215 | 0.0665 |
| Nb | 0.0070 | 0.0290 | 0.0031 | 0.0058 |
| Mo | 0.0037 | 2.3129 | 0.0375 | 0.0079 |

### 3.1.2 Aggregates

Crushed limestone aggregates with a maximum size of (12.5 mm) obtained from quarries in Abu-Hadriyah were used. It was first sieved into different size fractions and then washed with potable water to remove salt and dust contamination. Thereafter, it was air-dried for 48 hours and stored till used. The absorption and bulk specific gravity of the coarse aggregate were determined as per ASTM C 127 and were found to be 2.9% and 2.60, respectively. Also, dune sand with an average absorption of 0.57% and specific gravity of 2.56 was used as fine aggregate. Table 3.2 shows the grading of the coarse aggregates used in preparing the concrete specimens based on ASTM C 33. Potable water was used for mixing the concrete constituents for all ASTM G 109 specimens.

Table 3.2:Grading of Coarse Aggregates Used in Preparing the Concrete Specimens

| Size | Wt. Retained % | Cum. Weight. Retained | Passing % | ASTM C 33, No. 7 |
|---|---|---|---|---|
| 3/4” | 0 | 0 | 100 | - |
| 1/2” | 40 | 40 | 60 | 25-60 |
| 3/8” | - | - | - | - |
| 3/16” | 50 | 90 | 10 | 0-10 |
| 3/32” | 10 | 100 | 0 | 0-5 |

### 3.1.3 Cement and Silica Fume

ASTM C 150 Type I and silica fume were used in preparing all the concrete mixes. Table 3.3 shows the chemical composition of Portland cement and silica fume.

Table 3.3:Chemical Composition of Portland Cement and Silica Fume

| Constituents (wt %) | Type I Cement | Silica Fume |
|---|---|---|
| $SiO_2$ | 19.92 | 98.7 |
| $Al_2O_3$ | 6.54 | 0.21 |
| $Fe_2O_3$ | 2.09 | 0.046 |
| CaO | 64.70 | 0.024 |
| MgO | 1.84 | - |
| $SO_3$ | 2.61 | 0.015 |
| $K_2O$ | 0.56 | 0.048 |
| $Na_2O$ | 0.28 | 0.085 |
| $C_3S$ | 55.9 | - |
| $C_2S$ | 19 | - |
| $C_3A$ | 7.5 | - |
| $C_4AF$ | 9.8 | - |

## 3.2 Test Variables

In order to fulfil the objectives of this investigation, the following test variables were selected to simulate moderate and severe environmental conditions in the eastern province of Saudi Arabia:

1) Four different steel bars (black (BB), Stainless steel (SS), MMFX and stainless-clad (SCS))
2) Temperature (25 and 55 ºC).

3) Chloride concentration (500, 1000 and 2000 ppm).
4) Sulfate concentration (0, 500 and 2000 ppm).

Tables 3.4 through 3.6 show the types of steel bars, temperature range and chloride sulfate concentration and the relevant tests, while Tables 3.7 and 3.8 show the details of concrete specimens used for determining corrosion resistance of the specialty steel bars utilizing ASTM G109 test method.

Table 3.4:Potentiodynamic Tests on Steel Samples in Presence of Chloride and varying Temperatures

| Steel name | Chloride Concentration | Temperature | Evaluation |
|---|---|---|---|
| Black steel | 500 ppm | 25 C˚ 55 C˚ | Potentiodynamic polarization |
| | 1000 ppm | | |
| | 2000 ppm | | |
| Stainless steel | 500 ppm | 25 C˚ 55 C˚ | |
| | 1000 ppm | | |
| | 2000 ppm | | |
| MMFX | 500 ppm | 25 C˚ 55 C˚ | |
| | 1000 ppm | | |
| | 2000 ppm | | |
| Stainless steel Clad | 500 ppm | 25 C˚ 55 C˚ | |
| | 1000 ppm | | |
| | 2000 ppm | | |

Table 3.5:Details of Potentiodynamic Tests on Steel Samples in the Presence of Chloride and Sulfate

| Steel name | Chloride Concentration | Sulfate Concentration | | Temperature | Evaluation |
|---|---|---|---|---|---|
| Black steel | 500 ppm | 500 | | 25 C˚ 55 C˚ | Potentiodynamic polarization |
| | 1000 ppm | | | | |
| | 2000 ppm | 500 | 2000 | | |
| Stainless steel | 500 ppm | 500 | | 25 C˚ 55 C˚ | |
| | 1000 ppm | | | | |
| | 2000 ppm | 500 | 2000 | | |
| MMFX | 500 ppm | 500 | | 25 C˚ 55 C˚ | |
| | 1000 ppm | | | | |
| | 2000 ppm | 500 | 2000 | | |
| Stainless steel Clad | 500 ppm | 500 | | 25 C˚ 55 C˚ | |
| | 1000 ppm | | | | |
| | 2000 ppm | 500 | 2000 | | |

Table 3.6:Details of Steel Samples for SEM

| Steel bars | Chloride Concentration (ppm) | Sulfate Concentration (ppm) | Temperature (°C) | No. of Steel Specimens | Evaluation Properties |
|---|---|---|---|---|---|
| Mild steel | - | - | - | 1 | Microstructure |
| Stainless steel | - | - | - | 1 | |
| MMFX | - | - | - | 1 | |
| Stainless-clad | - | - | - | 1 | |
| Mild steel | 1000 | - | 25<br>55 | 2 | |
| Stainless steel | 1000 | - | 25<br>55 | 2 | |
| MMFX | 1000 | - | 25<br>55 | 2 | |
| Stainless-clad | 1000 | - | 25<br>55 | 2 | |
| Mild steel | 1000 | 500 | 25 | 2 | |
| Stainless steel | 1000 | 500 | 25 | 2 | |
| MMFX | 1000 | 500 | 25 | 2 | |
| Stainless-clad | 1000 | 500 | 25 | 2 | |

Table.3.7:Over view of the Concrete Specimens for Laboratory Exposure

| Steel name | No. of prismatic specimens | Dimensions in (mm) | Test |
|---|---|---|---|
| Black steel | 12 | 280 x 150 x 115 | ASTM G109 |
| Stainless steel | 12 | 280 x 150 x 115 | |
| MMFX | 12 | 280 x 150 x 115 | |
| Stainless steel Clad | 12 | 280 x 150 x 115 | |

Table3.8:Uncracked Concrete Specimens for Laboratory Exposure

| Steel bars | Sodium Chloride Concentration (%) | Sodium Sulfate Concentration (%) | Magnesium Sulfate Concentration (%) | No. of Steel Specimens (Replicates) | Test |
|---|---|---|---|---|---|
| Mild steel | 3 | - | - | 3 | ASTM G109 |
| Stainless steel | 3 | - | - | 3 | |
| MMFX | 3 | - | - | 3 | |
| Stainless-clad | 3 | - | - | 3 | |
| Mild steel | 3 | 0.25 | 0.25 | 3 | |
| Stainless steel | 3 | 0.25 | 0.25 | 3 | |
| MMFX | 3 | 0.25 | 0.25 | 3 | |
| Stainless-clad | 3 | 0.25 | 0.25 | 3 | |
| Mild steel | 3 | 1.5 | 1.5 | 3 | |
| Stainless steel | 3 | 1.5 | 1.5 | 3 | |
| MMFX | 3 | 1.5 | 1.5 | 3 | |
| Stainless-clad | 3 | 1.5 | 1.5 | 3 | |
| Mild steel | 15 | 1.0 | 1.0 | 3 | |
| Stainless steel | 15 | 1.0 | 1.0 | 3 | |
| MMFX | 15 | 1.0 | 1.0 | 3 | |
| Stainless-clad | 15 | 1.0 | 1.0 | 3 | |

## 3.3 Electro-Chemical Testing

### 3.3.1 Steel Specimens Design

Steel specimens of 28 mm length, 16 mm diameter for black bar and stainless steel, 14 mm diameter for the MMFX and 20 mm diameter for the stainless-clad bar were prepared and the surface of each sample was cleaned by using sand paper and acetone. Both ends of the steel samples were coated with epoxy resin, as shown in Figure 3.1. The top side of steel specimen was drilled to be fitted with coarse-thread stainless steel holder. The exposed area of the reinforcing steel was in the range of (12.98 to 17.62) $cm^2$. Completed specimens are shown in Figure 3.2.

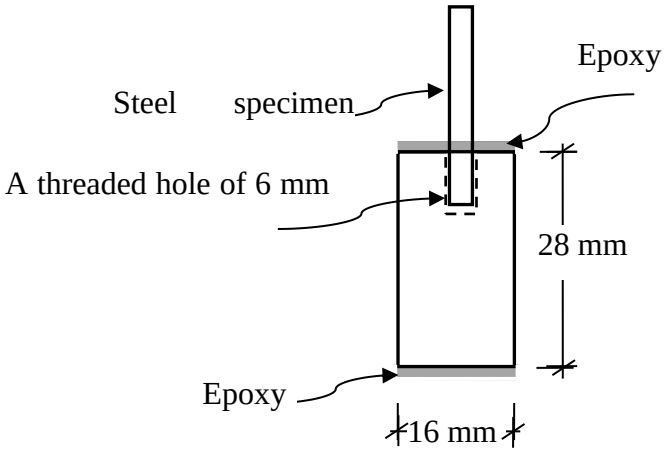


Figure 3.1: Schematic Representation of the Steel Specimen.

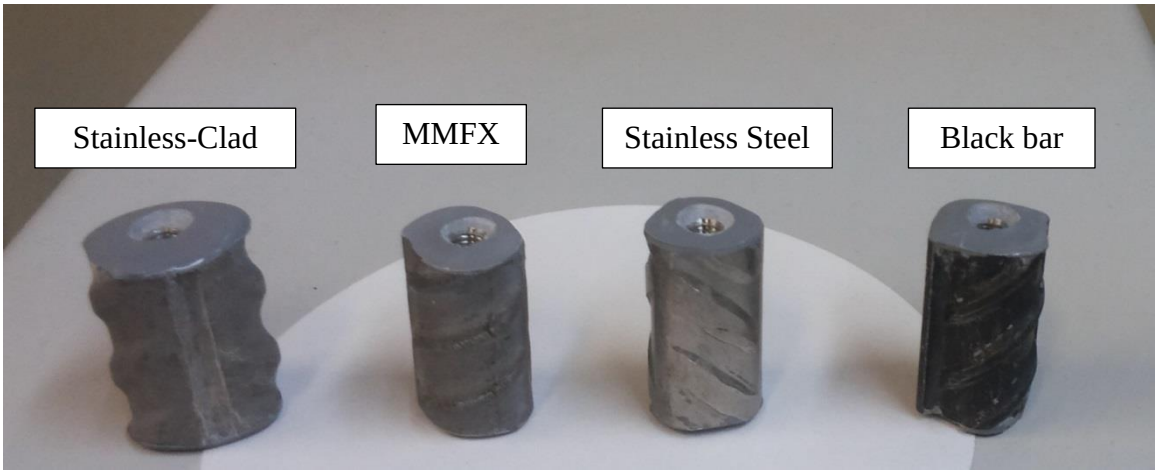


Figure 3.2:Specimens Ready for Testing

### 3.3.2 Simulated Concrete Pore Solution

The simulated concrete pore solution was prepared based on the analysis of concrete specimens at KFUPM which indicates that one liter of concrete pore solution contains 974 g of distilled water, 14 g of potassium hydroxide (KOH), 10 g of sodium hydroxide (NaOH), and 2 g of calcium hydroxide [$Ca(OH)_2$]. The simulated concrete pore solution has a pH of more than 13.4. Reagent grade of KOH, NaOH and Ca $(OH)_2$ were utilized to prepare the concrete pore solution.

### 3.3.3 Test procedures

The steel specimens, as described in Section 3.3.1, were placed in the corrosion cell containing simulated concrete pore solution and varying temperature and sulfate and/or chloride concentration. Thereafter, potentiodynamic polarization test was conducted.

In order to conduct the proposed test procedures, specialized equipment was used (ACM instrument). The main components of this system includes: computer operated

potentiostat, controlled magnetic stirrer for stirring the solution during test period, corrosion cell, and thermometer for measuring the temperature of the solution.

### 3.3.4 Description of the Corrosion Cell Preparation and Curing of Specimens

Three electrode cell was used for the potentiodynamic measurements. It mainly consists of three electrodes which are immersed in the solution as follows:

- Stainless steel plate was used as counter electrode.
- Saturated calomel electrode (SCE) was used as the reference electrode.
- Working electrode (the tested steel specimen itself).

The steel specimens were prepared as described in 3.3.1. In order to attach the steel specimen to the specimen holder, a threaded hole of 6 mm diameter and 8 mm deep was drilled in each sample. The specimen holder was covered with a Teflon tube to prevent any possibility of crevice corrosion. The electrolyte level was kept below the attaching point all the time. Figure 3.3 show the working electrode, reference and counter electrode.

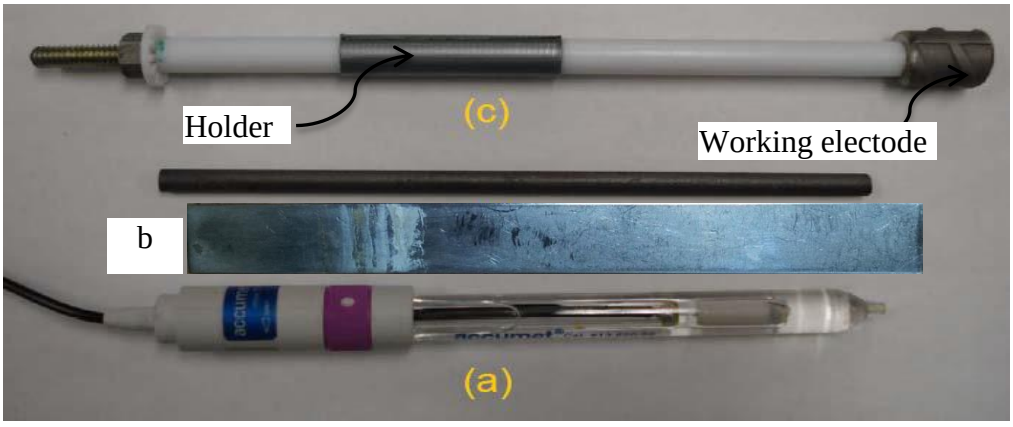


Figure 3.3:Electrodes Used in Electrochemical Testing (a) Reference Electrode (b) Counter Electrode (c) Working Electrode

### 3.3.5 Potentiodynamic Testing

The potentiodynamic method measures the current for a large potential sweep from the cathodic to the anodic region of the corrosion potential. The potentiodynamic studies were conducted on bare steel exposed to electrolyte representing the concrete pore solution admixed with the selected inhibitors, selected chloride concentration and selected temperature. The potentiodynamic potential-current curves were recorded by changing the electrode potential from - 900 to + 900 mV with a scan rate of 15mV/minute, as shown in Figure 3.4. The schematic illustration in Figure 3.5 displays the main terminologies for a typical potentiodynamic polarization diagram (PDP), which is plotted in terms of applied potential vs the logarithm of the measured corrosion current density. From this Figure, we can notice many futures which can be used to interpret the behavior of steel specimens under PDP test. The open circuit potential is located at Point (A) at which the sum of cathodic and anodic reaction on the working electrode is zero (often this point equals to corrosion potential). As the applied potential increases from A to B, anodic polarization moves to region (B), which is the passive region (increase in the applied potential without increase in the measured current). Point (C) is known as the active potential, and as the applied potential increases above this value, the current moves to region (D), which is called active region. At region (D), the current density increases with the increase in the applied potential and steel oxidation is the dominant reaction taking place. The increase in current continues with the increase in the applied potential till it reaches point (E), which is the limit point of anodic scan. In some cases, sudden increase in the measured current may be noted without an increase in the potential, which indicates presence of pitting

corrosion and the corresponding potential called the pitting potential, as shown in Figure 3.6.

In the cathodic scan, the applied potential increased in the negative direction, as anodic scan point (A) represents the open circuit potential. As the applied potential increases in the negative direction the current moves into region (F), which represents the oxygen reduction reaction (cathodic polarization). This increase continues till point (H), which is the limit point for cathodic scan.

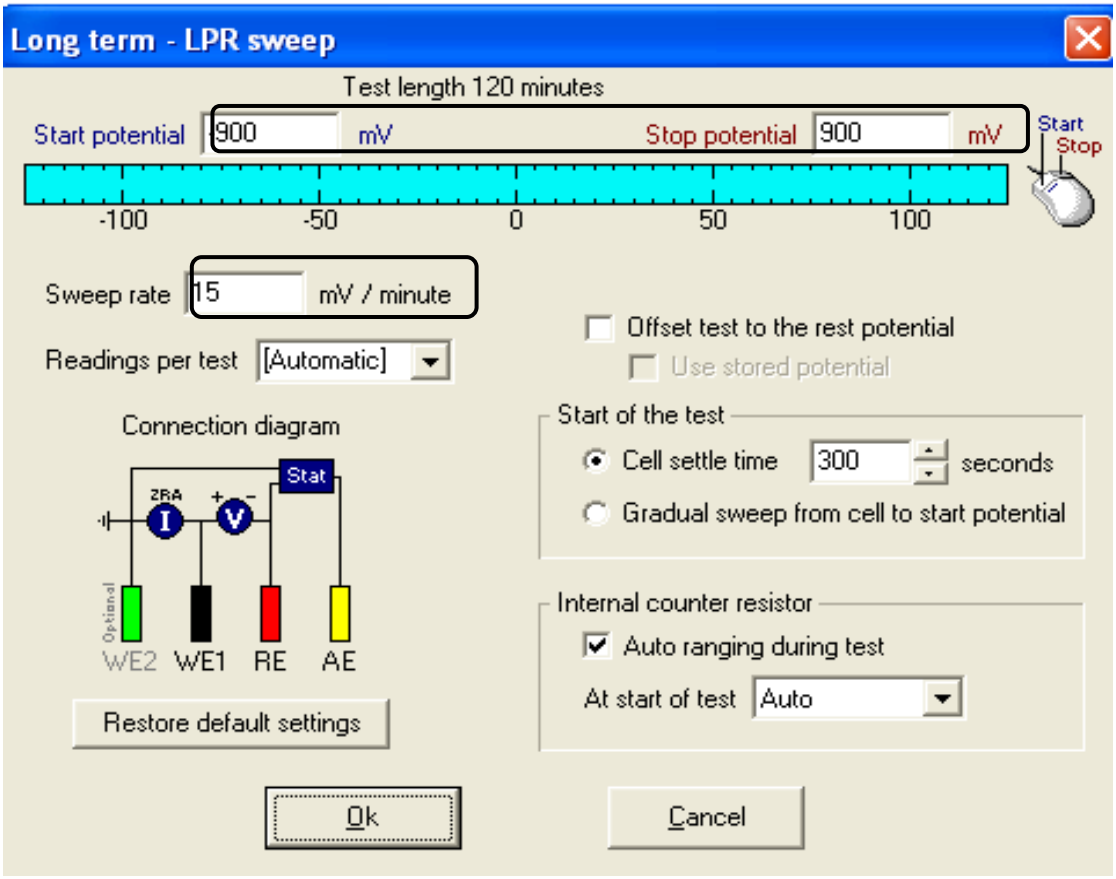


Figure 3.4:Potential Range and Scanning Rate as Appeared

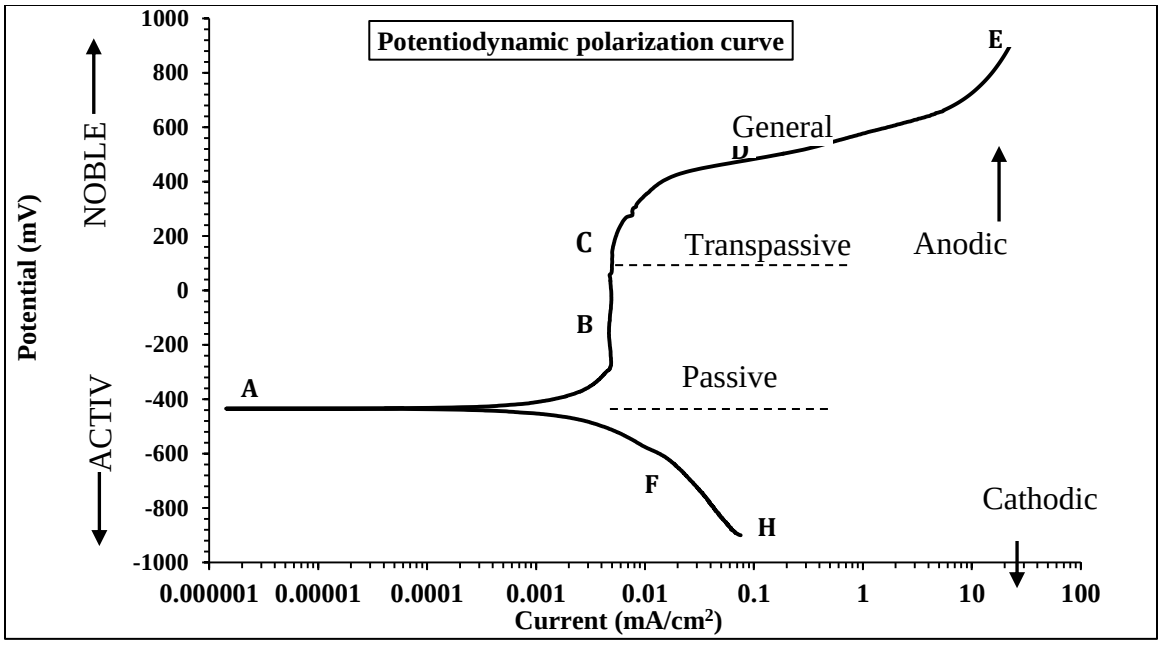


Figure 3.5:Schematic Illustration of Potentiodynamic Polarization with Various Terminologies

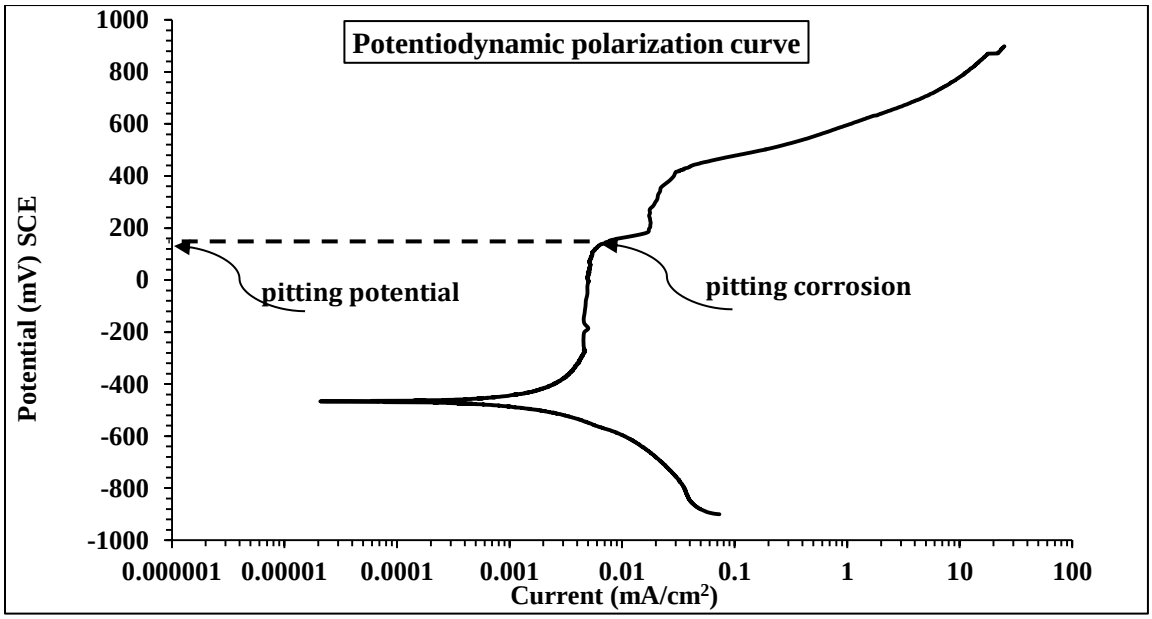


Figure 3.6:Schematic Illustration of Potentiodynamic Polarization with Pitting Corrosion

Significant information can be obtained from the potentiodynamic polarization scan, some of which include the following:

i. The potential area over which the metal remains at passive stage.
ii. The corrosion rate of the metal sample in the passive area and the ability of the metal sample to be passivated,
iii. The localized corrosion of metal samples, and
iv. Passivity condition.

### 3.3.6 Corrosion Current Density

For this test, ACM instrument with three electrodes was used to conduct the potentiodynamic scan. The steel specimen with 28 mm length as described in Section 3.3.1, was connected to the working electrode terminal while reference electrode and the auxiliary stainless steel plate were connected to the respective terminals of the ACM potentiostat machine. This specimen was polarized by applying a potential of ±900 mV of the corrosion potential with scan rate of 15 mV/minute and the resulting current between the working and counter electrodes is measured. Figure 3.7 shows a schematic representation of the set-up which was used to measure the corrosion current density. Also, Figure 3.8 shows general view of the experimental setup of corrosion current density test.

Figure 3.9 depicts the main terminologies in a polarization diagram which is plotted between the applied potential and log measured current. The solid lines represent cathodic and anodic reactions, whereas the dashed lines represent the linear part of each reaction.

The intersection of these dashed lines gives the open circuit potential ($E_{corr}$) on the vertical excise and corrosion current density on the horizontal axis. The anodic polarization curve is predominant at positive direction (Nobel), while cathodic polarization curve is predominant at negative direction (active). Then, the corrosion current density can be calculated using the Stern-Geary formula [36]:

$$I_{corr} = B/R_p \quad (3.1)$$

Where:

$I_{corr}$ = corrosion current density ($\mu A/cm^2$);

$R_p$ = polarization resistance, KOhms-$cm^2$;

$B = (\beta a * \beta c) / (2.3(\beta a + \beta c))$;

Where: βc and βa are the cathodic and anodic Tafel constants, respectively.

The Tafel constants can be determined either by polarizing the steel to ±250 mV of the corrosion potential or polarizing the steel to ±900 mV of the corrosion potential (potentio-dynamic).In case of the absence of sufficient data on Tafel constants, value of 100 mV is to be used for steel in a highly resistant medium [37]. A good correlation between the linear polarization technique and the weight loss determined by gravimetric methods was observed by Gonzalez et al [38] by using a B value of 52 mV in the passive state and 26 mV for steel in the active state. In our investigation, βc = βa = 120 mV was used throughout which corresponds to B = 26 mV. These values have been found to be useful in the corrosion experiments at KFUPM.

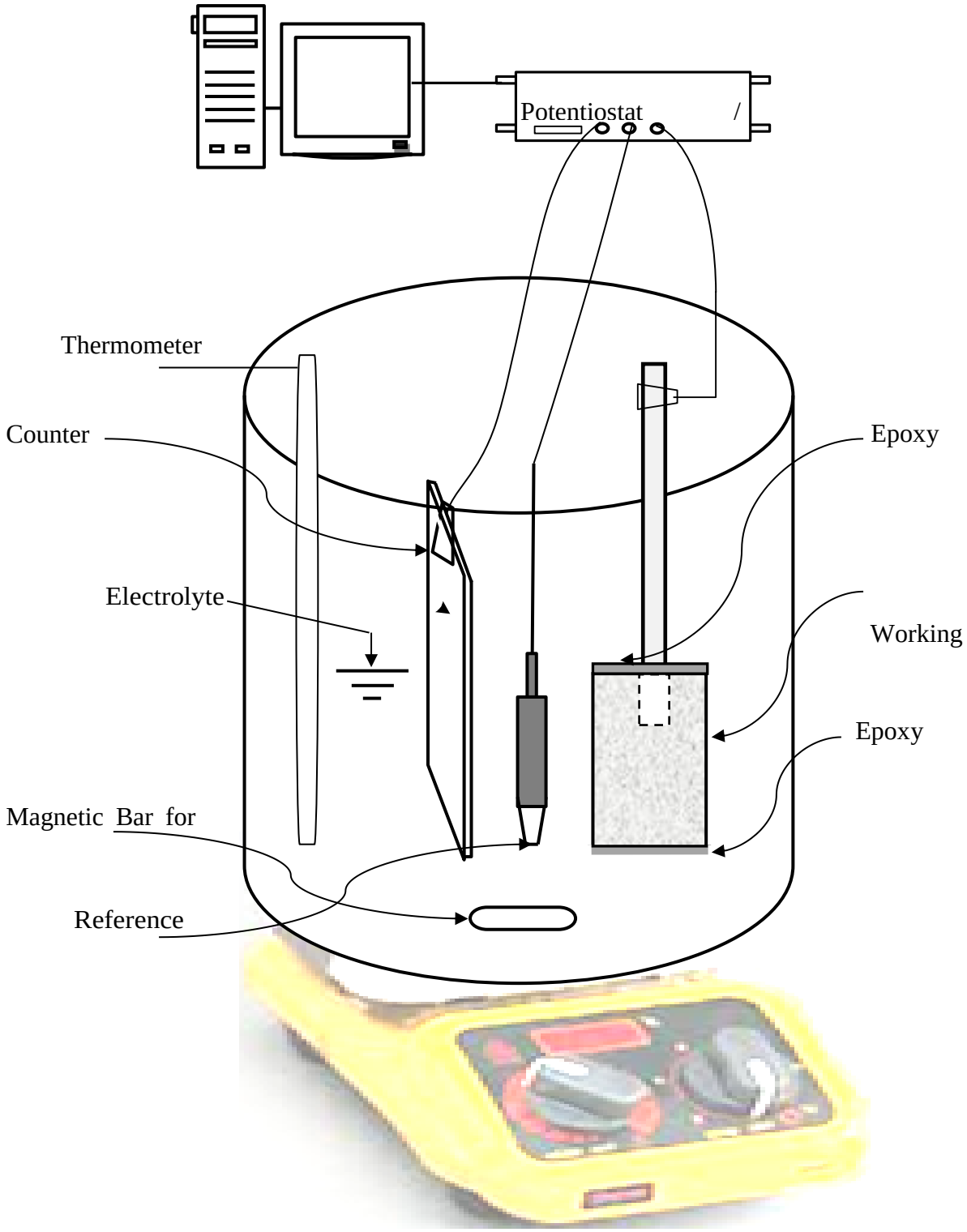


Figure 3.7:Schematic Representation of the Experimental Setup Used for Electro- Chemical Measurements


Figure 3.8:General View of the Experimental Setup for Electro-Chemical Measurements.

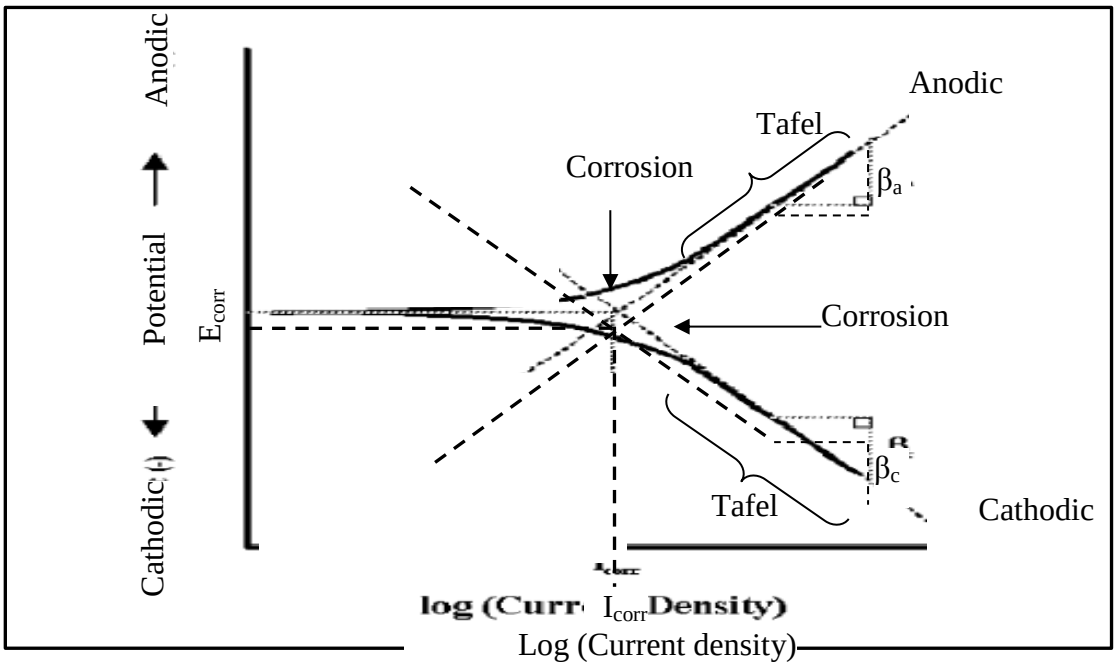


Figure 3.9Main Parts of Tafel Polarization Diagram.

### 3.3.7 Scanning Electron Microscopy (SEM)

The scanning electron microscope (SEM) uses beam of high-energy electrons instead of light to generate variety of signals at the surface of solid samples. These signals reveal information about the sample including its chemical composition, external morphology (texture), and orientation of materials making up the sample, and crystalline structure. In this research, the surface of steel samples exposed to simulated concrete pore solution at different temperatures and chloride or chloride plus sulfate concentrations were evaluated using SEM to know the surface conditions. In order to conduct the proposed SEM test procedures, specialized equipment (JSM-5800LV SEM instrument) was used. The main components of this system includes: sample chamber, electron column, three visual display monitors and EDS detector, as shown in Figure 3.10.

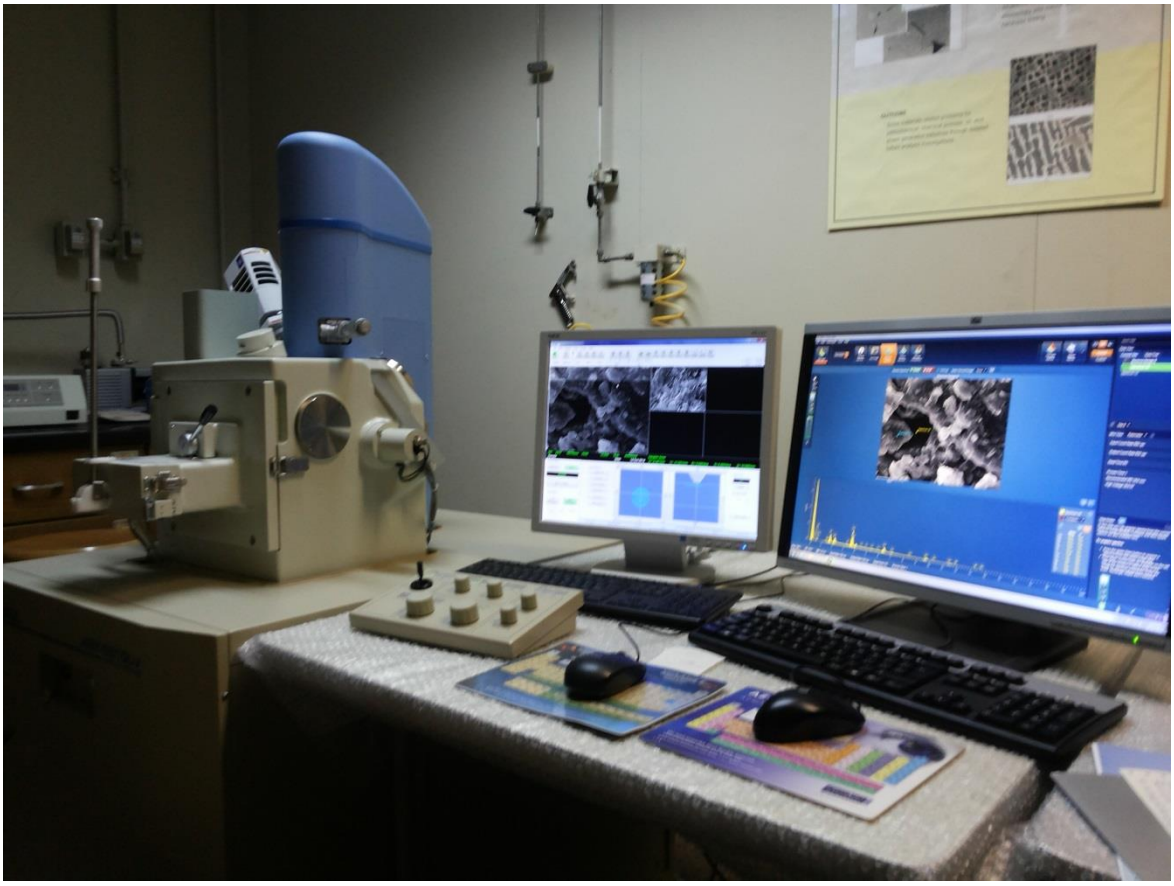

Figure 3.10:Photographic Documentation of SEM Instrument showing the main Components

## 3.4 Preparation of Concrete Specimens f Macro-Cell Current Measurements

The concrete specimens were prepared with the four different steel bars and ponded with four different chemical solutions.

### 3.4.1 Concrete Specimens Design

The concrete specimens was designed according to ASTM G 109, with 16 mm diameter for the black and stainless steel bars, 14 mm diameter for the MMFX and 16mm for the stainless-clad steel bar . These bars were cut into 360 mm long pieces. One end of steel

specimen was drilled and tapped to be fitted with a coarse-thread stainless steel rod. The steel screwed bars were cleaned with acetone. Electroplater's tape was used to cover 78 mm from each end of the steel samples leaving 204 mm long piece of sample exposed for testing. Electrical connections and the ends of steel bars were coated with a two-part epoxy. Then, the steel bars were placed into wooden molds with the following dimensions: 280 x 150 x 115 mm (inner dimensions) in two layers. These bars must be placed in the middle of the mold. The top layer consisted of one steel reinforcement bar with a clear cover depth of 25.4 mm. While the bottom reinforcement layer consisted of two steel reinforcement bars that were placed 31.75 mm from bottom of the mold. Figure 3.11 is a schematic representation of an ASTM G 109 test specimen. Photographic documentation of the completed specimens is shown in Figure 3.12.

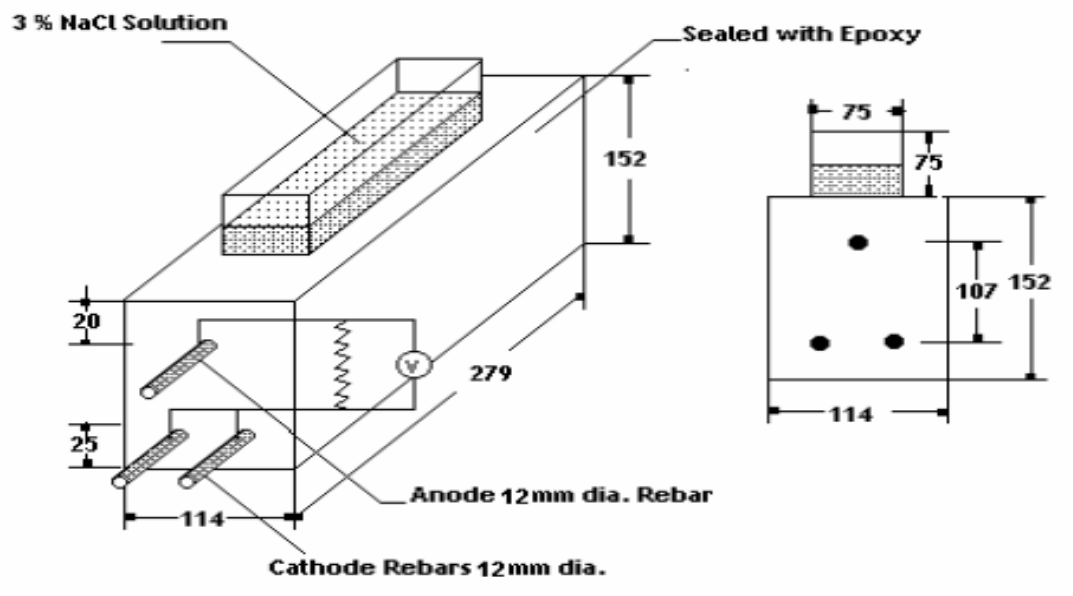


Figure 3.11:Schematic Representation of ASTM G 109 Specimen.


Figure 3.12:Completed G 109 Test Concrete Specimens

### 3.4.2 Concrete Proportioning

Concrete mixtures were used to cast the concrete specimens for macro cell current studies. ASTM C 150 Type I (ordinary Portland) cement and silica fume were used in all of the concrete mixtures. The coarse aggregate used was crushed limestone with a maximum size of 12.5 mm. Also, dune sand with an average absorption of 0.57% and specific gravity of 2.56 was used as fine aggregate. Each concrete mixture contained one type of the five selected corrosion inhibitors. The concrete specimens were prepared with the mix design shown in Table 3.9.

Table 3.9: Concrete Mixture Proportions for ASTM G 109 Specimens

| Ingredients | Weight ($kg/cm^3$) | |
|---|---|---|
| Cement (kg) | 355 | |
| Water (kg) | 170 | |
| Silica fume (kg) | 25 | |
| Coarse aggregate | Opening Size (mm) | Weight (kg) |
| | 19 | 0.0 |
| | 12.5 | 449.09 |
| | 9.5 | 449.09 |
| | 4.75 | 112.27 |
| | 2.36 | 112.27 |
| Sand (kg) | 748.48 | |
| W/(C+SF) ratio | 0.444 | |
| Superplasticizers(%) | 1.2 | |

### 3.4.3 Fabrication of Specimens

A band saw was used to cut all reinforcement to the required length 360 mm. Thereafter, the reinforcement bar was drilled on a lathe machine, and the threading was done on one end of the bar. Both ends of all reinforcing bars were wrapped with electroplaters tape for a length of 76 mm from each end of the steel samples, as shown in Figures 3.13 and 3.14. Neoprenes tubing of appropriate diameters were then placed on each end to provide a second barrier layer and to protect the tape from any physical damage during handling (see Figure 3.15). A stainless steel screw with stainless steel nut was threaded into one end of the bar, and then two part waterproof epoxy was placed on both end of each bar, covering both the tubing and steel. The bars were then placed into the wooden mold so that an equal length was protruding from both ends, as shown in Figure 3.16. For ASTM G 109 test, the bottom two reinforcing bars are the cathode and the top reinforcing bar is the anode.

Figure 3.13:Reinforcing Bars for ASTM G 109 Specimens

Figure 3.14: Steel Bars End with Electroplaters Tape

Figure 3.15:Complete Reinforcing Bar End Treatment

Figure 3.16:Completed Reinforcing Bars in Formwork

### 3.4.4 Mixing and Casting

The concrete constituents were mixed in a revolving drum type mixer (Figure 3.17) for about 10 to 15 minutes till a uniform mixture was achieved. The superplasticizers were added to the mixes by dissolving them in the mixing water. Thereafter, the molds were filled with concrete in roughly two equal layers (76.2 mm height each layer) and vibrated for consolidation by using a small vibrating table, as shown in Figure 3.18. ASTM G 109 requires three replicates to be made; hence three replicates were cast for each type of steel bars. The top of the specimens were finished with a steel float, as shown in Figure 3.19.

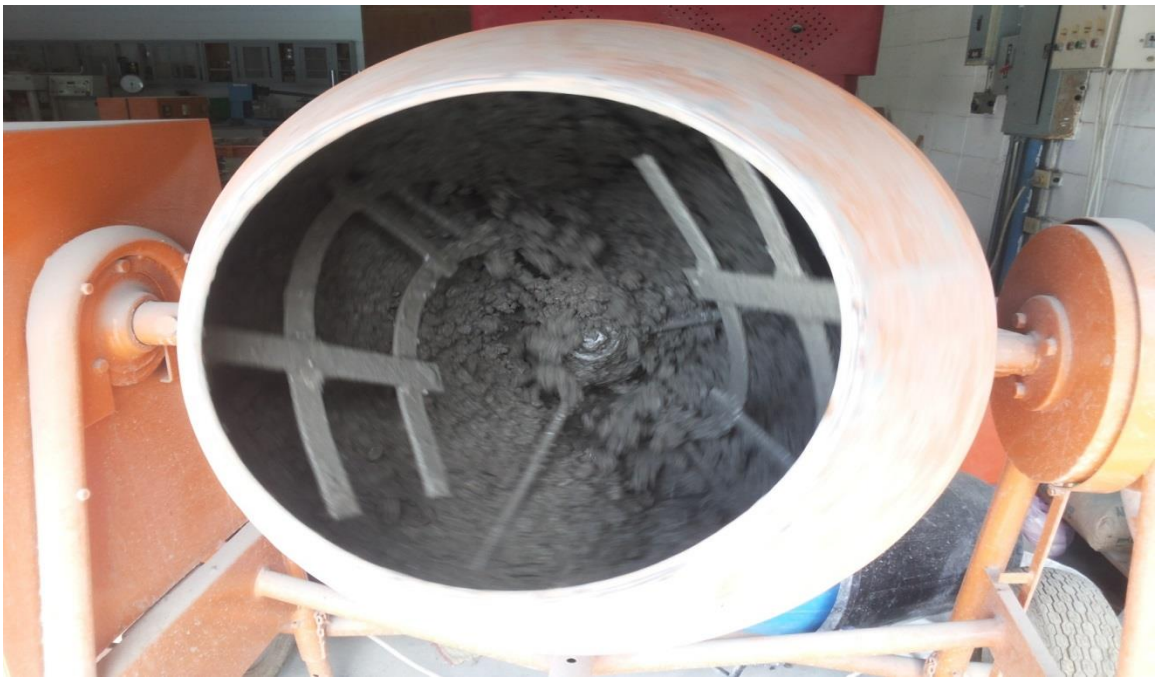

Figure 3.17:Photograph for Revolving Drum Mixer

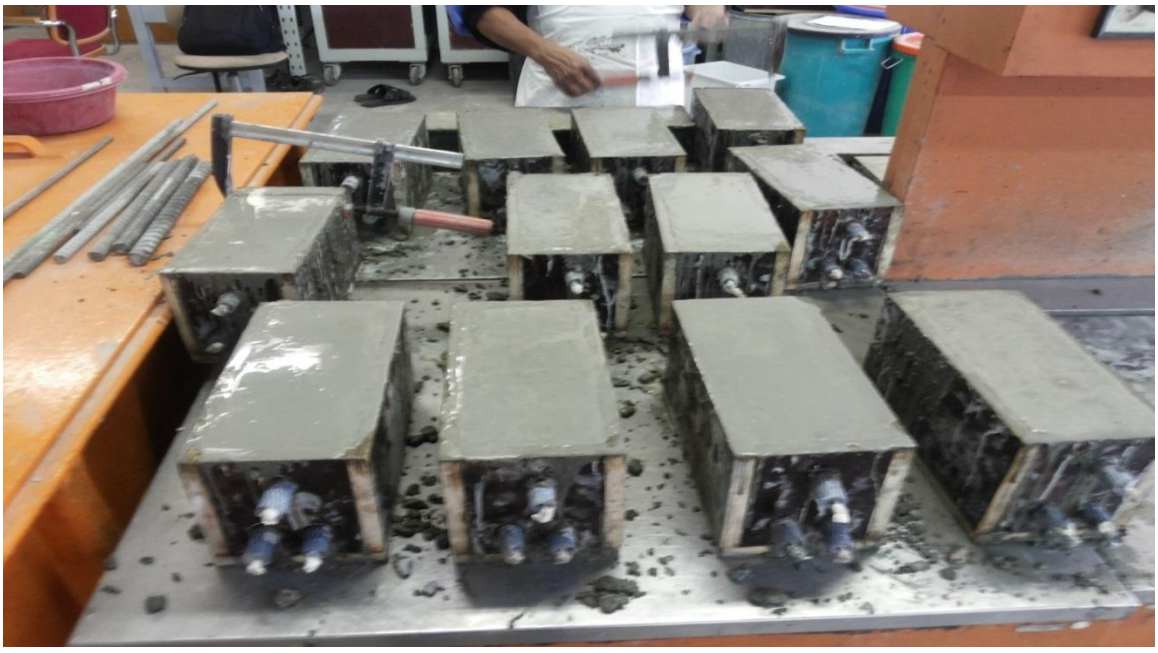

Figure 3.18:Concrete Specimens on the Vibrating Table

Figure 3.19:Finishing the Surface of Concrete Specimens

### 3.4.5 Curing

After casting, the concrete specimens were cured by covering them with plastic sheet for approximately 24 hours. Then, the specimens were demoded and cured by covering them with wet burlap for 28 days. A total of 48 specimens were covered with wet burlap and plastic sheets, as shown in Figures 3.20. These burlaps were wetted twice daily (at early morning and evening). After two weeks of drying, as shown in Figure 3.21, the four vertical sides and the top, except on the inside of the Plexiglas dams were sealed with epoxy. Then, wires were attached to each of the screws on one end of each top reinforcing bars (anode electrode), and the bottom two wires were connected together to form one wire (cathode electrode). A 100 Ohm resister was connected between the bottom and the top wires. Completed specimens are shown in Figure 3.22.

Figure 3.20:Curing of Specimens by Covering them with Wet Burlap.

Figure 3.21: Drying the Specimens after 28 Days of Curing.

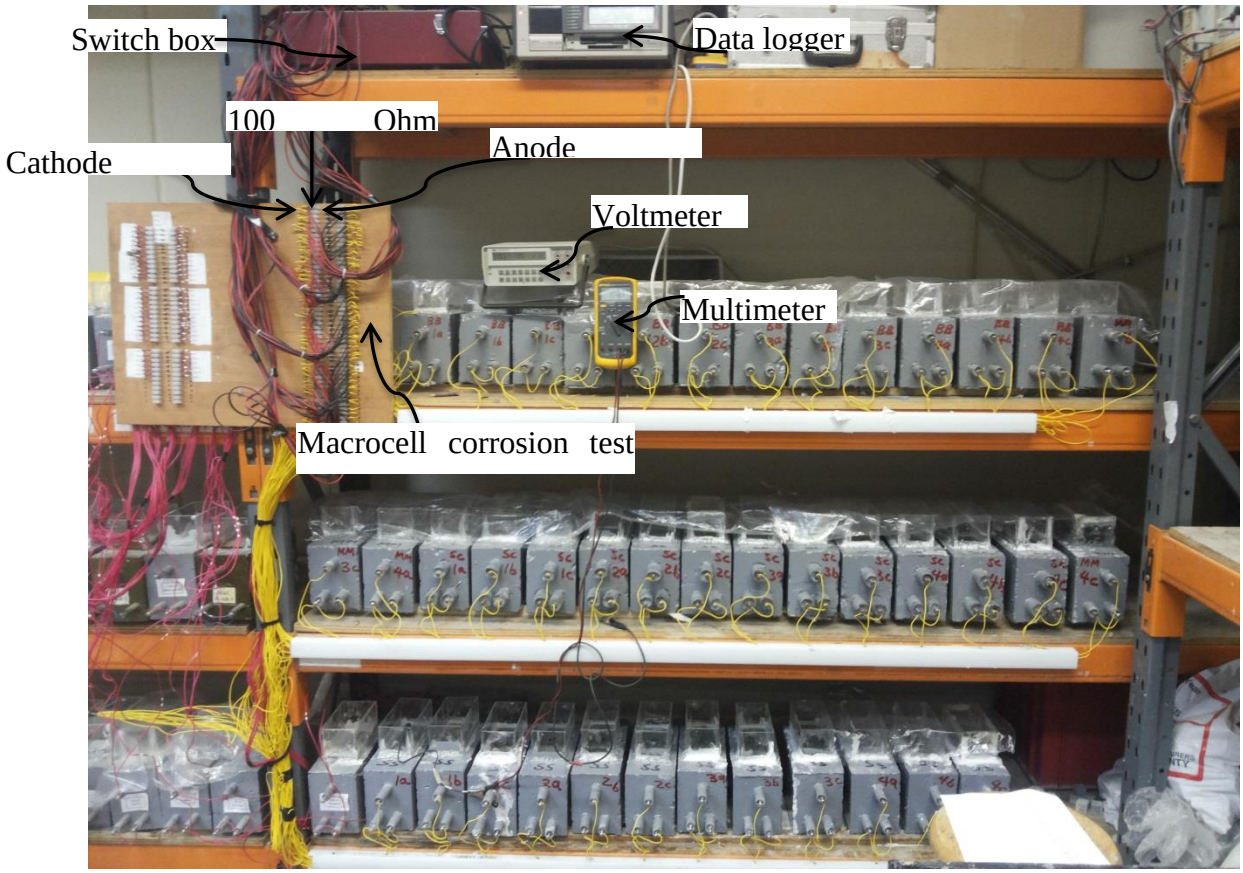


Figure 3.22:Experimental Setup for Macro Cell Corrosion Measurements.

## 3.5 Testing

The concrete specimens were stored on steel shelves in the laboratory to ensure their bottom surfaces are exposed to air during all period of the test. The specimens were ponded with 400 ml (half the height of Plexiglas dam) of four different solutions representing different environmental conditions which are:

i. 3% NaCl solution

ii. 3% NaCl solution admixed with 0.5% $SO_4^{2-}$ (0.25 $Na_2SO_4$ and 0.25 $MgSO_4$)

iii. 3% NaCl admixed with 3% $SO_4^{2-}$ (1.5% $Na_2SO_4$ and 1.5% $MgSO_4$ )

iv. 15% NaCl admixed with 2% $SO_4^{2-}$ (1% $Na_2SO_4$ and 1% $MgSO_4$ sabka solution

The concrete specimens were ponded using the above mentioned four different solution for two weeks. At the end of the two weeks of ponding, the solutions were removed by vacuuming it off. Thereafter, specimens were allowed to dry for further two weeks. Thereafter, specimens were ponded again, and this cycle of wetting and drying was repeated for six months.

### 3.5.1 Corrosion Potential

The corrosion potential of each specimen was measured with respect to the reference saturated calomel electrode (SCE). Since measuring the potential requires a path of moisture between the concrete and the electrode, corrosion potentials were only measured during the ponding period. One reading was taken over the top reinforcing bar at the beginning of the second week of wetting cycle (i.e. the bottom bar was cathode). Measurement of corrosion potential is shown in Figure 3.23.


Figure 3.23:Measurement of Corrosion Potentials.

### 3.5.2 Macro-Cell Current Measurement

Macro-cell corrosion current was measured between the top and bottom layers of the reinforcing steel. The test measures the current flowing from the top bar which is being exposed to a chloride environment, while the bottom bars were free of chloride environment because they acted as the cathode, and the top steel was the anode. The 100-Ohm resistor connects the top and bottom layers of steel, and the voltage readings were measured across the resistors with a high impedance voltmeter and a data logger. Then, using Ohm's Law, the macro-cell current was calculated (the voltage was divided by the resistance values of the resistor to obtain current). Measurement of macro-cell corrosion current is shown in Figure 3.24.


Figure 3.24:Measurements of Macro-Cell Corrosion Current.

### 3.5.3 Determination of Chloride Concentration

For each ASTM G 109 specimen tested, the chloride concentration at the rebar level was determined. A 19 mm diameter hole was drilled above the top reinforcing bar to obtain at least 3 grams of concrete powder up to a depth of 20 mm from the top surface. The loose dust was blown out of the hole just before reaching the 20 mm depth in order to collect the right sample. Then, the dust was collected by drilling vertically between 20 to 25 mm in a sequential process. Each sample was stored in a plastic bag until all the samples were taken. For the determination of free chloride content, 3 grams of concrete powder was transferred to a 100-ml beaker and 50 ml of hot distilled water was added. The sample was

heated gently and thoroughly mixed by a stirrer. The solution was allowed to settle for 24 hours and filtered using No. 1 filter paper. After that, the filtered solution was poured into 100 ml flask then, distilled water was added to make the solution 100 ml (standardization of volume) [42,43]. After this, 0.1 ml of solution was mixed with 2 ml of ferric ammonium sulfate plus 2 ml of mercuric thiocyanate. Finally, the above solution was placed in the compartment of Spectronic 21 (spectrophotometer machine) [43, 44]. This machine is equipped with a screen display that can be programmed to display the chloride absorption value automatically when appropriate inputs are fed. Figure 3.25 shows the spectrophotometer machine used in the investigation.


Figure 3.25:Spectronic 21 Machine

# CHAPTER 4

# RESULTS AND DISCUSSION

This chapter presents the results and discussion of mechanical properties of the steel specimens used for this research work and also the result of the tests conducted on the black bar and the corrosion resistant steel bars and their possible interpretation. Broadly speaking, the data developed fall in the following categories.

1. Mechanical properties of the selected steel bars.

2. Combined effect of sulfate and/or chloride and temperature on the corrosion behavior of all the tested steel specimens using LPR and PDP techniques.
3. Effect of the selected chemical compositions simulating different severe environmental conditions on reinforcement corrosion of sound concrete specimens using ASTM G 109.

## 4.1 MECHANICAL PROPERTIES OF THE STEEL SPECIMENS

The micro hardness of the selected steel bars was evaluated using the Buler microhardnes machine. The metallographic preparation of the specimens was done as per the procedures outlined in ASTM E3 and the micro hardness was determined as per ASTM E384. The micro-hardness of the selected steels is summarized in Table 4.1 and shown in Figure 4.1

Table 4.1 :Micro-hardness of the selected steel.

| Indentation #. | Micro-hardness (HV) | | | |
|---|---|---|---|---|
| | Black bar | Stainless steel | Stainless-clad | MMFX |
| 1 | 296.1 | 316.7 | 190.8 | 395.8 |
| 2 | 283.8 | 312.1 | 175.4 | 393.3 |
| 3 | 229.2 | 327.6 | 177.8 | 394.9 |
| 4 | 217.7 | 325.7 | 162.4 | 394.9 |
| 5 | 211.5 | 296.7 | 276.5 | 393.3 |
| 6 | 208.0 | 301.0 | 270.0 | 397.4 |
| 7 | 226.0 | 326.3 | 292.5 | 404.1 |
| 8 | 228.8 | 267.7 | 222.5 | 405.8 |
| 9 | 227.4 | 267.7 | 204.1 | 405.8 |
| 10 | 209.6 | 282.3 | 199.6 | 399.0 |
| 11 | 205.3 | 302.1 | 200.5 | 398.2 |
| 12 | 203.5 | 320.3 | 266.8 | 399.5 |
| 14 | 220.4 | 270.0 | 179.1 | 397.4 |
| 15 | 220.8 | 275.6 | 220.8 | 394.1 |
| 16 | 271.3 | 249.5 | 245.1 | 394.9 |
| 17 | 312.7 | 303.7 | 189.4 | 393.3 |
| 18 | - | - | 185.7 | - |
| 19 | - | - | 191.1 | - |
| 20 | - | - | 217.4 | - |
| Average value | 235.7 | 296.5 | 214.1 | 397.6 |

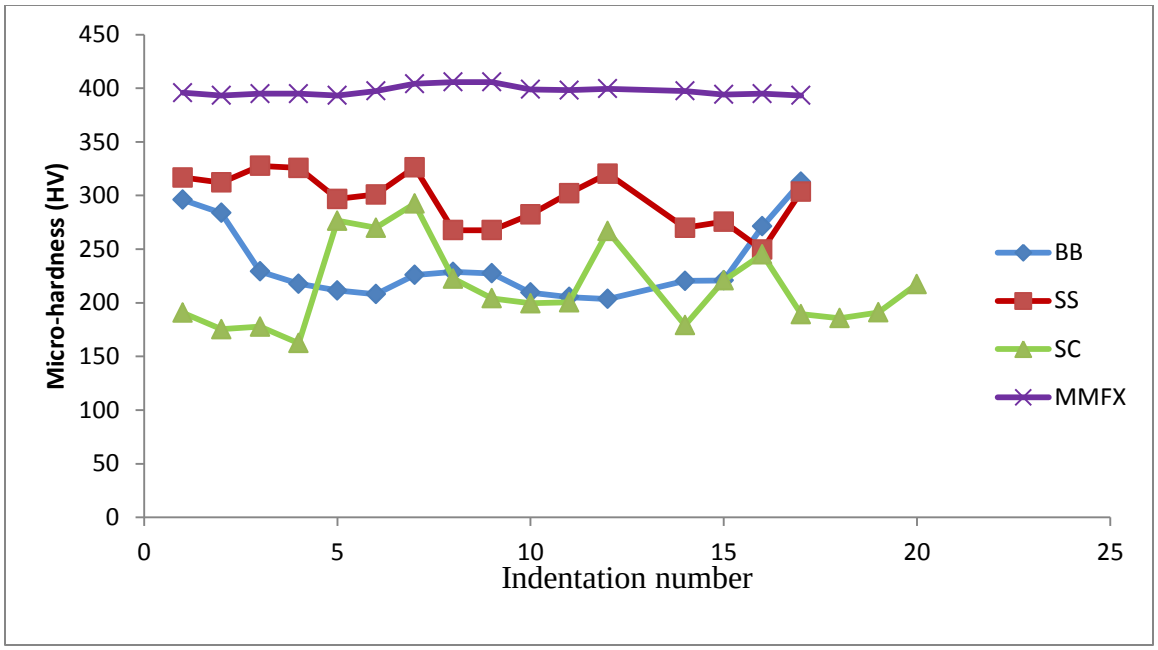


Figure 4.1:Micro-Hardness Variation across the cross-section of the steel specimens

The micro-hardness of MMFX steel bar is the maximum among the selected steel bars. This may be attributed to the densification of microstructure of this steel bar, which is ascribable to its manufacturing process. The micro-hardness of black steel and stainless clad bars was almost similar and the lowest. The micro-hardness of stainless steel bars was more than that of black steel bar; however, it was less than that of MMFX steel bars.

The tensile test was conducted at room temperature (24.8 °C) utilizing a 600 kN Instron universal testing machine. The strain was calculated over a gauge length of 200 mm utilizing an extensometer fitted with a linear variable displacement transducer (LVDT). The tensile properties of the selected steel bars are summarized in Table 4.2 and stress-strain curves are depicted in Figure 4.2.

The yield and ultimate tensile strength of black, stainless steel and stainless clad bars are almost similar. However, these values for the MMFX bars are significantly high. The yield and ultimate strength of these bars are approximately twice that of the black bars. However, the elongation of these bars is almost half of the others bars; indicating that these bars will be very rigid compared to the other bars. The stress strain curves indicate a well-defined yield in the black bars while such a behavior is not noted in the stainless steel and stainless clad bars. A sudden failure at the ultimate stress is indicated in the MMFX bars.

Table 4.2:Tensile properties of the selected steel bars.

| Property | Black bar | Stainless steel | Stainless-clad | MMFX |
|---|---|---|---|---|
| Tensile stress at yield (Offset 0.2 %) (MPa) | 570 | 610 | 400 | 1,000 |
| Tensile stress at yield (Offset 0.5 %) (MPa) | 610 | 670 | 440 | 1,100 |
| Ultimate tensile strength (MPa) | 710 | 740 | 680 | 1,200 |
| Elongation (%) | 24 | 23 | 21 | 9 |

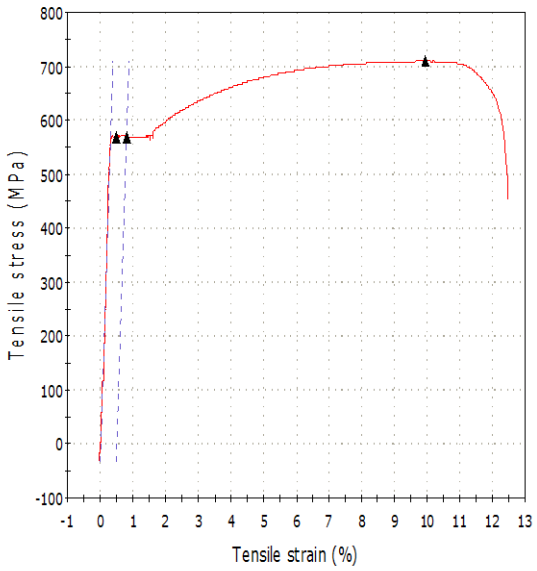


Carbon Steel

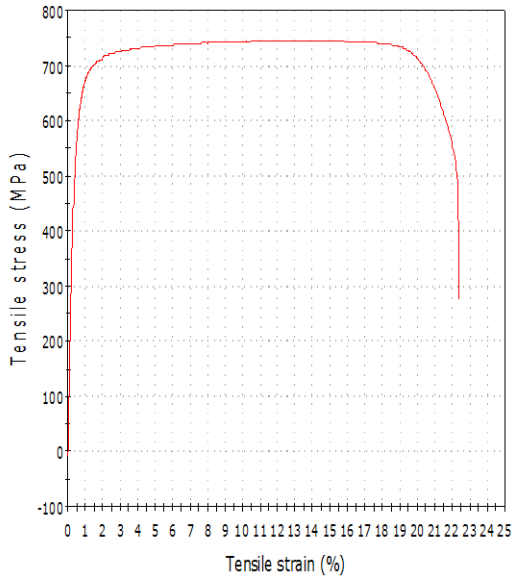


Stainless steel

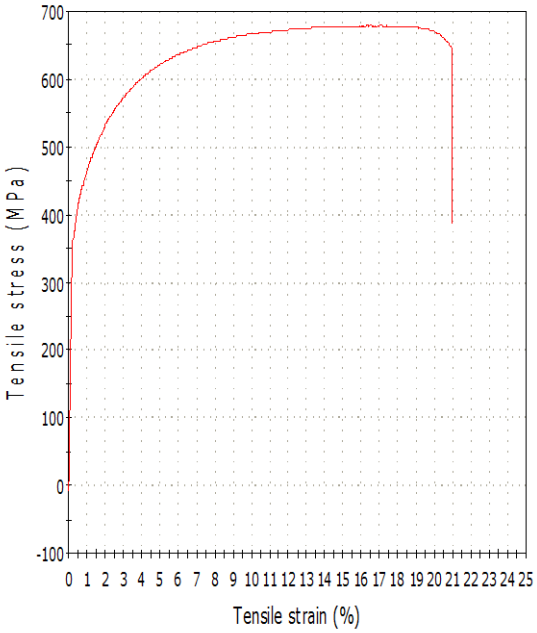


Stainless-Clad Steel

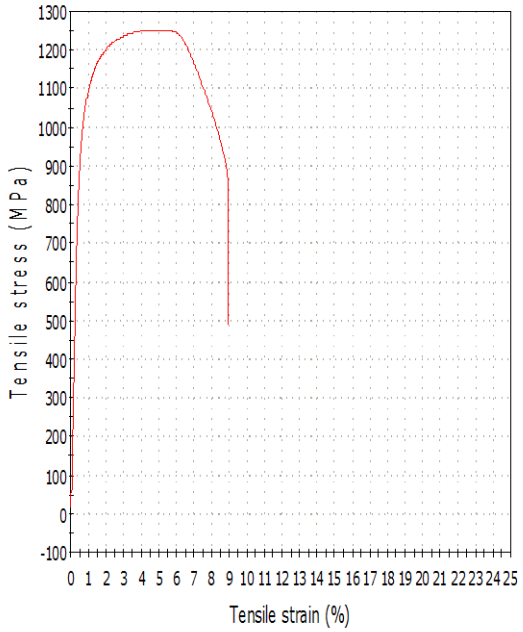


MMFX

Figure 4.2:Stress-strain curves for the selected steel bars.

## 4.2 PERFORMANCE OF STEEL SPECIMENS IN SCPS

Linear polarization resistance (LPR) and Potentiodynamic polarization (PDP) techniques are considered as a reliable method to evaluate the mechanism of corrosion. The PDP curves can be utilized to determine the nature and extent of corrosion. The effect of chloride and/or sulfate and temperature on the mechanism of corrosion of mild steel, MMFX, stainless-clad steel bar and stainless steel placed in simulated concrete pore solution (SCPS) is described in the following sub-sections.

### 4.2.1 Effect of Chloride and Temperature on Corrosion Mechanism

The PDP curves for steel bars exposed to simulated concrete pore solution contaminated with 2,000 ppm chloride and maintained at temperatures of 25 $^0$C or 55 $^0$C are depicted in Figures 4.3 through 4.6. An anodic shift was noted due to an increase in the temperature of the pore solution. As is apparent an anodic shift leads to an increase in the corrosion current density.

The PDP curves for carbon steel bars, shown in Figure 4.3 indicates mostly general corrosion. Minor pitting was noted at about -50 mV in the steel bars exposed to 55 C. Pitting corrosion was noted in the MMFX bars, as is exhibited in Figure 4.4. The pitting potentials at 25 $^0$C is approximately +230 mV and at 55 $^0$C is approximately +100 mV. Similarly, pitting was noted in stainless-clad bars at +300 mV and +175 mV as shown in Figure 4.5, for exposure temperature of 25 $^0$C and 55 $^0$C, respectively. Higher pitting

potentials noted in the stainless clad bars compared to the MMFX steel bars is indicative of the fact that the former bars are more corrosion-resistant than the latter bars.

Figure 4.6 depicts the PDP curves for the stainless steel bars. Pitting was noted at a potential of 200 mV and 175 mV for temperatures of 25 and 55 C, respectively.

The PDP curves depicted in Figures 4.3 through 4.6 exhibit pitting tendency in the MMFX, stainless clad and stainless steel bars. However, minor pitting was noted in the carbon steel bars. However, it should be noted that the rate of corrosion, measured in terms of Icorr in the black bars was more than that of MMFX, stainless clad and stainless steel bars.

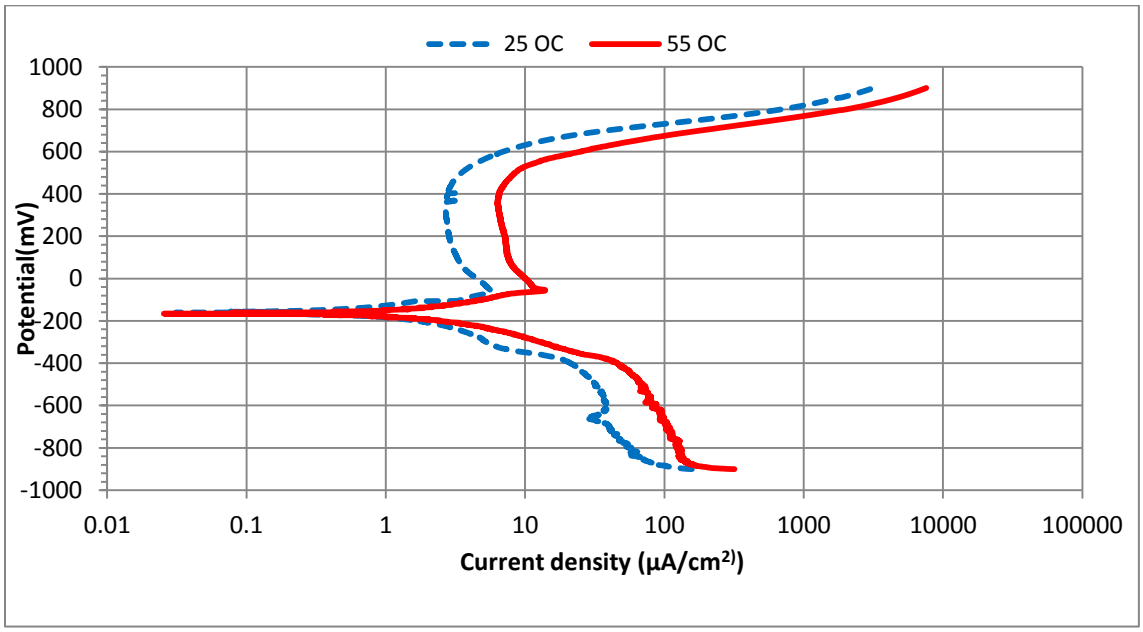


Figure 4.3:PDP curves of carbon steel bar immersed in SCPS contaminated with 2000 ppm chloride ions maintained at 25 $^{O}$C and 55 $^{O}$C.

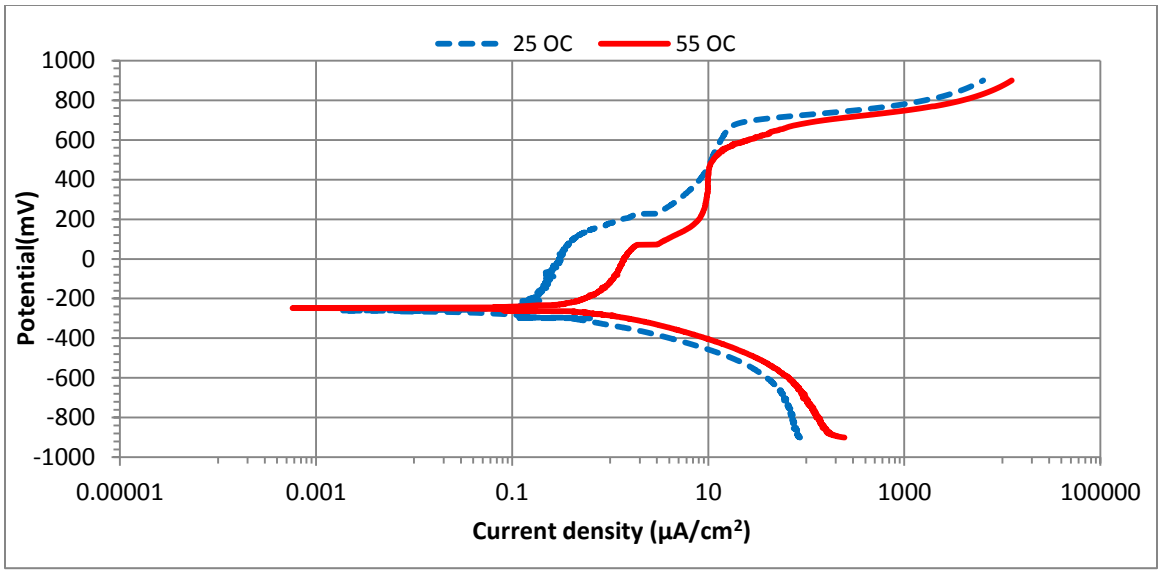


Figure 4.4:PDP curves for MMFX steel bars immersed in SCPS contaminated with 2000 ppm chloride and maintained at 25 $^{0}$C and 55 $^{0}$C.

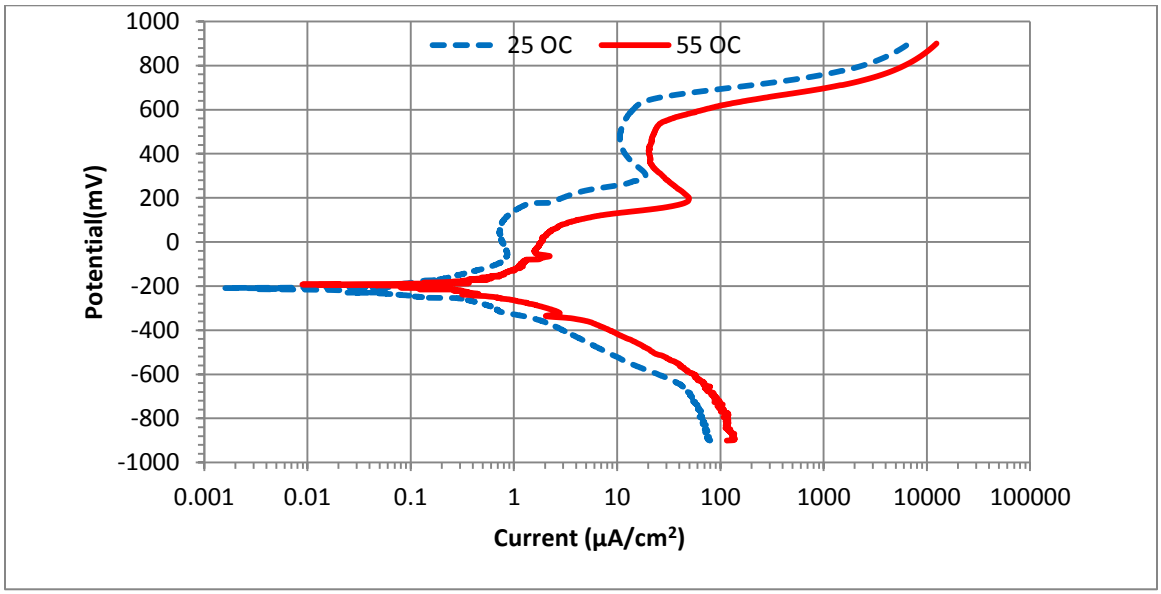


Figure 4.5:PDP curves for stainless-clad bars immersed in SCPS contaminated with 2000 ppm chloride maintained at 25 $^{O}$C and 55 $^{O}$C.

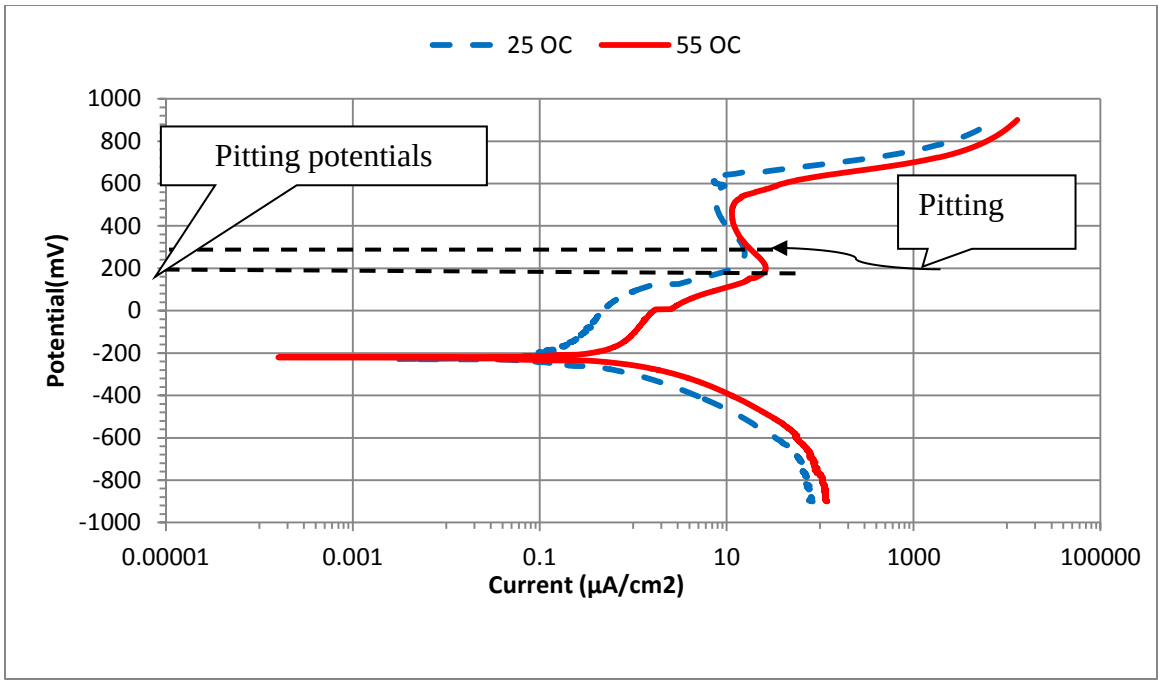


Figure 4.6:PDP curves for stainless steel bar immersed in SCPS contaminated with 2,000 ppm chloride and maintained at 25 $^{O}$C and 55 $^{O}$C.

### 4.2.2 Effect of Chloride and Temperature on the Corrosion Current Density of the Steel Bars

Figure 4.7 depicts the corrosion current density (Icorr) on the selected steel bars exposed to SCPS contaminated with 500 ppm chloride ions and temperature of 25 $^{0}$C and 55 $^{0}$C. The Icorr was observed to be maximum in the black steel bars. The Icorr was 0.3 and 1.5 µA/cm$^2$ for exposure temperature of 25 and 55 °C. The Icorr for stainless clad bars for the two temperatures used was 0.13 µA/cm$^2$ and 0.30 µA/cm$^2$. The Icorr for 25 and 55 C temperatures for the MMFX bars were 0.10 µA/cm$^2$ and 0.12 µA/cm$^2$, respectively, while for stainless steel bars these values were 0.0554 µA/cm$^2$ to 0.1013 µA/cm$^2$. These results

indicate that the Icorr in the corrosion-resisting steel bars was much less than that in the black steel bars. Further, a significant increase in the Icorr value due to an increase in the temperature was noted in the black steel bars while such an increase was not noticeable in the corrosion-resisting steels.

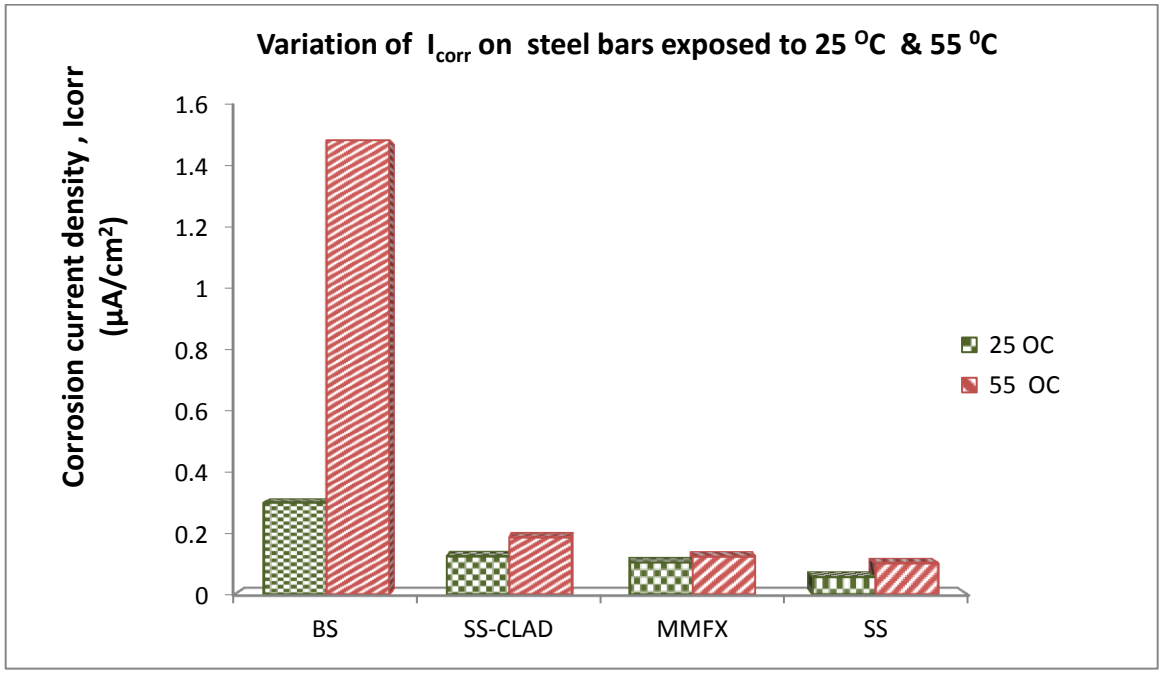


Figure 4.7:Corrosion current density on steel specimens exposed to SCPS contaminated with 500ppm chloride ions concentration.

Figure 4.8 depicts the Icorr values for steel specimens placed in SCPS contaminated with 1,000 ppm chloride and exposed to temperature of 25 $^{0}$C and 55 $^{0}$C. The Icorr values increased with the exposure temperature in this batch of specimens as well. The Icorr value for black bars exposed to 25 and 55 C was 0.629 µA/cm$^2$ and 1.93 µA/cm$^2$,

respectively. These values for the stainless clad bars were 0.1416 μA/cm$^2$ and 0.2030 μA/cm$^2$ while they were 0.1147 μA/cm$^2$ and 0.1404 μA/cm$^2$ for the MMFX bars. The Icorr values for stainless steel bars were 0.094 μA/cm$^2$ and 0.134 μA/cm$^2$.

Figure 4.9 depicts the Icorr on steel bars immersed in SCPS contaminated with 2,000 ppm chloride and exposed to temperature of 25 $^0$C and 55 $^0$C. The Icorr increased with the exposure temperature in this group of specimens also. Further, the Icorr in the specialty steel bars was less than that in the carbon steel bars. The $I_{corr}$ in the black bars exposed to 25 and 55 $^O$C was 0.9 μA/cm$^2$ and 2.06 μA/cm$^2$ respectively. These values for the stainless clad bars were 0.13 μA/cm$^2$ and 0.302 μA/cm$^2$. The $I_{corr}$ on MMFX bars increased from 0.14 μA/cm$^2$ to 0.23μA/cm$^2$ for an increase in temperature from 25 $^O$C to 55 $^O$C. Similarly, the $I_{corr}$ on stainless-steel bars increased from 0.101 μA/cm$^2$ to 0.150 μA/cm$^2$.

Figure 10 summarizes the combined effect of temperature and chloride concentration on the $I_{corr}$ on all the steel bars at varying chloride ion concentrations when exposed to 25 $^O$C and 55 $^O$C. The Icorr increased with the chloride concentration in all the steel bars. However, the increase in the Icorr was steeper in the carbon steel bars than the specialty steel bars, This can be explained by the fact that an increase in temperature usually accelerates the corrosive processes [45]. This leads to higher dissolution rates of the metal. There was almost negligible increase in the Icorr value in stainless steel and MMFX bars with the increase in temperature.

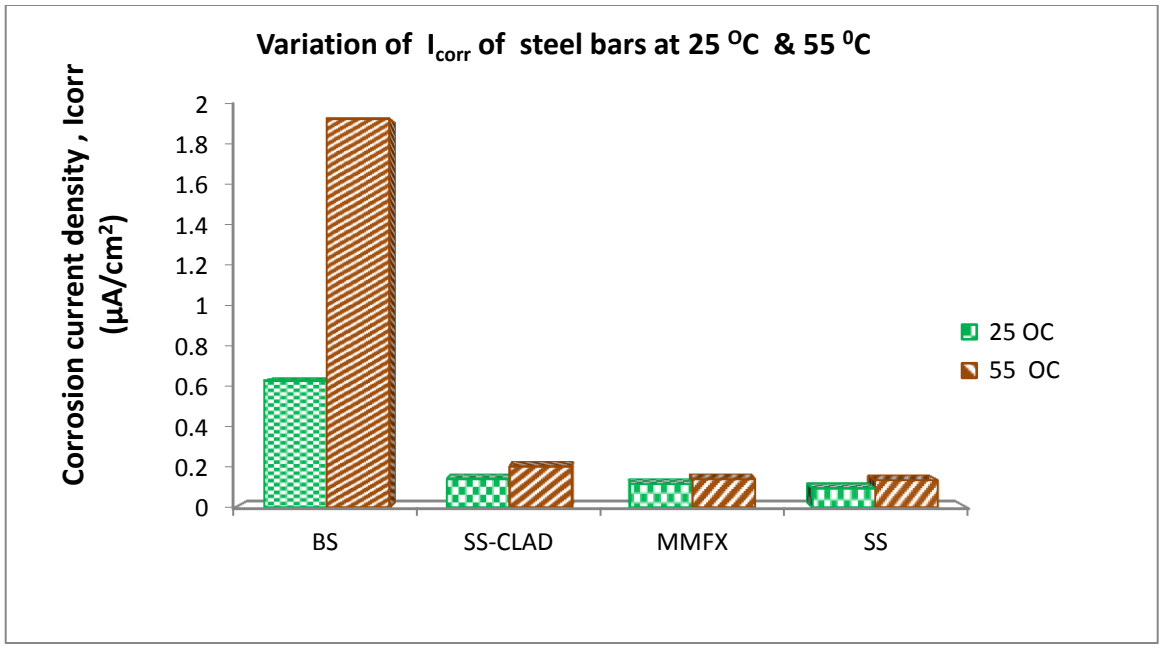


Figure 4.8: Corrosion current density on steel specimens exposed to SCPS contaminated with 100ppm chlorides ions concentration.

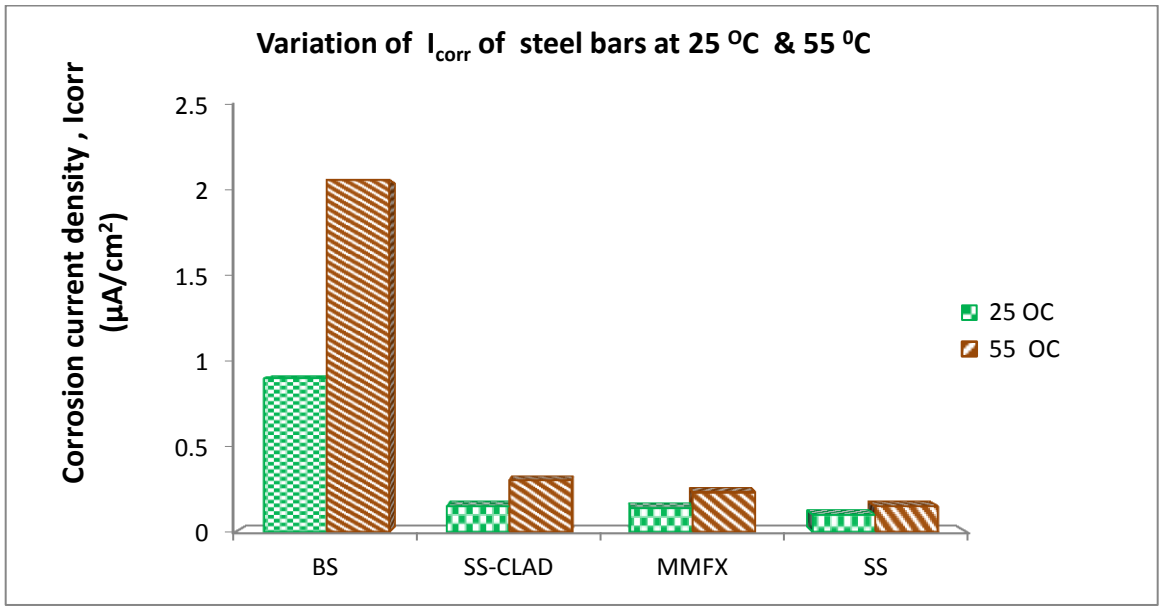


Figure 4.9:Corrosion current density on steel specimens exposed to SCPS contaminated 2000ppm chloride ions concentration.

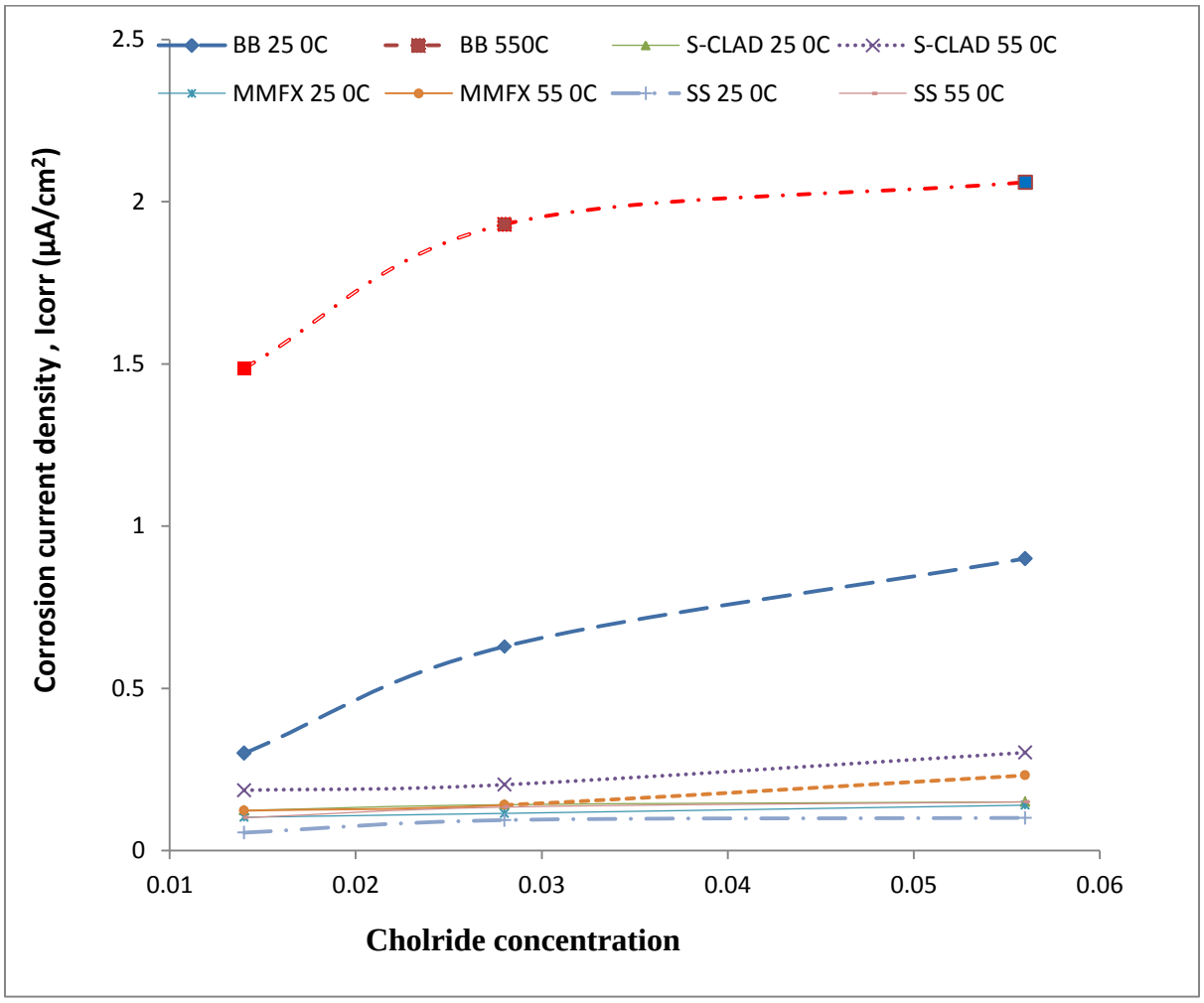


Figure 4.10: Effect of Chloride and Temperature on Corrosion Current Density.

### 4.2.3 Effect of Sulfate and/or Chloride and Temperature on Corrosion Mechanism

The PDP curves for steel bars exposed to simulated concrete pore solution contaminated with 2,000 ppm chloride and 500 ppm sulfates and maintained at temperatures of 25 $^0$C or 55 $^0$C are depicted in Figures 4.11 through 4.14. An anodic shift was noted due to an increase in the temperature and an inclusion of sulfate ions in the pore solution. As is apparent an anodic shift leads to an increase in the corrosion current density.

The PDP curves for carbon steel bars, shown in Figure 4.11 indicates mostly general corrosion. Pitting corrosion was noted in the MMFX bars, as is exhibited in Figure 4.12, the pitting potentials at 25 $^0$C was approximately +300mV and at 55 $^0$C was approximately +200mV. Similarly, pitting was noted in stainless-clad bars at +300 mV and +200 mV, for exposure temperature of 25 $^0$C and 55 $^0$C, respectively as depicted in Figure 4.13. Higher pitting depth was noted in stainless clad bars compared to the MMFX steel bars is indicative of the fact that the former bars are more corrosion-resistant than the latter bars this may be due to the dense microstructure of the MMFX bar.

Figure 4.14 depicts the PDP curves for the stainless steel bars. Pitting was noted at a potential of +200 mV and +220 mV for temperatures of 25 and 55 C, respectively.

The PDP curves depicted in Figures 4.16 through 4.19 exhibit pitting tendency in the MMFX, stainless clad and stainless steel bars. However, minor pitting was noted in the carbon steel bars. However, it should be noted that the rate of corrosion, measured in terms of Icorr in the black bars was more than that of MMFX, stainless clad and stainless steel bars.

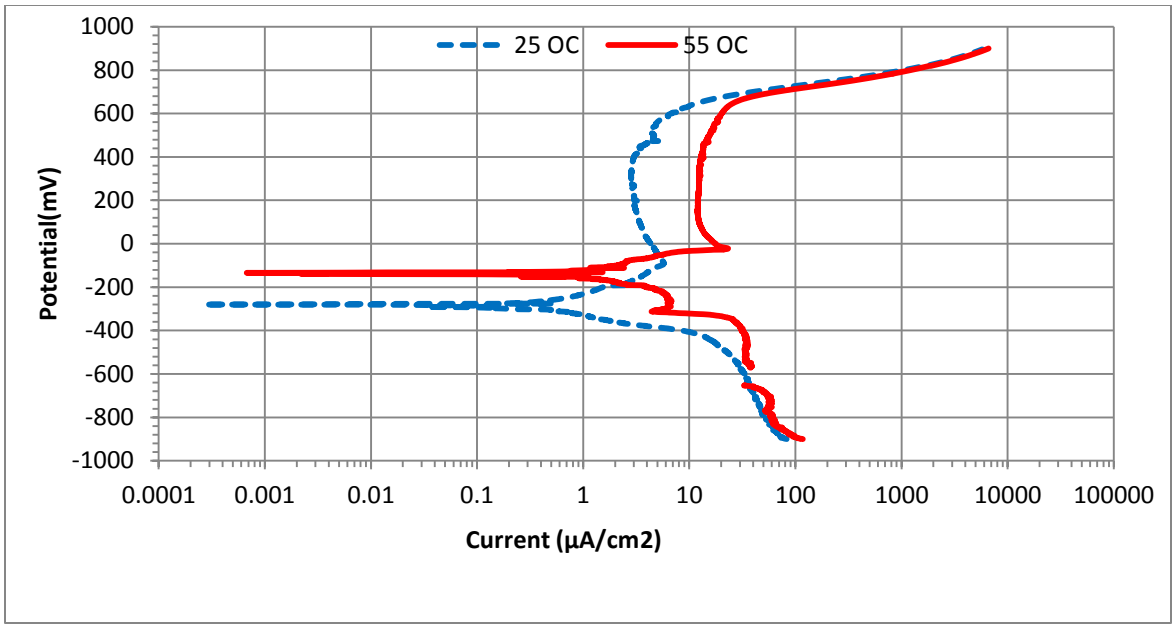


Figure 4.11 : Potentiodynamic curves of black steel bar immersed in pore solutions with 2000ppm Chloride ions and 500ppm sulfate ions at 25 $^{0}$C and 55 $^{0}$C

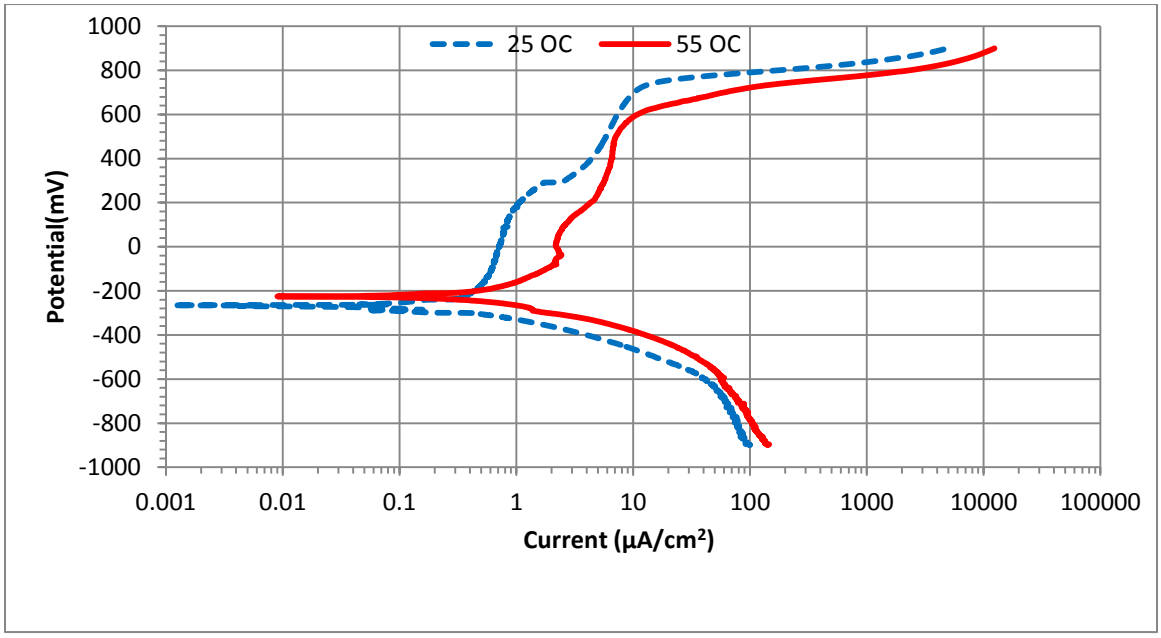


Figure 4.12: Potentiodynamic Tefel curves of MMFX steel bar immersed in pore solutions with 2000ppm Chloride ions and 500ppm Sulfate ions at 25 $^{0}$C and 55 $^{0}$C.

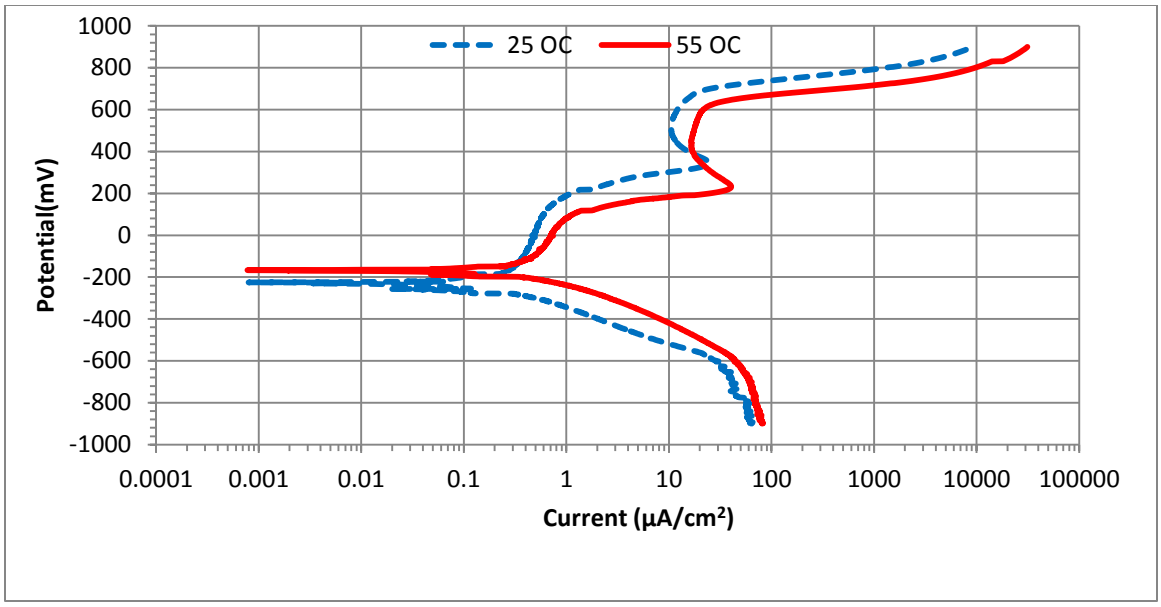


Figure 4.13: **:** Potentiodynamic Tefel curves of stainless-Clad steel bar immersed in pore solutions with 2000ppm Chloride ions and 500ppm Sulfate ions at 25 $^{0}$C and 55 $^{0}$C.

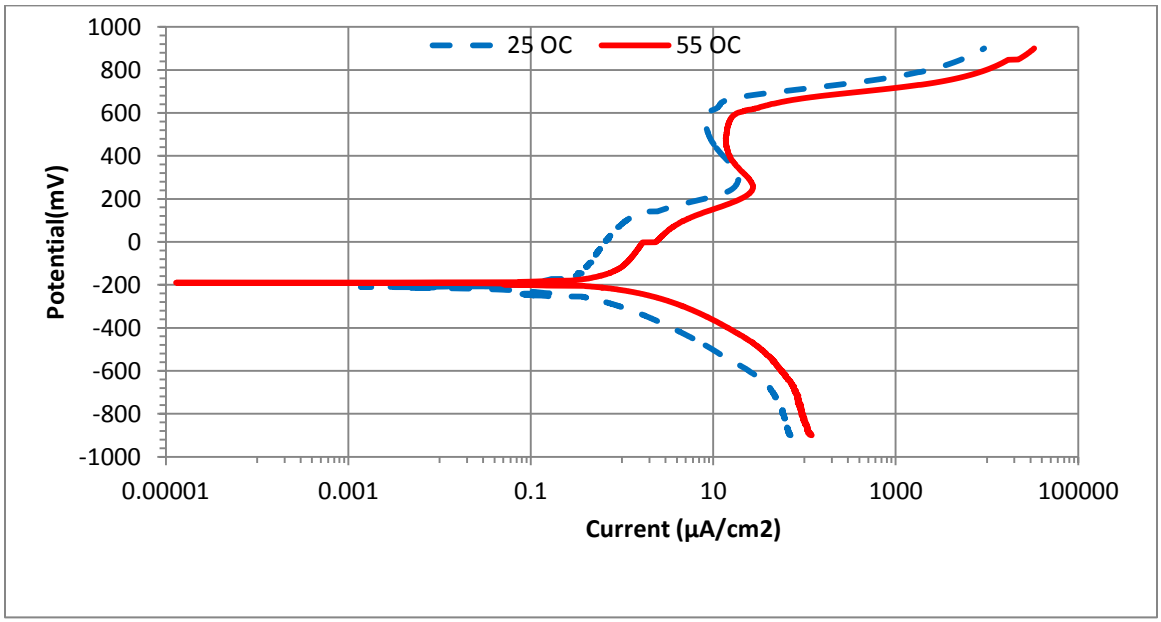


Figure 4.14: Potentiodynamic Tefel curves of stainless steel bar immersed in pore solutions with 2000ppm Chloride ions and 500ppm Sulfate ions at 25 $^{0}$C and 55 $^{0}$C

### 4.2.4 Effect of Sulfate and/or Chloride and Temperature on Corrosion Current Density of Steel Bars

Figure 4.15 depicts the corrosion current density (Icorr) on the selected steel bars exposed to SCPS contaminated with 500 ppm chloride ions only, 500 ppm chloride and 500 sulfate ions admixed together at temperature of 25 $^0$C and 55 $^0$C. For the black steel bars, The Icorr was 0.3 and 1.5 μA/cm$^2$ for exposure temperature of 25 °C and 55 °C for the 500 ppm chloride ions only but the Icorr increased to 0.4633 μA/cm$^2$ and 1.6974 μA/cm$^2$ for the combined chloride and sulfate concentration, This increment has been justified by Saleem et al. [40] that reported the result of the study carried out at King Fahd University of Petroleum and Mineral, it was concluded that reinforcement corrosion may be accelerated due to the concomitant presence of chloride and sulphate ions, compared to specimens contaminated with only chloride ions. The authors attributed this increase to the two reasons stated below:

Firstly, the concomitant presence of chloride and sulphate ions increases the concentration of free chloride ions in the pore solution compared to the specimens contaminated with only sodium chloride. This increase in the chloride concentration is attributed to the simultaneous reaction of $C_3A$ with both chloride and sulphate ions. This increased chloride concentration is not only detrimental from the depassivation perspective but will also reduce the resistivity of concrete.

Secondly, the electrical resistivity of concrete contaminated with sodium chloride plus sodium sulphate may be lower than that in the specimens contaminated with only sodium chloride'.

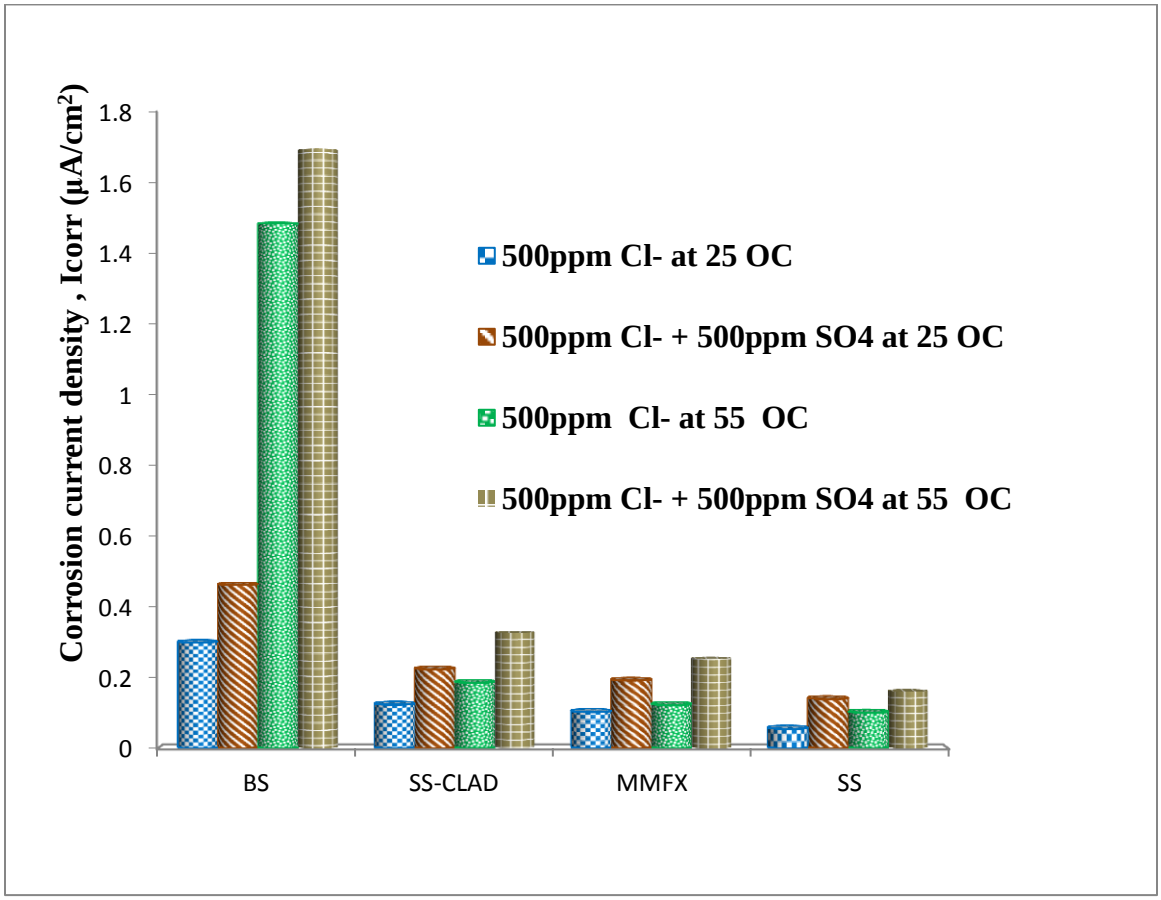


Figure 4.15: Corrosion current density on steel specimens exposed to SCPS contaminated with 500 ppm chloride ions and 500 ppm sulfate ions concentration

Dehwah et al. [41] also observed an increased in the $OH^-$ concentration in cement pastes admixed with sodium chloride plus sodium sulfate when compare to the one admixed with only sodium chloride. He attributed this increased in $OH^-$ concentration in to the cation type associated with the sulfate and chloride ions. When sodium chloride and sodium

sulfate are added to cement, $Cl^-$ and $SO_4^{2-}$ react with the cement hydration products, namely $Ca(OH)_2$ and $C_3A$, forming calcium-chloroaluminate, ettringite and monosulfate while $Na^+$ and $OH^-$ ions are released in the pore solution, thereby increasing its alkalinity.

According to Yonezawa et al. [42], when both NaCl and $Na_2SO_4$ are both admixed in concrete, The NaCl will first reacts with $Ca(OH)_2$, to form $CaCl_2$ releasing $Na^+$ and $OH^-$ in the pore solution. The $CaCl_2$ then reacts with tricalcium aluminate ($C_3A$) to form calcium-chloroaluminate hydrate (Friedel's salt) as indicated in the following equations:

$$2NaCl + Ca(OH)_2 \rightarrow CaCl_2 + 2Na^+ + 2OH^- \quad \text{.....4.1}$$

$$3CaO.Al_2O_3.10H_2O + CaCl_2 \rightarrow 3CaO.Al_2O_3.10H_2O \,.\, CaCl_2 \quad \text{.....4.2}$$

$$(Mg, Na_2)SO_4 + Ca(OH)_2 \rightarrow CaSO_4.2H_2O + (Mg, Na_2)(OH)_2 \quad \text{.....4.3}$$

$$3(CaSO_4.2H_2O) + C_3AH_{12} \rightarrow C_3A.3CaSO_4.H_{32} \quad \text{.....4.4}$$

The Icorr for stainless clad bars for the two temperatures used was 0.124 μA/cm$^2$ and 0.186 μA/cm$^2$ for the 500 ppm chloride ions only but the Icorr increased to 0.224 μA/cm$^2$ and 0.3272 μA/cm$^2$ for the combined chloride and sulfate concentration. The Icorr for 25 $^o$C and 55 $^o$C temperatures for the MMFX bars were 0.10 μA/cm$^2$ and 0.12 μA/cm$^2$, respectively for the 500 ppm chloride ions only but the Icorr increased to 0.1924 μA/cm$^2$ and 0.2533 μA/cm$^2$ for the combined chloride and sulfate concentration, while for stainless steel bars these values were 0.0554 μA/cm$^2$ to 0.1013 μA/cm$^2$ for the 500 ppm chloride ions only but the Icorr increased to 0.1399 μA/cm$^2$ and 0.1607 μA/cm$^2$ for the combined chloride and sulfate concentration. These results indicate that the Icorr in the corrosion-

resisting steel bars was much less than that in the black steel bars. Further, a significant increase in the Icorr value due to an increase in the temperature was noted in the black steel bars while such an increase was not noticeable in the corrosion-resisting steels.

Figure 4.16 depicts the Icorr values for steel specimens immersed in the SCPS contaminated with 1000 ppm chloride ions only, 1000 ppm chloride and 500 sulfate ions admixed together at of temperature of 25 $^0$C and 55 $^0$C. The Icorr values increased with the exposure temperature in this batch of specimens as well. The Icorr was 0.629 μA/cm$^2$ and 1.93 μA/cm$^2$ for exposure temperature of 25 °C and 55 °C for the 1000 ppm chloride ions only but the Icorr increased to 0.658 μA/cm$^2$ and 2.92 μA/cm$^2$ for the combined chloride and sulfate concentration. These values for the stainless clad bars were 0.142 μA/cm$^2$ and 0.203 μA/cm$^2$ for the 1000 ppm chloride ions only but the Icorr increased to 0.229 μA/cm$^2$ and 0.347 μA/cm$^2$ for the combined chloride and sulfate concentration while they were 0.115 μA/cm$^2$ and 0.140 μA/cm$^2$ for the MMFX bars for the 1000 ppm chloride ions only but the Icorr increased to 0.224 μA/cm$^2$ and 0.3157 μA/cm$^2$ for the combined chloride and sulfate concentration for exposure temperature of 25 °C and 55 °C respectively. The Icorr values for stainless steel bars were 0.094 μA/cm$^2$ and 0.134 μA/cm$^2$ for the 1000 ppm chloride ions only but the Icorr increased to 0.160 μA/cm$^2$ and 0.245 μA/cm$^2$ for the combined chloride and sulfate concentration.

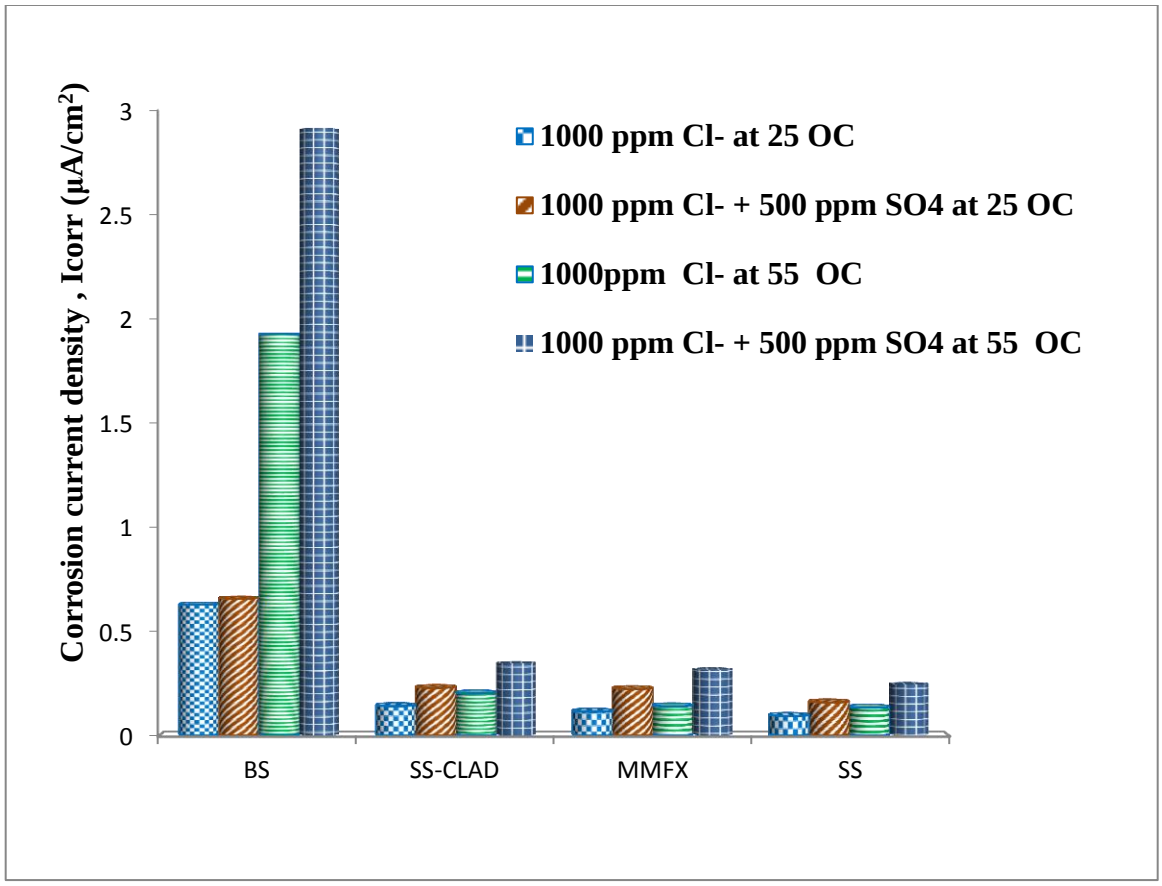


Figure 4.16 :Corrosion current density on steel specimens exposed to SCPS contaminated with 1000 ppm chloride ions and 500 ppm sulfate ions concentration

Figure 4.17 depicts the Icorr values for steel specimens immersed in SCPS contaminated with 2000 ppm chloride ions only, 2000 ppm chloride and 500 sulfate ions admixed together at of temperature of 25 $^0$C and 55 $^0$C. The Icorr values increased with the exposure temperature in this batch of specimens as well. For the black bar, the Icorr was 0.9 µA/cm$^2$ and 2.06 µA/cm$^2$ for exposure temperature of 25 °C and 55 °C for the 2000 ppm chloride ions only but the Icorr increased to 1.2 µA/cm$^2$ and 2.996 µA/cm$^2$ for the combined chloride and sulfate concentration. These values for the stainless clad bars were

0.150 μA/cm$^2$ and 0.302μA/cm$^2$ for the 2000 ppm chloride ions only but the Icorr increased to 0.365 μA/cm$^2$ and 0.401 μA/cm$^2$ for the combined chloride and sulfate concentration while they were 0.115 μA/cm$^2$ and 0.140 μA/cm$^2$ for the MMFX bars for the 2000 ppm chloride ions only but the Icorr increased to 0.14 μA/cm$^2$ and 0.232 μA/cm$^2$ for the combined chloride and sulfate concentration for exposure temperature of 25 °C and 55 °C respectively. The Icorr values for stainless steel bars were 0.101 μA/cm$^2$ and 0.15μA/cm$^2$ for the 2000 ppm chloride ions only but the Icorr increased to 0.18 μA/cm$^2$ and 0.244 μA/cm$^2$ for the combined chloride and sulfate concentration.

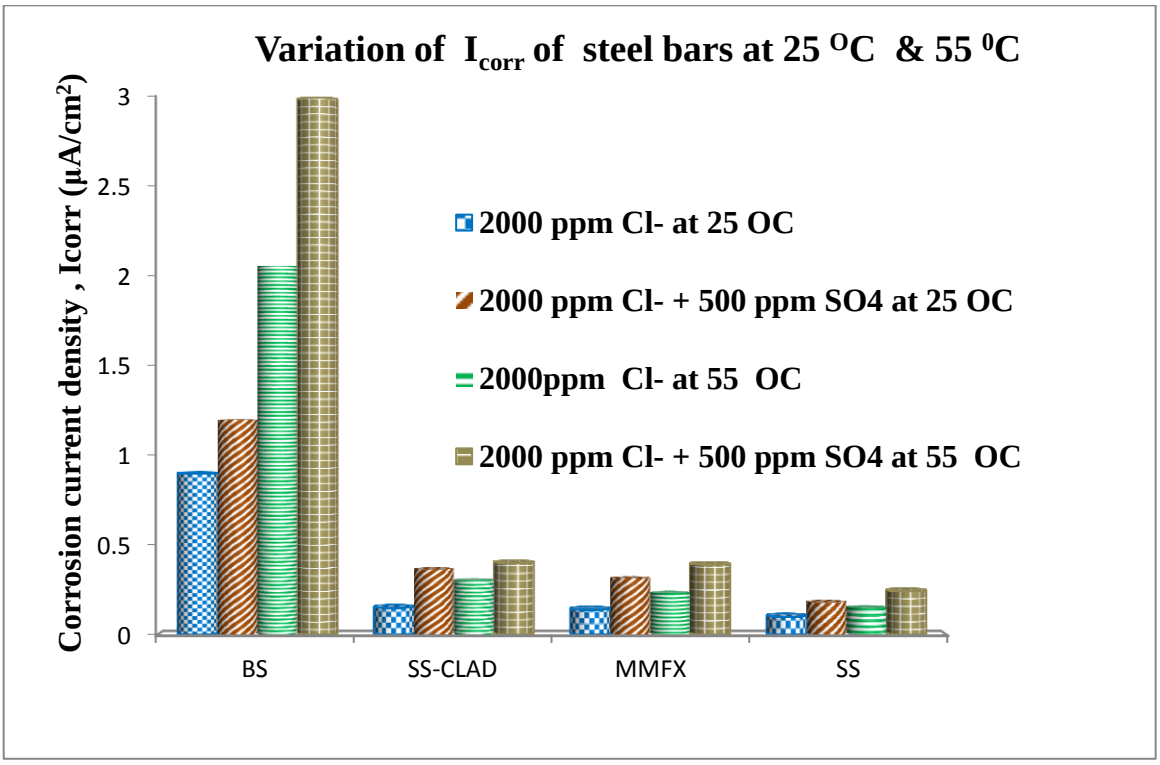


Figure 4.17: Corrosion current density on steel specimens exposed to SCPS contaminated with 2000 ppm Cl- and 500 ppm sulfate ions concentration

Figure 4.18 depicts the Icorr values for steel specimens immersed in SCPS contaminated with 2000 ppm chloride ions only, 2000 ppm chloride and 2000 ppm sulfate ions admixed together at of temperature of 25 $^{0}$C and 55 $^{0}$C. The Icorr values increased with the exposure temperature in this batch of specimens as well. For the black bar, the Icorr was 0.9 μA/cm$^2$ and 2.06 μA/cm$^2$ for exposure temperature of 25 °C and 55 °C for the 2000 ppm chloride ions only but the Icorr increased to 1.27 μA/cm$^2$ and 3.423 μA/cm$^2$ for the combined chloride and sulfate concentration. These values for the stainless clad bars were 0.150 μA/cm$^2$ and 0.302 μA/cm$^2$ for the 2000 ppm chloride ions only but the Icorr increased to 0.469 μA/cm$^2$ and 0.656 μA/cm$^2$ for the combined chloride and sulfate concentration while they were 0.115 μA/cm$^2$ and 0.140 μA/cm$^2$ for the MMFX bars for the 2000 ppm chloride ions only but the Icorr increased to 0.484 μA/cm$^2$ and 0.520 μA/cm$^2$ for the combined chloride and sulfate concentration for exposure temperature of 25 °C and 55 °C respectively. The Icorr values for stainless steel bars were 0.101 μA/cm$^2$ and 0.150 μA/cm$^2$ for the 2000 ppm chloride ions only but the Icorr increased to 0.224 μA/cm$^2$ and 0.307 μA/cm$^2$ for the combined chloride and sulfate concentration.

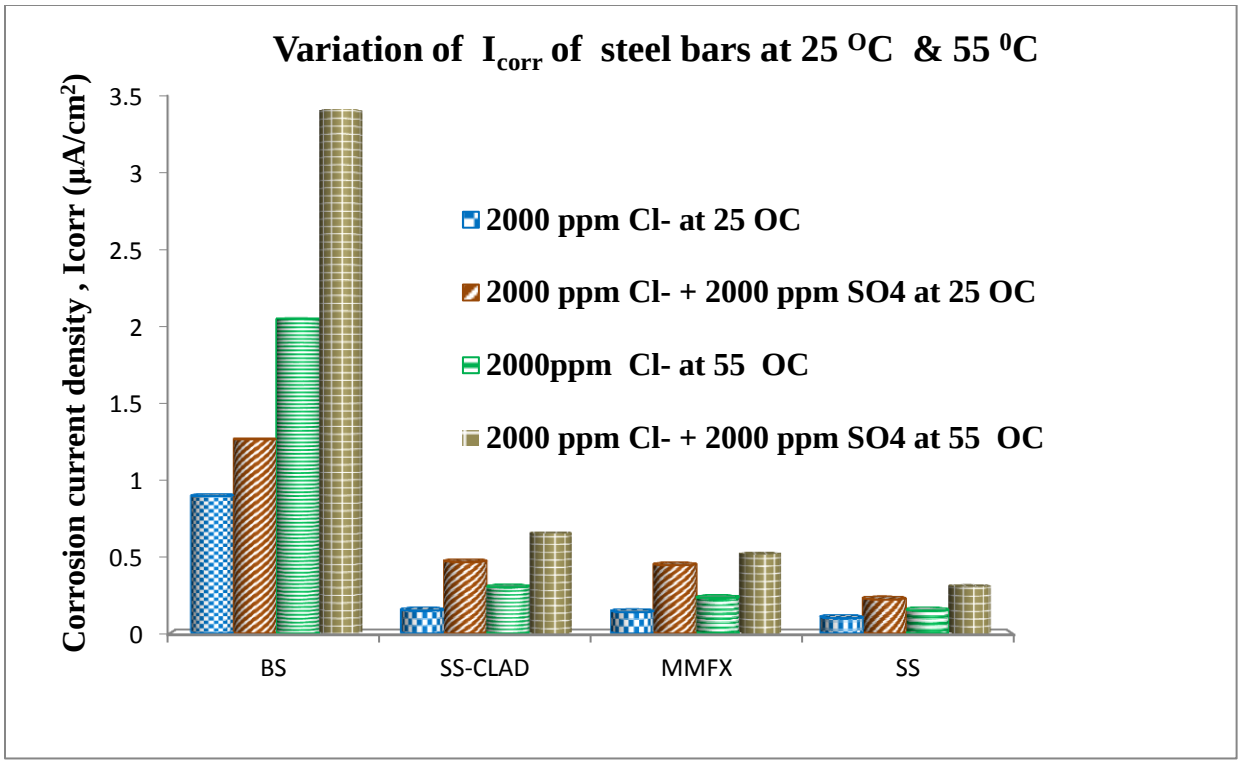


Figure 4.18 : Corrosion current density on steel specimens exposed to SCPS contaminated with 2000ppm Cl- and 2000 ppm sulfate ions concentration

Figure 4.15 summarizes the combined effect of temperature and chloride and sulfate concentrations on the $I_{corr}$ of all the steel bars at varying chloride ion concentrations when exposed to 25 and 55 $^{0}$C. The Icorr increased with the increased in the sulfate ions concentration in all the steel bars. However, the increase in the Icorr was steeper in the carbon steel bars than the specialty steel bars, This can be explained by the fact that an increase in temperature usually accelerates the corrosive processes [43]. This leads to higher dissolution rates of the metal. There was almost negligible increase in the Icorr value in stainless steel and MMFX bars with the increase in temperature.

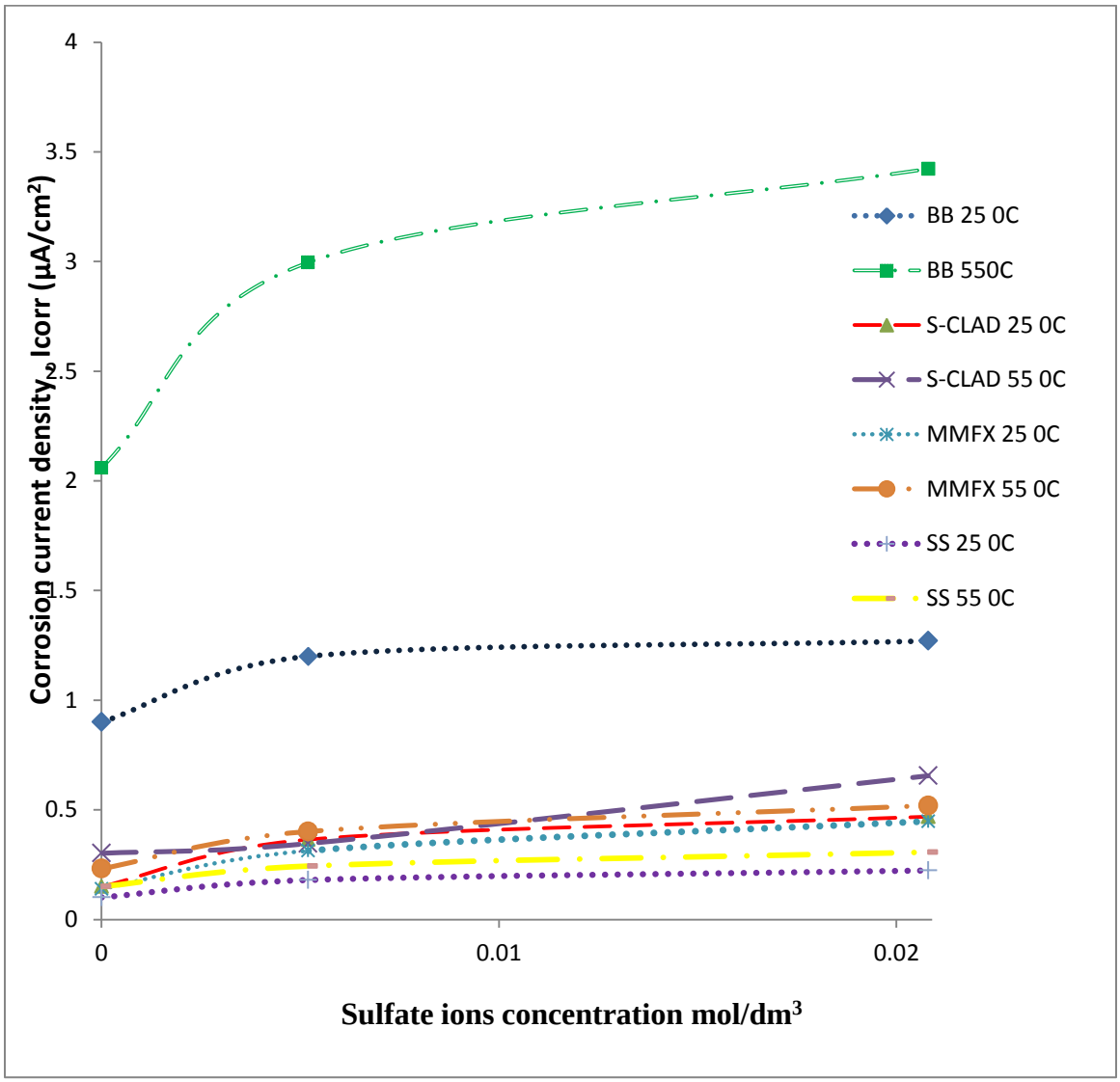


Figure 4.19: Effect of Sulfate and Temperature variation on Corrosion Current Density with 2000 ppm Chloride ions

### 4.2.5 Scanning Electron Microscopy (SEM) and Energy-Dispersive X-ray Spectroscopy (EDX) Results of Steel Specimens Immersed in SCPS

The scanning electron micrographs and the energy dispersive X-ray results of the fine gold coated surface of the steel specimens after polarization test when exposed to SCPS contaminated with sulfate and/or chloride ions are shown in Figures 4.20 through 4.21.

Figure 4.20a depicts the SEM, while Figure 4.20b and Figure 4.20c depict the EDX results for the mild steel exposed to SCPS contaminated with 1000ppm Chloride ions at 25 ºC, there was general corrosion on the surface of the bar in form of iron-oxide. The steel surface was rough and covered with corrosion products. However, a more corroded surface area was noted on the specimens immersed in SCPS contaminated with 1,000 ppm chloride and exposed to 55 ºC (Figure 4.21). Furthermore, a more general corrosion with little pitting was noted on the black bar specimens immersed in SCPS contaminated with 1,000 ppm chloride and 500ppm sulfate ions exposed to 55 ºC due to the formation of iron-oxide as reviewed in EDX result (Figure 4.22).

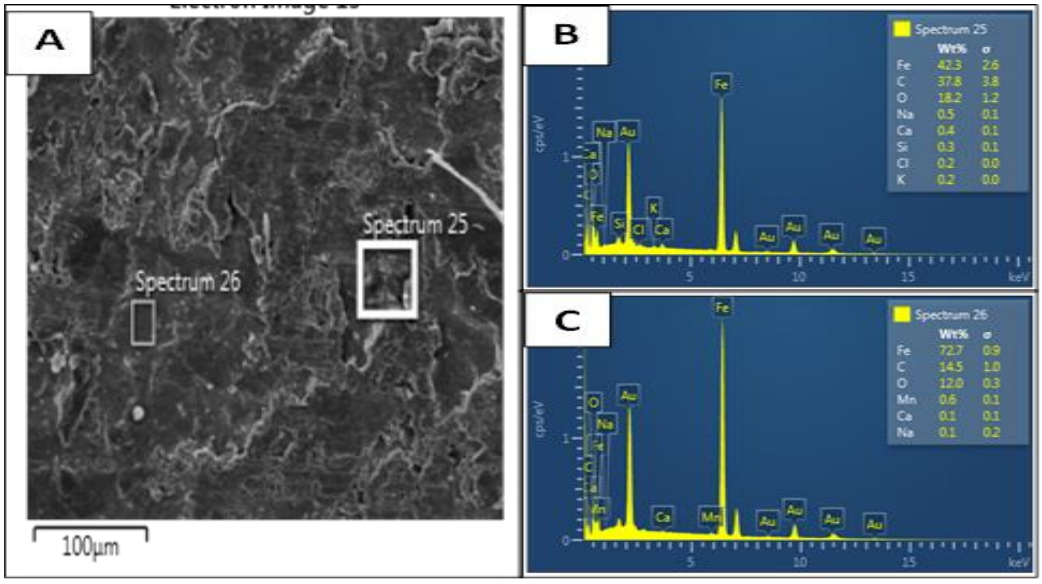


Figure 4.20: SEM (300X) and EDX results for black bar after polarization in SCPS Contaminated with 1000 ppm Cl ions at 25 ºC

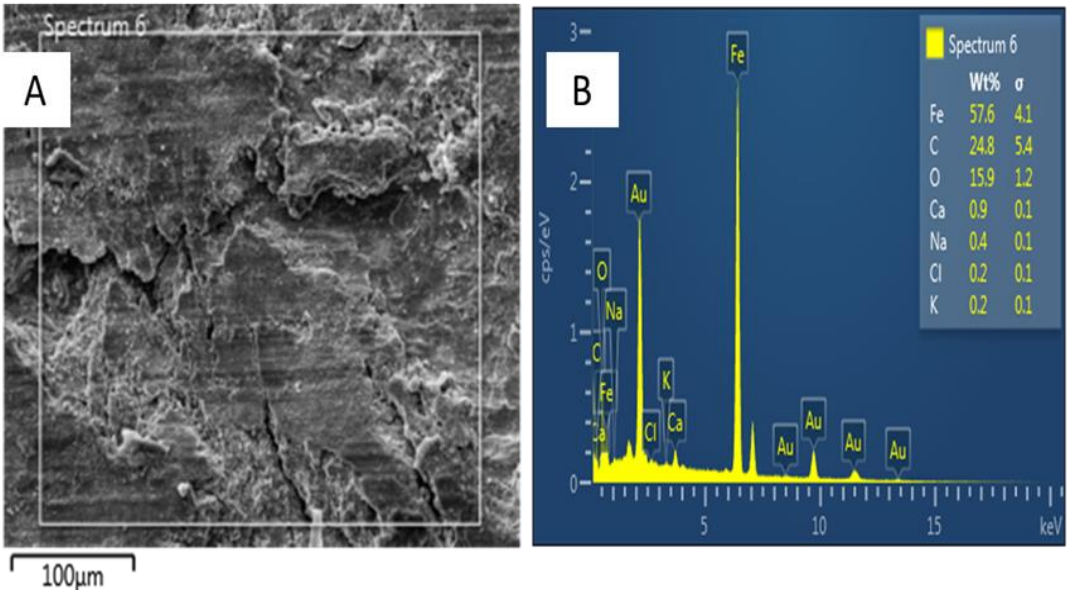


Figure 4.21: SEM (300X) and EDX results for black bar after polarization in SCP Contaminated with 1000 ppm Cl ions at 55 ºC.

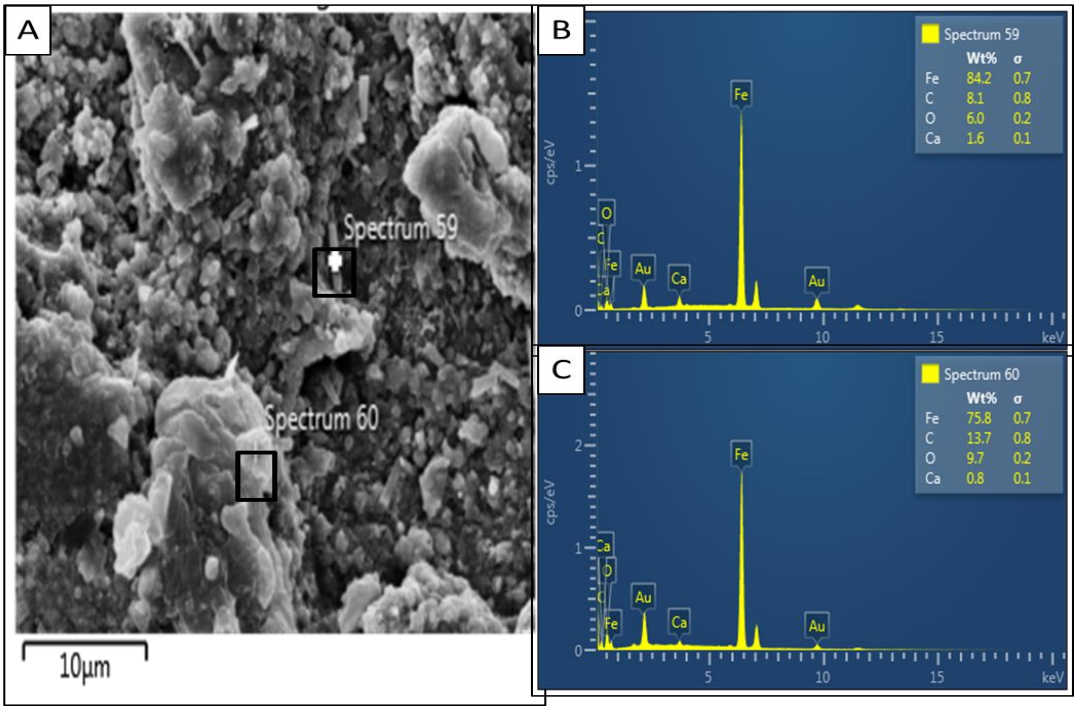


Figure 4.22: SEM (300X) and EDX results for black bar after polarization in SCPS Contaminated with 1000 ppm Cl ions plus 500ppm sulfate ions at 55 ºC.

Figure 4.23a depicts the SEM image, while Figure 4.23b and Figure 4.23c depict the EDX results for MMFX steel before polarization, the SEM shows a well dense microstructure without any trace of corrosion while the EDX shows the chromium content of the two distinct spectrums examined.

Figure 4.24a depicts the SEM, while Figure 4.24b and Figure 4.24c depict the EDX for MMFX steel exposed to SCPS contaminated with 1000 ppm Chloride ions at 25 ºC, Two distinct spectrums were observed, spectrum 33 and spectrum 34, spectrum 33 shows the area without any formation of corrosion product nor protective layer, while spectrum 34 reviews the formation of protective chromium-oxide on the surface of the bar which is responsible for the low corrosion density as reported in the previous section.

Figure 4.25a depicts the SEM, while Figure 4.25b, Figure 4.25c and 4.25d depict the EDX results for MMFX steel exposed to SCPS contaminated with 1000 ppm Chloride ions at 55 ºC, three distinct spectrums were observed, spectrum 49, spectrum 50 and spectrum 51. Spectrum 49 shows high content of chromium-oxide which dominate large portion of the surface area while spectrum 50 shows very little percentage composition of chromium and high content of carbon, this may signifies a very little uniform corrosion around this area. While spectrum 51 reviews the non- corroded area of the bar.

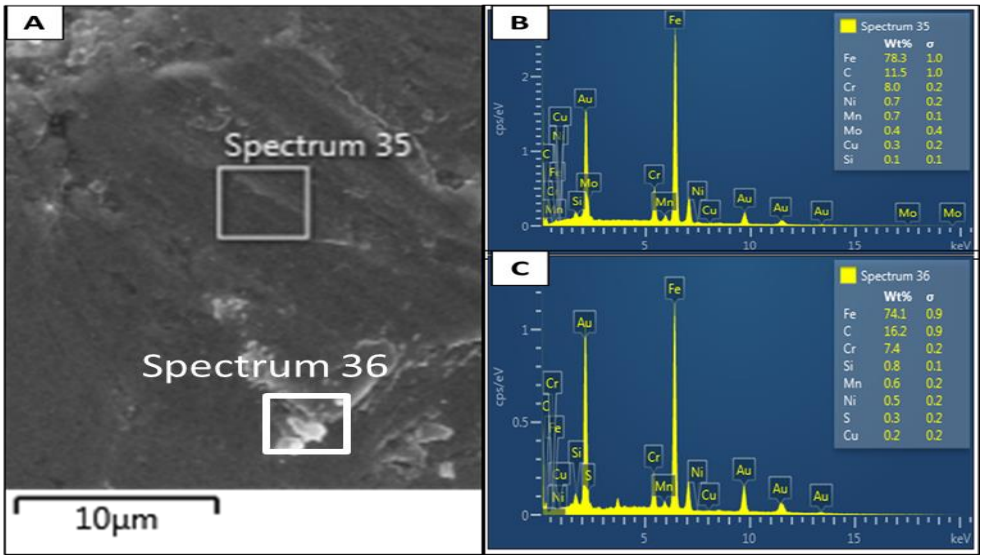


Figure 4.23: SEM (300X) and EDX results for bare MMFX steel bar

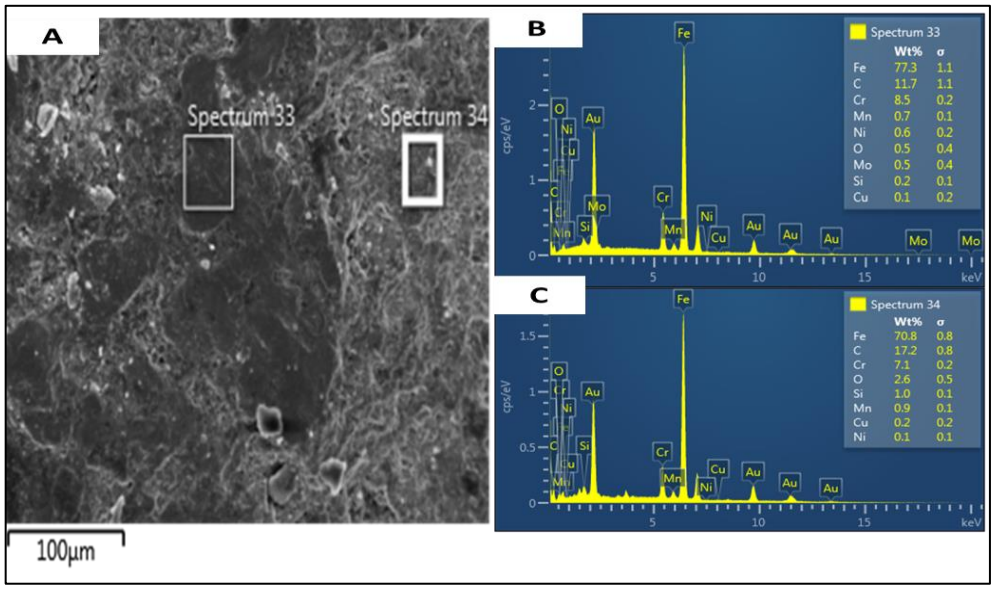


Figure 4.24: SEM (300X) and EDX results MMFX black bar after polarization in SCPS Contaminated with 1000 ppm $Cl^-$ at 25 ºC.

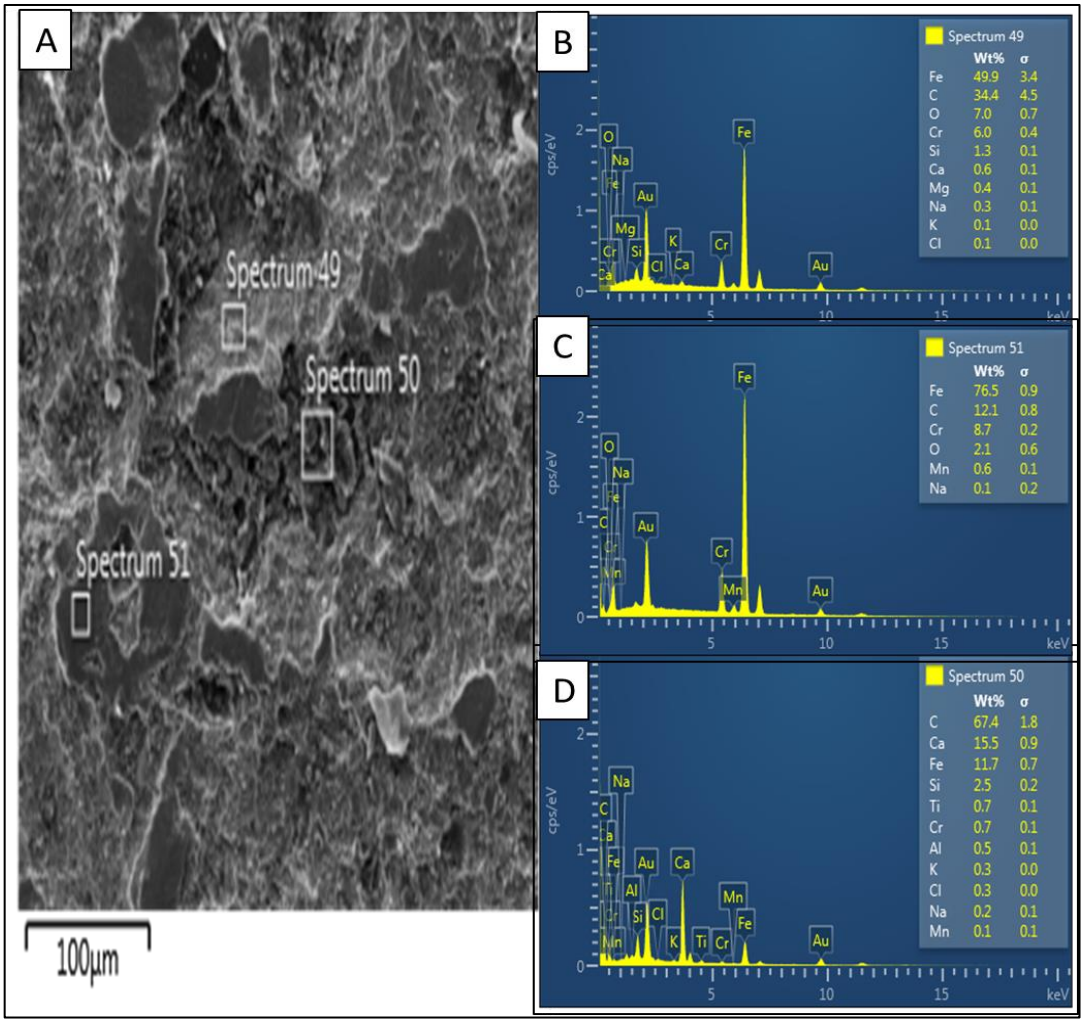


Figure 4.25: SEM (300X) and EDX results MMFX black bar after polarization in SCPS Contaminated with 1000 ppm $Cl^-$ at 55 ºC.

However, a more rough uniform corroded surface with formation of protective chromium-oxide on the surface area was noted on the specimens immersed in SCPS contaminated with 1,000 ppm chloride and 500 ppm sulfate ions exposed to 25 ºC as reviewed in EDX result (Figure 4.26). Furthermore, little pitting was noted on the MMFX bar specimens immersed in SCPS contaminated with 1,000 ppm chloride and 500 ppm exposed to 55 ºC as reviewed in EDX result (Figure 4.27)

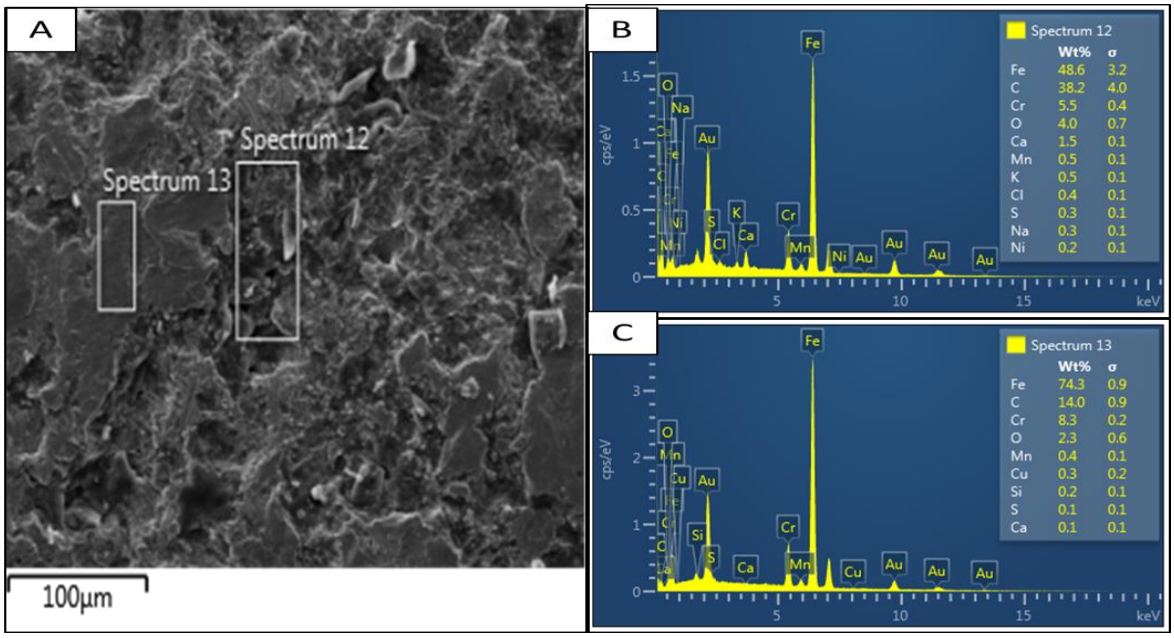


Figure 4.26: : SEM (300X) and EDX results for MMFX bar after polarization in SCPS Contaminated with 1000 ppm Cl ions plus 500 ppm sulfate ions at 25 ºC.

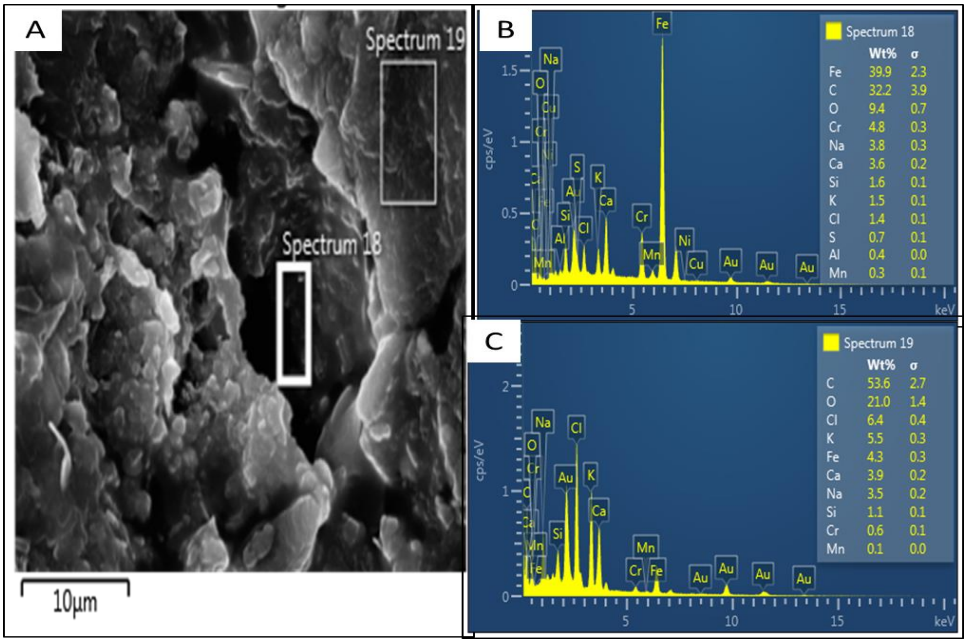


Figure 4.27:SEM (300X) and EDX results for MMFX bar after polarization in SCPS Contaminated with 1000 ppm Cl ions plus 500 ppm sulfate ions at 55 ºC.

Figure 4.28a depicts the SEM, while Figure 4.28b depicts the EDX results for stainless clad steel exposed to SCPS contaminated with 1000 ppm chloride ions at 25 ºC. Spectrum 1 shows the area covered with protective film of chromium-oxide which is responsible for the low corrosion density as reported in the previous section.

Figure 4.29a depicts the SEM image, while Figure 4.29b and 4.24c depict the EDX results for stainless clad steel exposed to SCPS contaminated with 1000 ppm Chloride ions at 55 ºC, two distinct spectrums were observed, spectrum 67 and spectrum 68. Spectrum 68 shows high content of chromium-oxide which dominate large portion of the surface area while spectrum 67 shows smaller percentage composition of chromium and high content of carbon, this may signifies a small localized pitting corrosion around this area.

However, a deep pitting corrosion was noted on the specimens immersed in SCPS contaminated with 1,000 ppm chloride and 500 ppm sulfate ions exposed to 25 ºC as shown in EDX result (Figure 4.30). Furthermore, a deeper pitting was seen on the stainless clad specimens immersed in SCPS contaminated with 1,000 ppm chloride and 500 ppm exposed to 55 ºC as reviewed in EDX result (Figure 4.31)

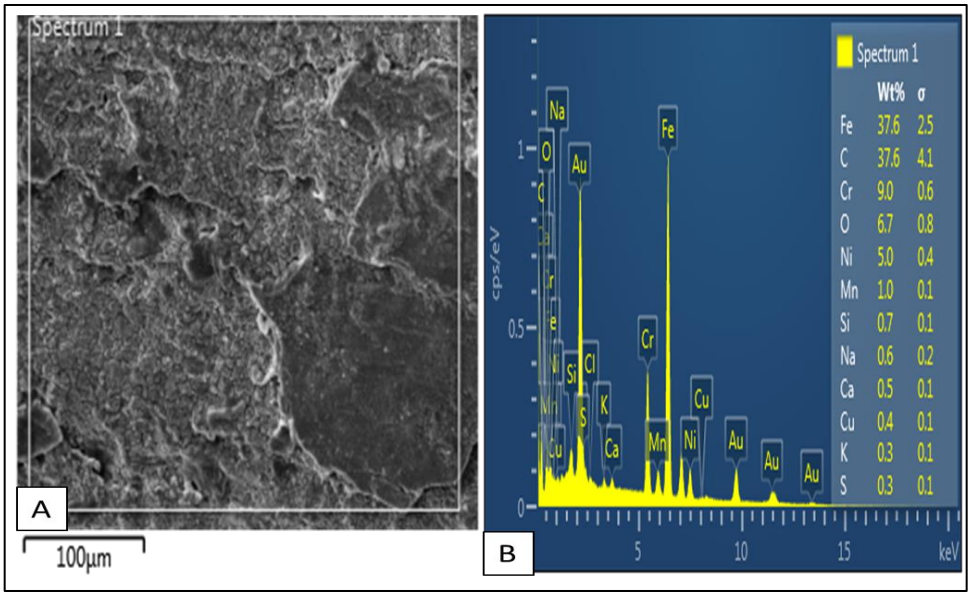


Figure 4.28:SEM (300X) and EDX results stainless-clad bar after polarization in SCPS Contaminated with 1000 ppm $Cl^-$ at 25 ºC.

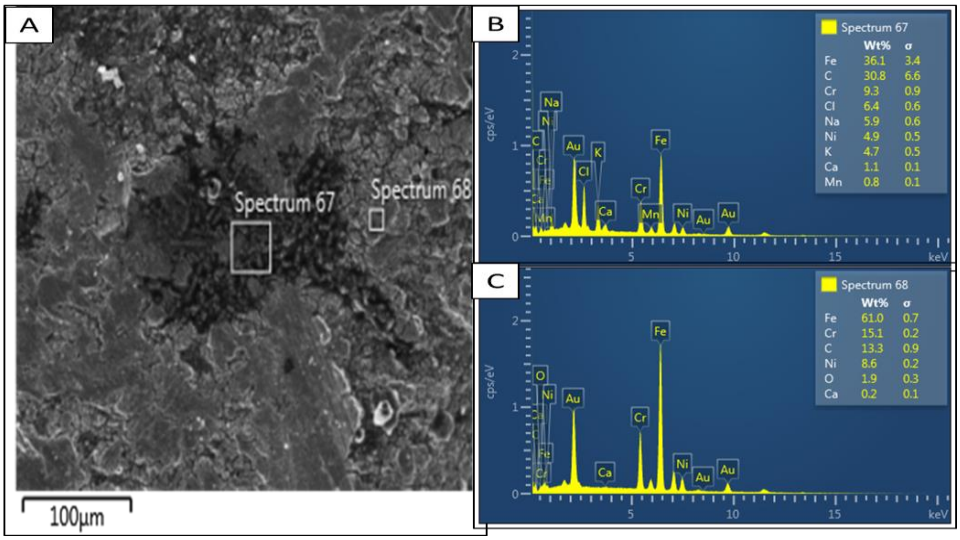


Figure 4.29:SEM (300X) and EDX results for stainless-clad bar after polarization in SCPS Contaminated with 1000 ppm Cl at 55 ºC.

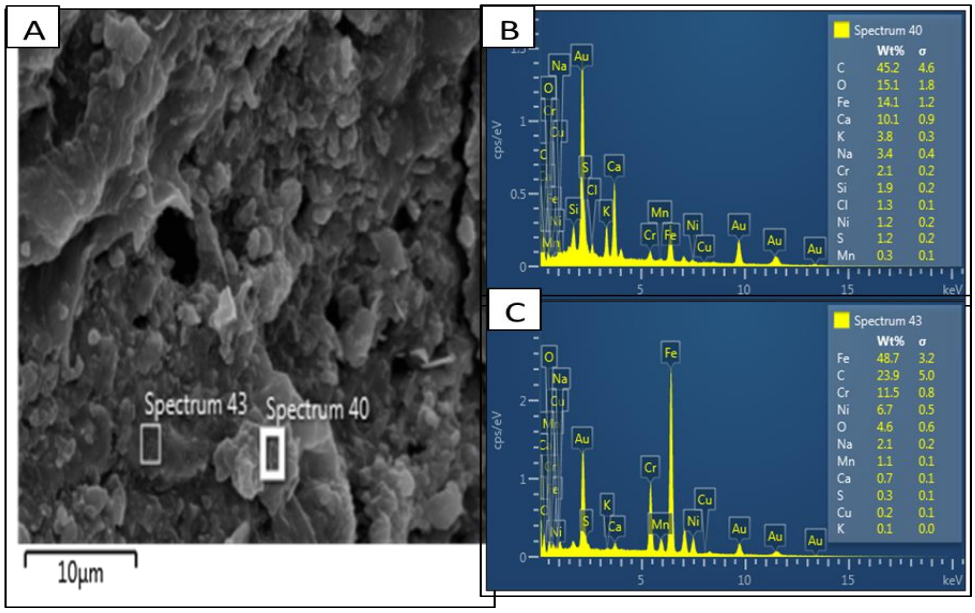


Figure 4.30:SEM (300X) and EDX results for stainless-clad bar bar after polarization in SCPS Contaminated with 1000 ppm Cl ions plus 500 ppm sulfate ions at 25 ºC.

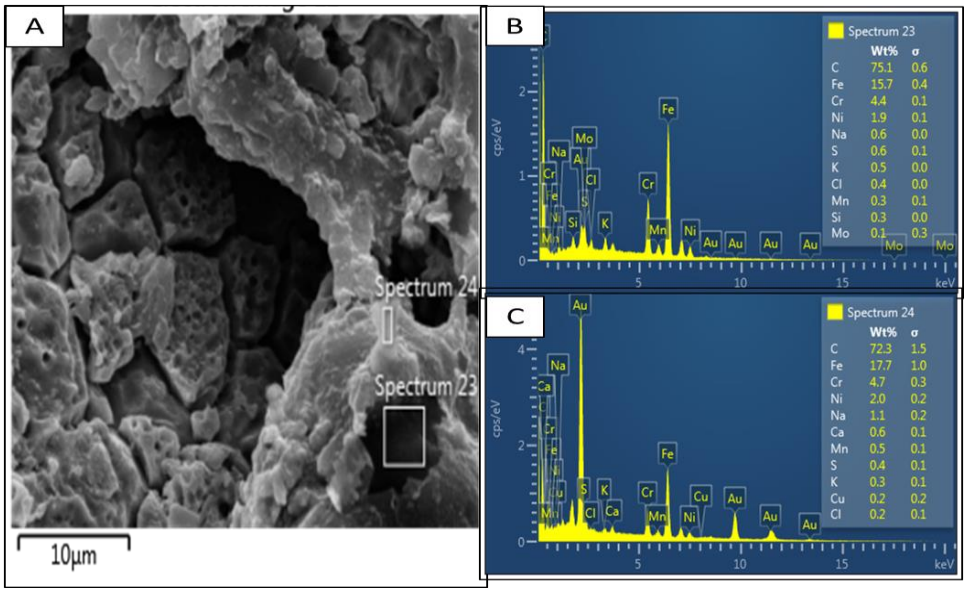


Figure 4.31:SEM (300X) and EDX results for stainless-clad bar after polarization in SCPS Contaminated with 1000 ppm Cl ions plus 500 ppm sulfate ions at 55 ºC.

Figure 4.32a depicts the SEM, while Figure 4.32b depicts the EDX results for stainless steel exposed to SCPS contaminated with 1000 ppm Chloride ions at 25 ºC. Spectrum 30 shows the area covered with protective film of chromium-oxide which is responsible for the low corrosion density as reported in the previous section.

Figure 4.33a depicts the SEM image, while Figure 4.33b depicts the EDX results for stainless steel exposed to SCPS contaminated with 1000 ppm Chloride ions at 55 ºC, No sign of corrosion was seen on the scanned surface.

However, pitting corrosion was noted on the specimens immersed in SCPS contaminated with 1,000 ppm chloride and 500 ppm sulfate ions exposed to 55 ºC as shown in EDX result (Figure 4.34).

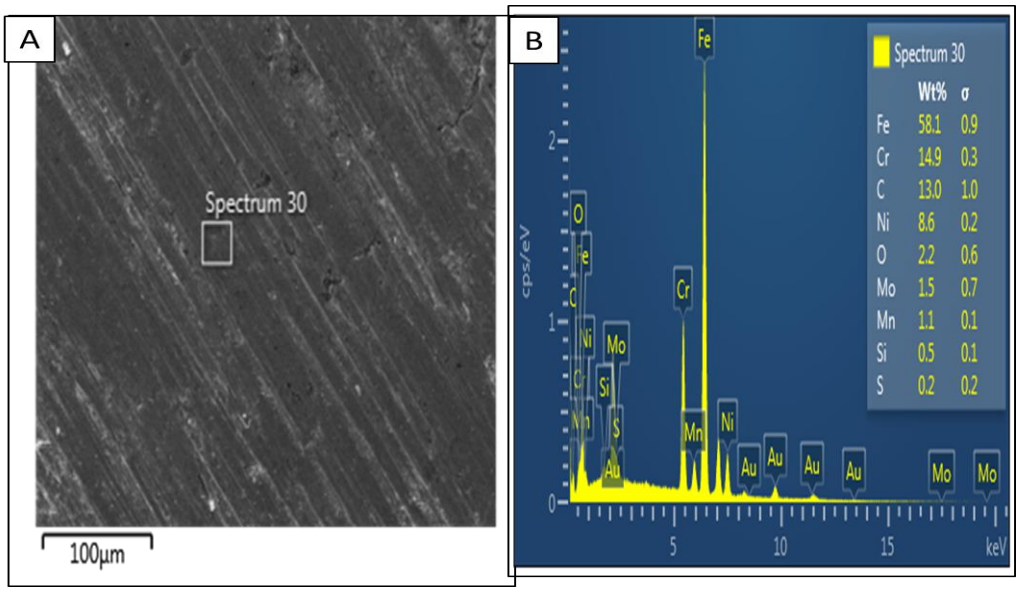


Figure 4.32:SEM (300X) and EDX results stainless bar after polarization in SCPS Contaminated with 1000 ppm $Cl^-$ at 25 ºC.

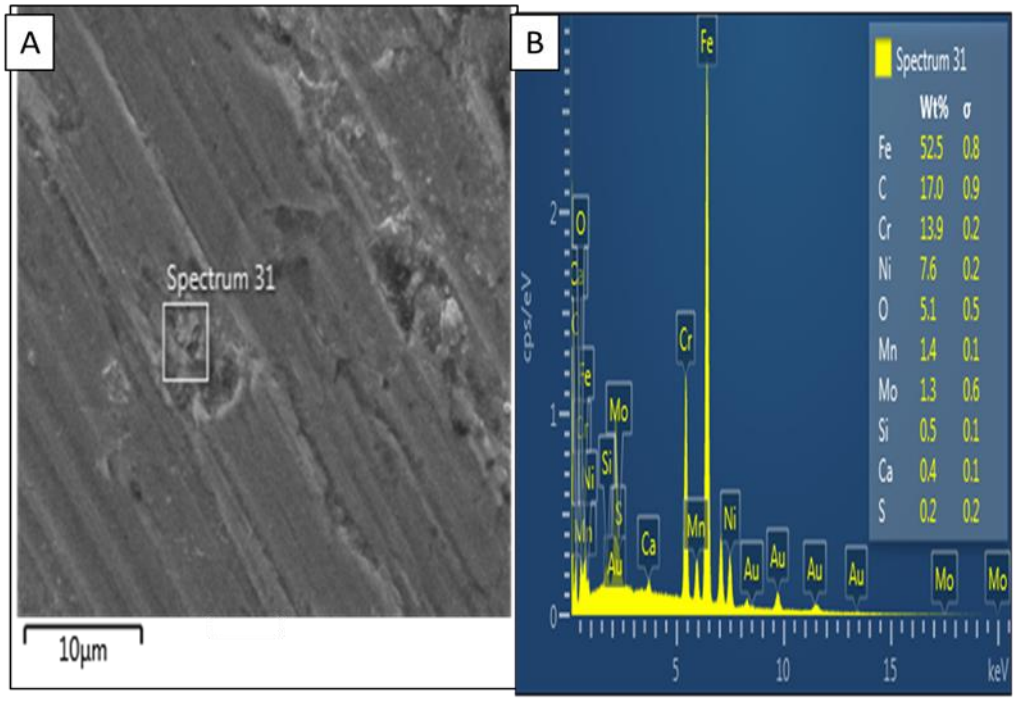


Figure 4.33:SEM (300X) and EDX results stainless bar after polarization in SCPS Contaminated with 1000 ppm $Cl^-$ at 25 ºC.

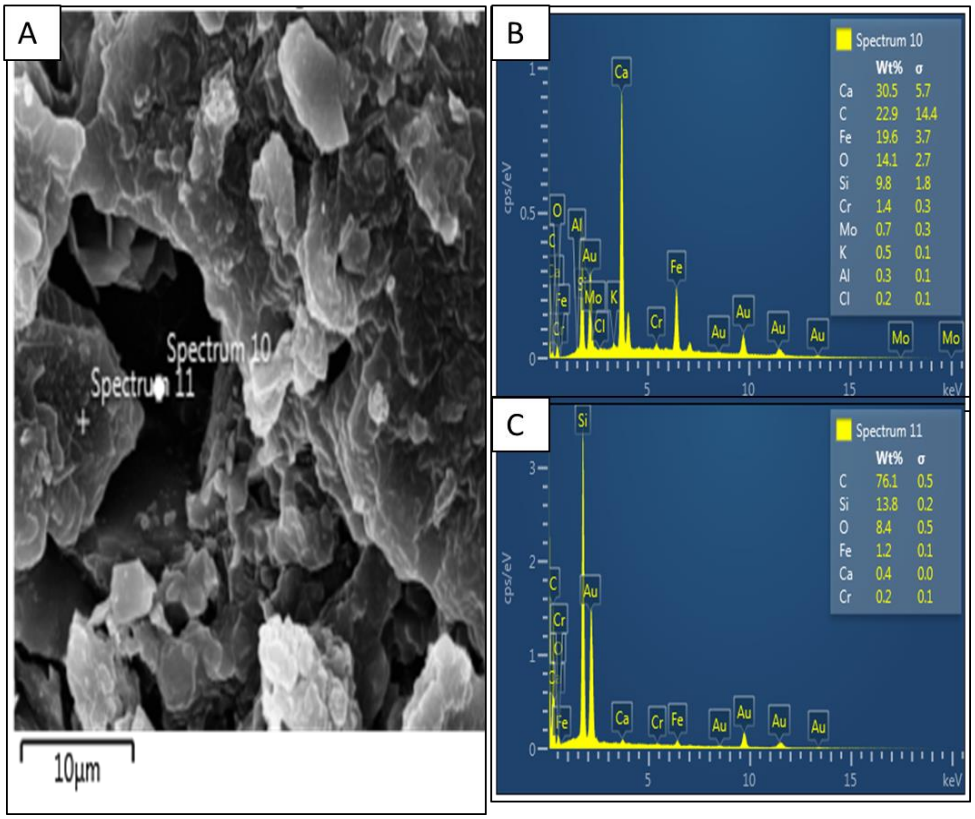


Figure 4.34:SEM (300X) and EDX results for stainless bar after polarization in SCPS Contaminated with 1000 ppm Cl ions plus 500ppm sulfate ions at 55 ºC.

## 4.3 EFFECT OF AGGRESSIVE MEDIUM ON REINFORCEMENT CORROSION USING ASTM G 109 METHOD

The effect of the chloride and sulfate solutions on black bar and corrosion resistant bars in concrete was evaluated using concrete specimens designed according to ASTM G 109. Macro-cell current and corrosion potentials were measured at regular intervals (every four weeks). The corrosion potentials were measured using high impedance voltmeter in conjunction with a SCE, while the macro-cell current was measured using macro-cell set-up as shown in Figure 4.35. Furthermore, visual inspection of the top bar and determination of the chloride concentration at the top bar level were also evaluated. The details of these tests were discussed in Chapter 3.

### 4.3.1 Corrosion Potentials

Corrosion is an electro-chemical process in which the corroding metal behaves like a small electro-chemical cell. This process of corrosion generates electrical potentials which can be detected and categorized by the half-cell. The equipment and method of measurement are presented in ASTM C 876 [39]. The free corrosion potential of the steel bar can be measured by determining the voltage difference between the steel bar and reference electrode which are immerged in electrolyte representing concrete pore solution. Also, the free corrosion potential of the steel bar for ASTM G 109 specimens was measured by determining the voltage difference between the top steel bar and reference electrode which are immerged in different form of electrolyte.

### 4.3.2 Macro-Cell Current

The macro-cell current was measured at regular intervals (once at the start of the second week of wetting cycle) for a period of 36 weeks (19 wetting cycles) for each specimen. The macro-cell current was measured for uncracked specimens as shown in Figure 35. The average macro-cell current for all the tested steel specimens in all the solutions described in Chapter 3 is shown in Tables 4.3 through 4.6, while Figures 4.36 through 4.41 show the average macro-cell current values plotted versus time.

Figure 4.35:Macro-Cell Set-up for Corrosion Monitoring

Table 4.3:Average Macro-Cell Current for Uncracked Specimens Ponded with 3% NaCl

| Average Macrocell Current (µA) | | | | | |
|---|---|---|---|---|---|
| **Date** | **Wet Cycle No.** | **Black bar** | **MMFX** | **Stainless-Clad Steel** | **Stainless-Steel** |
| 17/04/2014 | Starting wetting cycles | | | | |
| 24/04/2014 | 1 | 0.0000 | 0.0000 | 0.0000 | 0.0000 |
| 30/04/2014 | 2 | 0.0200 | 0.0133 | 0.0100 | 0.0100 |
| 8/05/2014 | 3 | 0.0200 | 0.0133 | 0.0100 | 0.0100 |
| 23/05/2014 | 4 | 0.0200 | 0.0133 | 0.0167 | 0.0100 |
| 05/06/2014 | 5 | 0.0267 | 0.0133 | 0.0200 | 0.0133 |
| 19/06/2014 | 6 | 0.0267 | 0.0167 | 0.0200 | 0.0133 |
| 03/07/2014 | 7 | 0.0300 | 0.0267 | 0.0200 | 0.0200 |
| 17/07/2014 | 8 | 0.0400 | 0.0267 | 0.0300 | 0.0200 |
| 31/07/2014 | 9 | 0.0400 | 0.0267 | 0.0300 | 0.0200 |
| 14/08/2014 | 10 | 0.0400 | 0.0300 | 0.0367 | 0.0266 |
| 04/09/2014 | 11 | 0.0500 | 0.0300 | 0.0367 | 0.0266 |
| 02/10/2014 | 12 | 0.0500 | 0.0300 | 0.0367 | 0.0266 |
| 30/10/2014 | 13 | 0.0600 | 0.0367 | 0.0422 | 0.0300 |
| 27/11/2014 | 14 | 0.0600 | 0.0333 | 0.0422 | 0.0300 |
| 25/12/2014 | 15 | 0.0600 | 0.0367 | 0.0380 | 0.0300 |
| 29/01/2015 | 16 | 0.0600 | 0.0333 | 0.0426 | 0.0300 |
| 26/02/2015 | 17 | 0.0600 | 0.0367 | 0.0426 | 0.0367 |
| 26/03/2015 | 18 | 0.0700 | 0.0400 | 0.0440 | 0.0367 |
| 23/04/2015 | 19 | 0.0800 | 0.0400 | 0.0440 | 0.0300 |

Table 4.4 :Average Macro-Cell Current for Uncracked Specimens Ponded with 3% NaCl and 0.5% of Sulfate ions.

| **Average Macrocell Current (μA)** | | | | | |
|---|---|---|---|---|---|
| **Date** | **Wet Cycle No.** | **Black bar** | **MMFX** | **Stainless-Clad Steel** | **Stainless-Steel** |
| 17/04/2014 | Starting wetting cycles | | | | |
| 24/04/2014 | 1 | 0 | 0.0000 | 0 | 0.0000 |
| 30/04/2014 | 2 | 0.0100 | 0.0100 | 0.0140 | 0.0010 |
| 8/05/2014 | 3 | 0.0200 | 0.0100 | 0.0140 | 0.0100 |
| 23/05/2014 | 4 | 0.0200 | 0.0167 | 0.0230 | 0.0167 |
| 05/06/2014 | 5 | 0.0267 | 0.0200 | 0.0230 | 0.0167 |
| 19/06/2014 | 6 | 0.0300 | 0.0200 | 0.0270 | 0.0200 |
| 03/07/2014 | 7 | 0.0330 | 0.0200 | 0.0270 | 0.0200 |
| 17/07/2014 | 8 | 0.0330 | 0.0200 | 0.0270 | 0.0167 |
| 31/07/2014 | 9 | 0.0400 | 0.0200 | 0.0270 | 0.0167 |
| 14/08/2014 | 10 | 0.0400 | 0.0300 | 0.0270 | 0.0200 |
| 04/09/2014 | 11 | 0.0400 | 0.0300 | 0.0270 | 0.0200 |
| 02/10/2014 | 12 | 0.0400 | 0.0300 | 0.0270 | 0.0233 |
| 30/10/2014 | 13 | 0.0500 | 0.0330 | 0.0270 | 0.0233 |
| 27/11/2014 | 14 | 0.0500 | 0.0330 | 0.0270 | 0.0233 |
| 25/12/2014 | 15 | 0.0550 | 0.0400 | 0.0310 | 0.0267 |
| 29/01/2015 | 16 | 0.0567 | 0.0400 | 0.0310 | 0.0300 |
| 26/02/2015 | 17 | 0.0600 | 0.0400 | 0.0310 | 0.0300 |
| 26/03/2015 | 18 | 0.0600 | 0.0400 | 0.0360 | 0.0300 |
| 23/04/2015 | 19 | 0.0700 | 0.0400 | 0.0400 | 0.0300 |

Table 4.5:Average Macro-Cell Current for Uncracked Specimens Ponded with 3% NaCl and 3% of Sulfate Solution.

| **Average Macrocell Current (μA)** | | | | | |
|---|---|---|---|---|---|
| **Date** | **Wet Cycle No.** | **Black bar** | **MMFX** | **Stainless-Clad Steel** | **Stainless-Steel** |
| 17/04/2014 | Starting wetting cycles | | | | |
| 24/04/2014 | 1 | 0 | 0 | 0 | 0 |
| 30/04/2014 | 2 | 0.0100 | 0.0100 | 0.010 | 0.0136 |
| 8/05/2014 | 3 | 0.0200 | 0.0100 | 0.010 | 0.0136 |
| 23/05/2014 | 4 | 0.0200 | 0.0100 | 0.010 | 0.0136 |
| 05/06/2014 | 5 | 0.0200 | 0.0200 | 0.010 | 0.0226 |
| 19/06/2014 | 6 | 0.0300 | 0.0200 | 0.017 | 0.0227 |
| 03/07/2014 | 7 | 0.0300 | 0.0200 | 0.020 | 0.0227 |
| 17/07/2014 | 8 | 0.0400 | 0.0300 | 0.020 | 0.0271 |
| 31/07/2014 | 9 | 0.0400 | 0.0300 | 0.020 | 0.0271 |
| 14/08/2014 | 10 | 0.0500 | 0.0330 | 0.023 | 0.0271 |
| 04/09/2014 | 11 | 0.0500 | 0.0300 | 0.023 | 0.0271 |
| 02/10/2014 | 12 | 0.0500 | 0.0300 | 0.020 | 0.0271 |
| 30/10/2014 | 13 | 0.0567 | 0.0300 | 0.023 | 0.0271 |
| 27/11/2014 | 14 | 0.0567 | 0.0367 | 0.023 | 0.0271 |
| 25/12/2014 | 15 | 0.0600 | 0.0367 | 0.027 | 0.0366 |
| 29/01/2015 | 16 | 0.0600 | 0.0400 | 0.027 | 0.0366 |
| 26/02/2015 | 17 | 0.0700 | 0.0400 | 0.030 | 0.0366 |
| 26/03/2015 | 18 | 0.0700 | 0.0400 | 0.030 | 0.0407 |
| 23/04/2015 | 19 | 0.008 | 0.0050 | 0.030 | 0.0407 |

Table 4.6:Average Macro-Cell Current for Uncracked Specimens Ponded with Sabkha Solution

| Average Macrocell Current (µA) | | | | | |
|---|---|---|---|---|---|
| **Date** | **Wet Cycle No.** | **Black bar** | **MMFX** | **Stainless-Clad Steel** | **Stainless-Steel** |
| 17/04/2014 | Starting wetting cycles | | | | |
| 24/04/2014 | 1 | 0 | 0.000 | 0.000 | 0.000 |
| 30/04/2014 | 2 | 1.15 | 0.017 | 0.012 | 0.010 |
| 8/05/2014 | 3 | 1.95 | 0.017 | 0.012 | 0.013 |
| 23/05/2014 | 4 | 2.3 | 0.023 | 0.015 | 0.020 |
| 05/06/2014 | 5 | 4.6 | 0.023 | 0.019 | 0.020 |
| 19/06/2014 | 6 | 7.955 | 0.027 | 0.023 | 0.023 |
| 03/07/2014 | 7 | 12.25 | 0.030 | 0.027 | 0.023 |
| 17/07/2014 | 8 | | 0.030 | 0.031 | 0.023 |
| 31/07/2014 | 9 | | 0.033 | 0.031 | 0.027 |
| 14/08/2014 | 10 | | 0.033 | 0.035 | 0.027 |
| 04/09/2014 | 11 | | 0.030 | 0.035 | 0.027 |
| 02/10/2014 | 12 | | 0.033 | 0.038 | 0.030 |
| 30/10/2014 | 13 | | 0.033 | 0.038 | 0.030 |
| 27/11/2014 | 14 | | 0.033 | 0.038 | 0.030 |
| 25/12/2014 | 15 | | 0.037 | 0.042 | 0.030 |
| 29/01/2015 | 16 | | 0.037 | 0.042 | 0.033 |
| 26/02/2015 | 17 | | 0.037 | 0.042 | 0.033 |
| 26/03/2015 | 18 | | 0.037 | 0.046 | 0.033 |
| 23/04/2015 | 19 | | 0.040 | 0.460 | 0.033 |

Figure 4.36 shows the average macro-cell current measured for all the steel samples ponded with 3% NaCl. From the data in this Figure, it is noted that a steady rise in the average measured macro-cell current was recorded for the black bar till it reached 0.08 μA after the 12 months of monitoring. The MMFX bar, Stainless-clad and Stainless steel bar maintain a very low macro-cell current of 0.04 μA , 0.044 μA and 0.03 μA respectively, after 12 months of ponding. All values measured for all the steel specimen is far below the threshold of 10 μA specified for corrosion to be initiated in the steel bars, this is due do the high quality concrete used for this experimental work which gives the steel bar protection against the ingress of the solutions.

Similar trends were also noted for the corrosion resistant steel specimens ponded with concomitant 3% NaCl and 0.5% Sulfate ions solution as shown in Figure 4.37 and also for 3% NaCl and 3% Sulfate ions solution as shown in Figure 4.38. Whereas, the steel specimen ponded with the sabkha solution shows very high macro-cell current for the black bar after $6^{th}$ wet cycle of ponding, a value of 12.25 μA was recorded , which is more than the threshold value of 10 μA as shown in Figure 4.39, which implies that corrosion has started after 77 days. Whereas, MMFX, stainless steel and stainless-clad bar remain passive by maintaining a very low corrosion current as shown in Figure 4.40 despite the aggressive nature of the sabkha solution, this is due to presence of chromium in the aforementioned corrosion resistance steel bars.

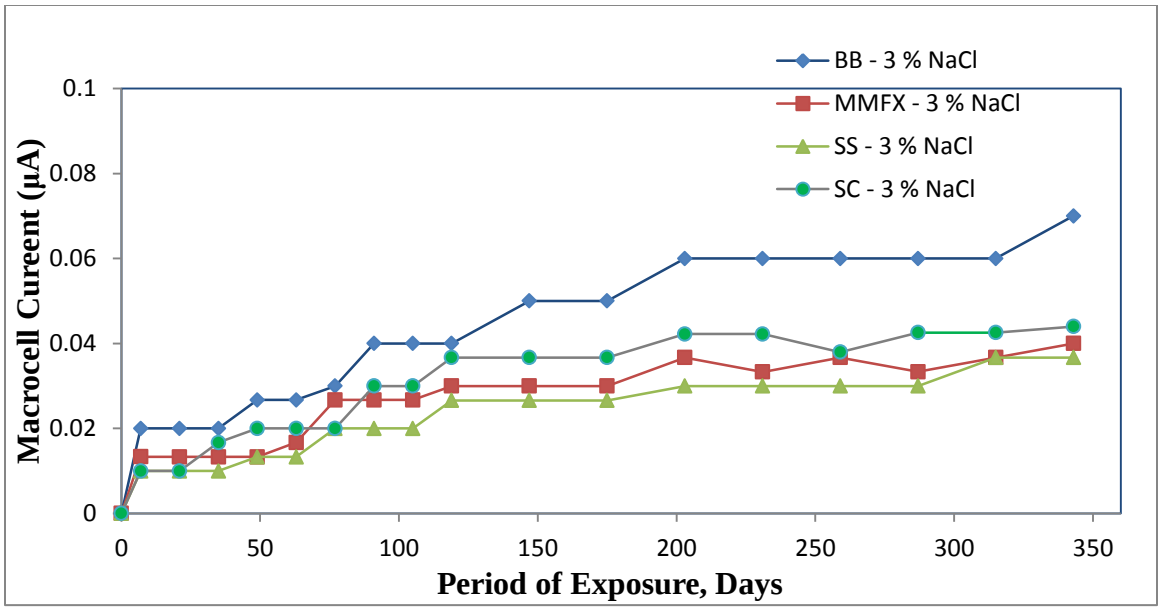


Figure 4.36: Comparison of the Average Macro-Cell Current of Steel Specimens Ponded with 3% NaCl.

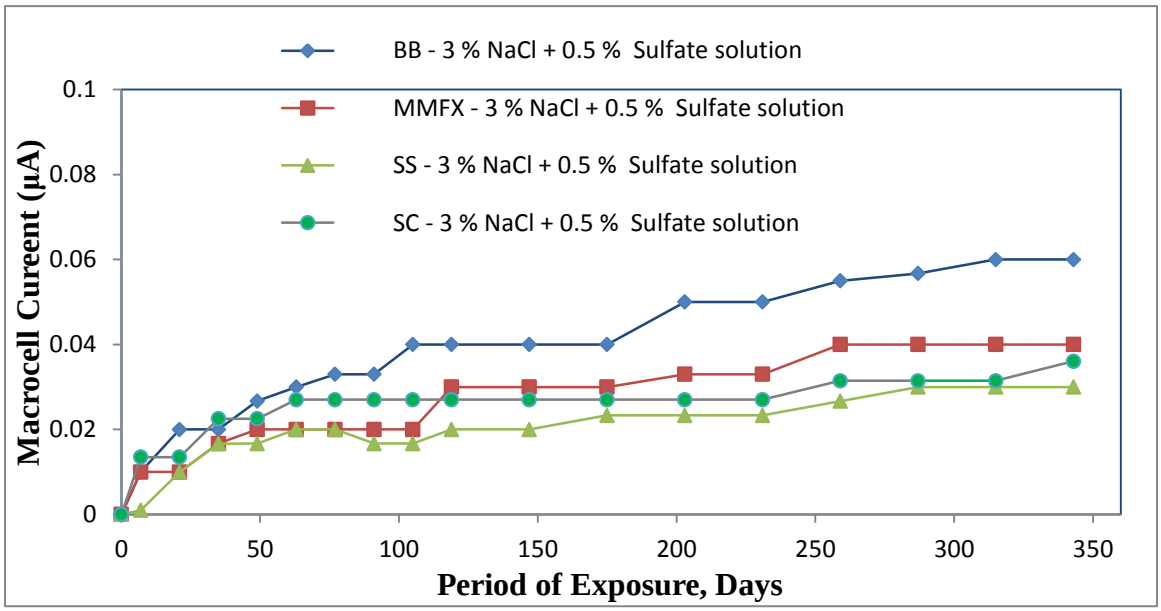


Figure 4.37: Comparison of the Average Macro-Cell Current of Steel Specimens Ponded with 3% NaCl and 0.5% of Sulfate Solution.

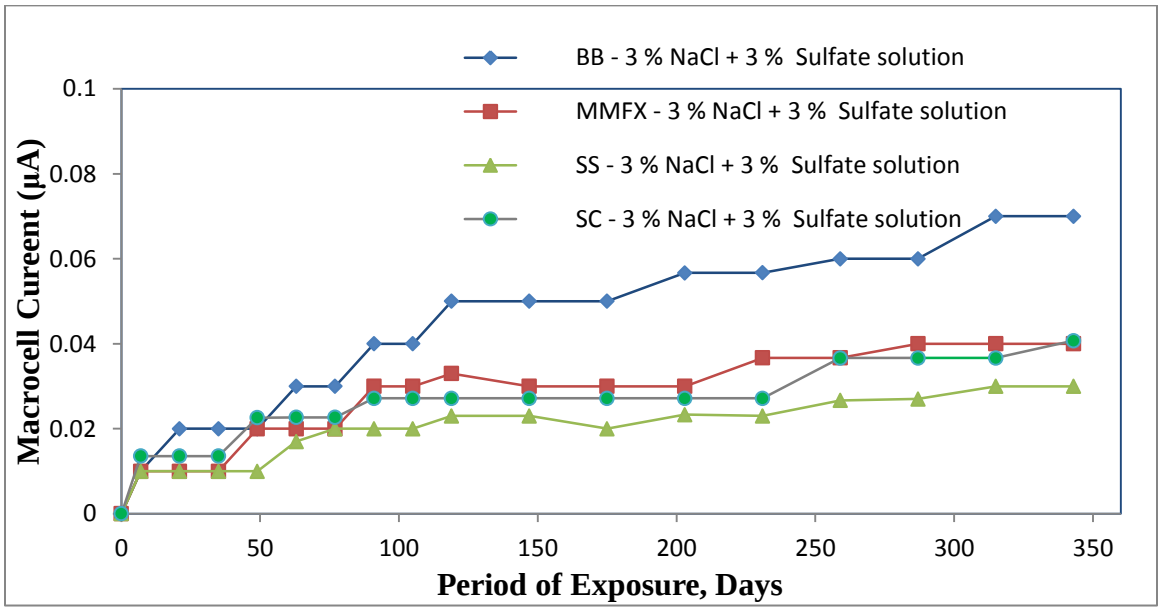


Figure 4.38:Comparison of the Average Macro-Cell Current of Steel Specimens Ponded with 3% NaCl and 3% of Sulfate Solution.

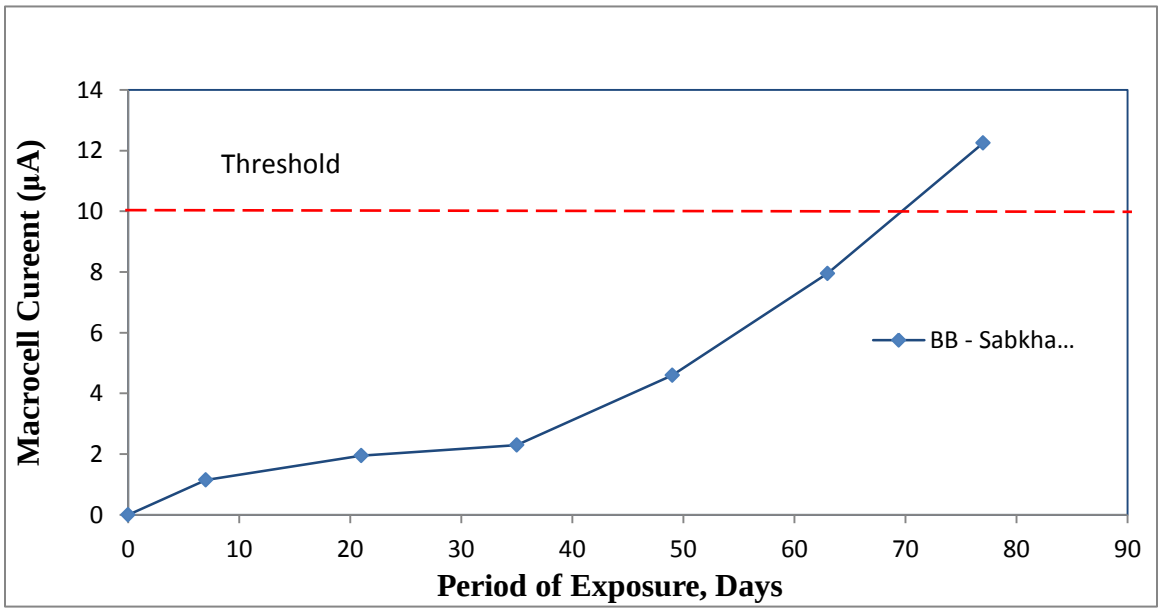


Figure 4.39:Comparison of the Average Macro-Cell Current of black Steel Specimens Ponded with Sabkha Solution.

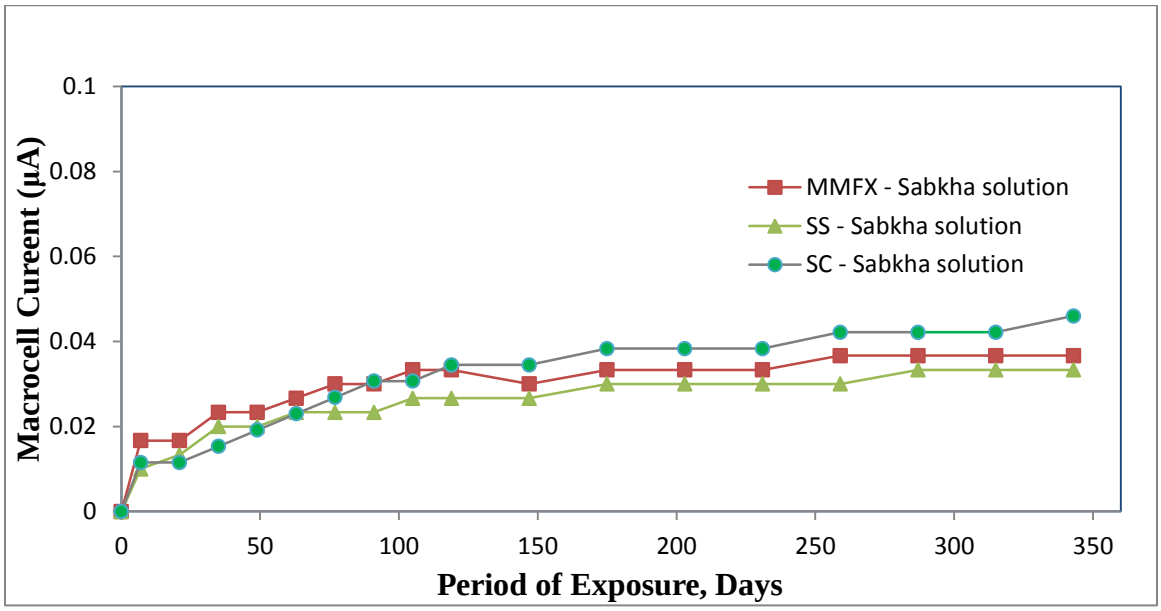


Figure 4.40: Comparison of the Average Macro-Cell Current of Corrosion resistant Steel Specimens Ponded with Sabkha Solution.

Overall, no significant macro-cell corrosion current could be noted in any of the concrete specimens with corrosion resistant bars, based on ASTM G 109 test, through the end of the 12- month evaluation period.

### 4.3.3 Total Current

ASTM G 109 requires the period of testing to continue till the average macro-cell current reaches 10 µA or greater, and at least half of the specimens show integrated macro-cell currents equal to or greater than 150 Coulombs. In those cases, where the admixtures being tested are corrosive, the tests are to be completed within three full cycles after an average integrated macro-cell current of 75 Coulombs is measured [43]. The total corrosion current which is the integration of the macro-cell current over time of each specimen was calculated using the following equation (as per ASTM G 109):

$$TC_j = TC_{j-1} + [(t_j - t_{j-1}) \times (i + i_{j-1})/2] \quad 4.5$$

Where:

TC: the total corrosion in Coulombs,

tj: the time in seconds when the macro-cell current was measured, and

ij: the macro-cell current in Amperes at time, tj.

The total current of the uncracked specimens is shown from Table 4.7 to 4.11.

Table 4.7 shows the average total current measured for all the steel samples ponded with 3% NaCl. From the data in this table, the average total current for black bar was 1.4 coulombs after 12 months of monitoring, while, MMFX bar, Stainless steel and Stainless-Clad bar have average macro-cell current of less than one coulomb respectively after 12

months. All values measured for all the steel specimen are far below the threshold of 150 coulomb specified for corrosion to be initiated in the steel bars, this is also due do the high quality concrete used for this experimental work which gives the steel bar protection from the ingress of the solutions.

Similar trends were also noted for the steel specimens ponded with concomitant 3% NaCl and 0.5% Sulfate ions solution and also for 3% NaCl and 3% Sulfate ions solution as shown in Table 4.8 and 4.9. Whereas, the steel specimen ponded with the sabkha solution shows very high average total current for the black bar with a value of 168 coulombs, which is more than the threshold value of 150 coulombs specified by the G109 standard, Whereas, MMFX, stainless steel and stainless-clad bar remain total currents of less than one coulomb.

Table 4.7: Total Current of the Steel Bars Ponded with 3% NaCl Solution.

| Specimen Types | Average Total Current (Coulombs |
|---|---|
| Black bar | 1.403 |
| MMFX | 0.632 |
| Stainless steel | 0.747 |
| Stainless Clad | 0.639 |

Table 4.8:Total Current of Steel Bars Ponded with 3% NaCl and 0.5 % Sulfate solution.

| Specimen Types | Average Total Current (Coulombs |
|---|---|
| Black bar | 1.588 |
| MMFX | 0.570 |
| Stainless steel | 0.670 |
| Stainless Clad | 0.885 |

Table 4.9:Total Current of the Steel Bars Immersed in 3% NaCl and 3% Sulfate Solution.

| Specimen Types | Average Total Current (Coulombs |
|---|---|
| Black bar | 1.600 |
| MMFX | 0.657 |
| Stainless steel | 0.728 |
| Stainless Clad | 0.896 |

Table 4.10:Total Current of the Steel Bars Ponded with Sabkha solution.

| Specimen Types | Average Total Current (Coulombs |
|---|---|
| Black bar | 168.376 |
| MMFX | 0.748 |
| Stainless steel | 0.838 |
| Stainless clad | 0.740 |

### 4.3.4 Macro-Cell Corrosion Potential

The average time-corrosion potential curves for steel in ASTM G 109 concrete specimens are shown in Figures 4.40 through 4.43. The individual time-corrosion potential curve for each specimen is shown in Appendices B and C. Furthermore, Tables 4.11 through 4.14 summarize the average data of corrosion potential measurements for the steel specimens.

The average corrosion potentials of the steel specimen in the uncracked concrete specimens was less than the ASTM C 876 threshold value of -270 mV SCE after 12 months of drying and wetting for the concrete specimens ponded with 3% NaCl, 3% NaCl and 0.5% Sulfate ions solution and also for 3% NaCl and 3% Sulfate ions solution as shown in Figure 4.38 to Figure 4.40, However, the corrosion potentials in the uncracked concrete specimens ponded with sabkha solutions reviews that black bar with corrosion potential of -327 mV exceeds the ASTM C 876 threshold value of -270 mV SCE after just one weeks of wetting, which indicates more than 90% probability of corrosion. While MMFX, stainless steel and stainless clad bar remains below the ASTM C 876 threshold value of -270 mV SCE. The maximum readings were in the range of -113 to -126 mV, which indicate less than 10% probability of corrosion.

Table 4.11:Corrosion Potential Data for Uncracked Specimens Ponded with 3% NaCl

| Corrosion potential (mV) SCE | | | | | |
|---|---|---|---|---|---|
| **Date** | **Wet Cycle No.** | **Black bar** | **MMFX** | **Stainless-Clad Steel** | **Stainless-Steel** |
| 17/04/2014 | Starting wetting cycles | | | | |
| 24/04/2014 | 1 | -94.5 | -160.3 | -145.2 | -153.7 |
| 30/04/2014 | 2 | -89.1 | -154.6 | -141.9 | -148.3 |
| 8/05/2014 | 3 | -81.6 | -152.5 | -138.3 | -143.3 |
| 23/05/2014 | 4 | -77.7 | -146.3 | -136.2 | -138.4 |
| 05/06/2014 | 5 | -73.8 | -143.5 | -134.3 | -137.1 |
| 19/06/2014 | 6 | -67.9 | -139.1 | -126.7 | -131.6 |
| 03/07/2014 | 7 | -61.1 | -133.8 | -123.1 | -127.4 |
| 17/07/2014 | 8 | -62.6 | -133.0 | -124.7 | -126.9 |
| 31/07/2014 | 9 | -62.8 | -137.4 | -124.9 | -126.9 |
| 14/08/2014 | 10 | -63.6 | -138.6 | -125.3 | -126.0 |
| 04/09/2014 | 11 | -59.9 | -134.3 | -122.3 | -120.7 |
| 02/10/2014 | 12 | -60.3 | -132.5 | -118.7 | -118.9 |
| 30/10/2014 | 13 | -55.2 | -130.6 | -113.6 | -113.9 |
| 27/11/2014 | 14 | -57.8 | -124.9 | -115.0 | -109.0 |
| 25/12/2014 | 15 | -60.8 | -121.6 | -108.9 | -111.1 |
| 29/01/2015 | 16 | -61.6 | -121.5 | -100.9 | -113.5 |
| 26/02/2015 | 17 | -71.0 | -118.7 | -99.1 | -115.5 |
| 26/03/2015 | 18 | -58.9 | -100.0 | -101.3 | -113.0 |

Table 4.12:Corrosion Potential Data for Uncracked Specimens Ponded with 3% NaCl and 0.5% of Sulfate Solution.

| Corrosion potential (mV) SCE | | | | | |
|---|---|---|---|---|---|
| **Date** | **Wet Cycle No.** | **Black bar** | **MMFX** | **Stainless-Clad Steel** | **Stainless-Steel** |
| 17/04/2014 | Starting wetting cycles | | | | |
| 24/04/2014 | 1 | -75.5 | -139.2 | -139.6 | -136.3 |
| 30/04/2014 | 2 | -49.6 | -125.0 | -137.6 | -116.1 |
| 8/05/2014 | 3 | -59.0 | -128.5 | -134.0 | -128.8 |
| 23/05/2014 | 4 | -40.9 | -116.4 | -130.2 | -114.7 |
| 05/06/2014 | 5 | -42.6 | -115.4 | -128.9 | -115.1 |
| 19/06/2014 | 6 | -45.7 | -117.7 | -125.7 | -117.4 |
| 03/07/2014 | 7 | -50.0 | -118.7 | -125.6 | -119.2 |
| 17/07/2014 | 8 | -41.3 | -112.8 | -128.1 | -108.2 |
| 31/07/2014 | 9 | -33.2 | -112.7 | -125.7 | -104.2 |
| 14/08/2014 | 10 | -35.3 | -114.6 | -126.8 | -105.6 |
| 04/09/2014 | 11 | -33.4 | -118.2 | -125.7 | -104.5 |
| 02/10/2014 | 12 | -34.1 | -118.4 | -124.4 | -103.7 |
| 30/10/2014 | 13 | -35.4 | -120.0 | -124.8 | -101.2 |
| 27/11/2014 | 14 | -31.8 | -103.2 | -125.7 | -102.3 |
| 25/12/2014 | 15 | -30.6 | -100.0 | -119.4 | -101.9 |
| 29/01/2015 | 16 | -20.5 | -91.7 | -115.9 | -91.9 |
| 26/02/2015 | 17 | -18.8 | -88.1 | -109.8 | -78.7 |
| 26/03/2015 | 18 | -31.5 | -99.4 | -126.2 | -91.1 |

Table 4.13:Corrosion Potential Data for Uncracked Specimens Ponded with 3% NaCl and 3% of Sulfate ions.

| Corrosion potential (mV) SCE | | | | | |
|---|---|---|---|---|---|
| **Date** | **Wet Cycle No.** | **Black bar** | **MMFX** | **Stainless-Clad Steel** | **Stainless-Steel** |
| 17/04/2014 | Starting wetting cycles | | | | |
| 24/04/2014 | 1 | -88.8 | -139.2 | -152.0 | -139.1 |
| 30/04/2014 | 2 | -80.0 | -125.0 | -147.3 | -131.9 |
| 8/05/2014 | 3 | -72.3 | -128.5 | -141.9 | -123.8 |
| 23/05/2014 | 4 | -65.7 | -116.4 | -134.7 | -118.3 |
| 05/06/2014 | 5 | -63.8 | -115.4 | -133.6 | -117.4 |
| 19/06/2014 | 6 | -54.0 | -117.7 | -130.8 | -115.4 |
| 03/07/2014 | 7 | -51.0 | -118.7 | -129.7 | -114.1 |
| 17/07/2014 | 8 | -47.6 | -112.8 | -129.6 | -106.6 |
| 31/07/2014 | 9 | -46.8 | -112.7 | -127.5 | -112.1 |
| 14/08/2014 | 10 | -48.2 | -114.6 | -128.2 | -108.7 |
| 04/09/2014 | 11 | -44.2 | -118.2 | -125.8 | -110.6 |
| 02/10/2014 | 12 | -41.5 | -118.4 | -125.1 | -112.3 |
| 30/10/2014 | 13 | -35.5 | -120.0 | -124.0 | -113.2 |
| 27/11/2014 | 14 | -37.9 | -103.2 | -124.8 | -100.9 |
| 25/12/2014 | 15 | -46.9 | -100.0 | -115.6 | -95.8 |
| 29/01/2015 | 16 | -44.3 | -91.7 | -116.9 | -100.8 |
| 26/02/2015 | 17 | -71.1 | -88.1 | -112.2 | -104.6 |
| 26/03/2015 | 18 | -58.3 | -99.4 | -121.9 | -100.5 |

Table 4.14:Corrosion Potential Data for Uncracked Specimens Ponded with Sabkha Solution

| Corrosion potential (mV) SCE | | | | | |
|---|---|---|---|---|---|
| **Date** | **Wet Cycle No.** | **Black bar** | **MMFX** | **Stainless-Clad Steel** | **Stainless-Steel** |
| 17/04/2014 | Starting wetting cycles | | | | |
| 24/04/2014 | 1 | -327.0 | -189.5 | -188.3 | -190.7 |
| 30/04/2014 | 2 | -328.0 | -186.8 | -190.5 | -188.9 |
| 8/05/2014 | 3 | -389.0 | -183.7 | -184.5 | -181.0 |
| 23/05/2014 | 4 | -391.0 | -183.1 | -182.6 | -179.0 |
| 05/06/2014 | 5 | -377.6 | -160.7 | -180.2 | -177.6 |
| 19/06/2014 | 6 | -342.5 | -177.1 | -179.5 | -175.6 |
| 03/07/2014 | 7 | -322.5 | -176.5 | -180.3 | -170.3 |
| 17/07/2014 | 8 | -323.0 | -176.1 | -181.2 | -170.2 |
| 31/07/2014 | 9 | -308.9 | -174.2 | -183.4 | -174.5 |
| 14/08/2014 | 10 | -311.0 | -174.5 | -184.1 | -174.5 |
| 04/09/2014 | 11 | -305.0 | -171.7 | -183.4 | -173.9 |
| 02/10/2014 | 12 | -300.5 | -170.7 | -182.8 | -174.1 |
| 30/10/2014 | 13 | -284.8 | -171.5 | -183.5 | -166.7 |
| 27/11/2014 | 14 | -265.4 | -177.0 | -188.6 | -170.0 |
| 25/12/2014 | 15 | -267.0 | -174.8 | -189.8 | -135.0 |
| 29/01/2015 | 16 | -245.0 | -173.6 | -192.8 | -136.1 |
| 26/02/2015 | 17 | -235.3 | -164.8 | -197.5 | -162.7 |
| 26/03/2015 | 18 | -260.9 | -166.6 | -189.8 | -163.8 |

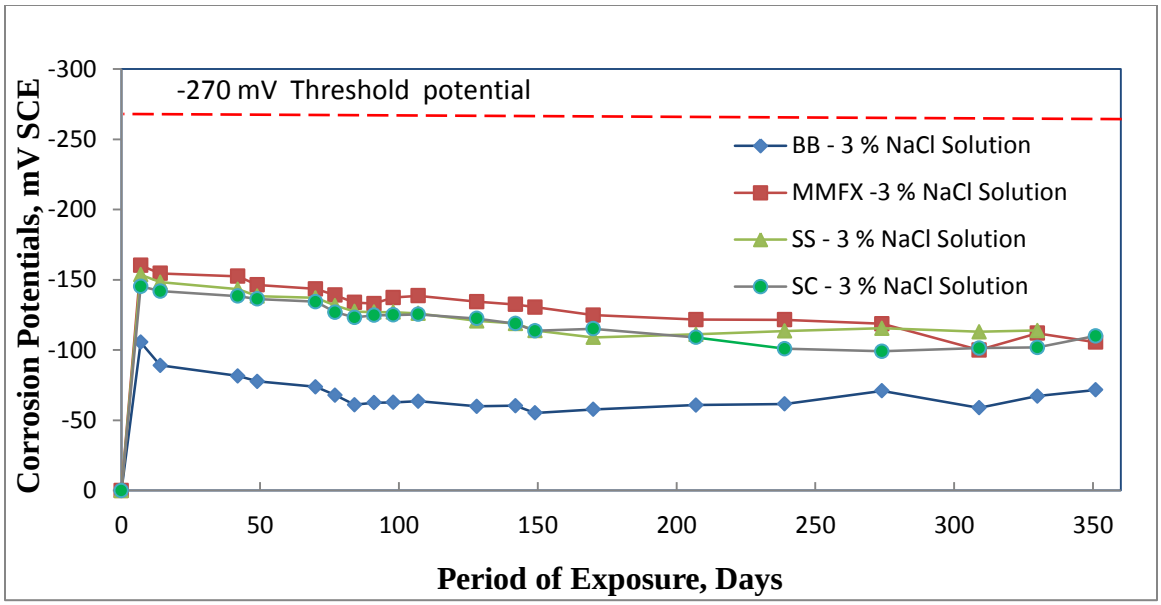


Figure 4.41:Comparison of the Average Corrosion Potential of Steel Specimens Ponded with 3% NaCl.

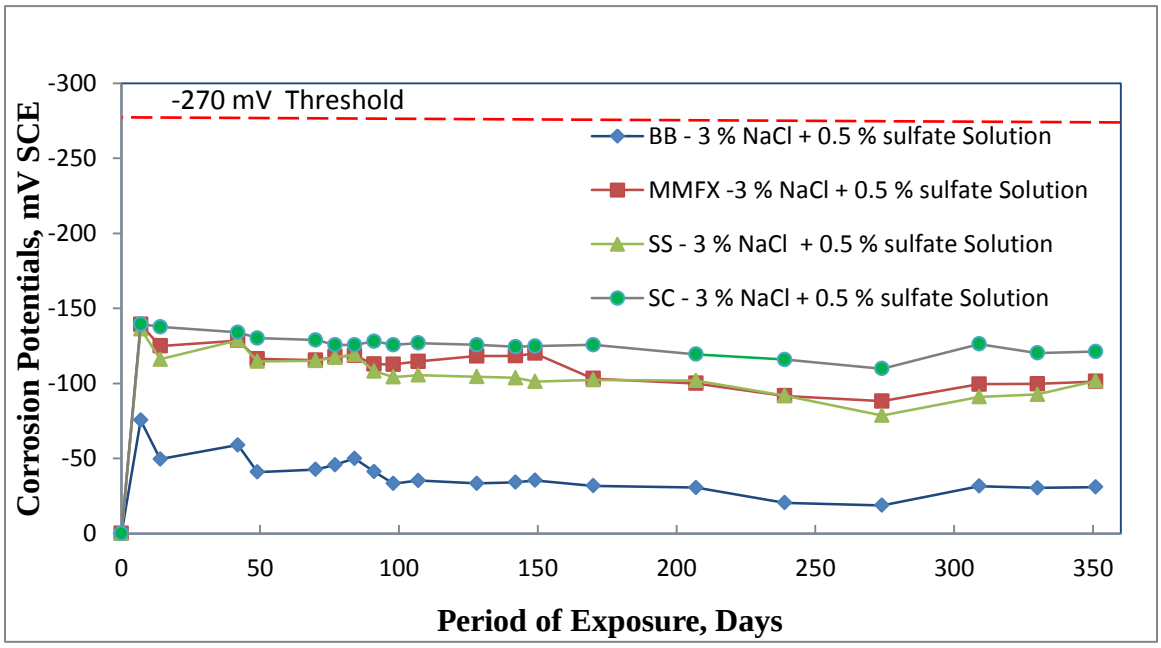


Figure 4.42:Comparison of the Average Corrosion Potential of Steel Specimens Ponded with 3% NaCl and 0.5% of Sulfate Solution.

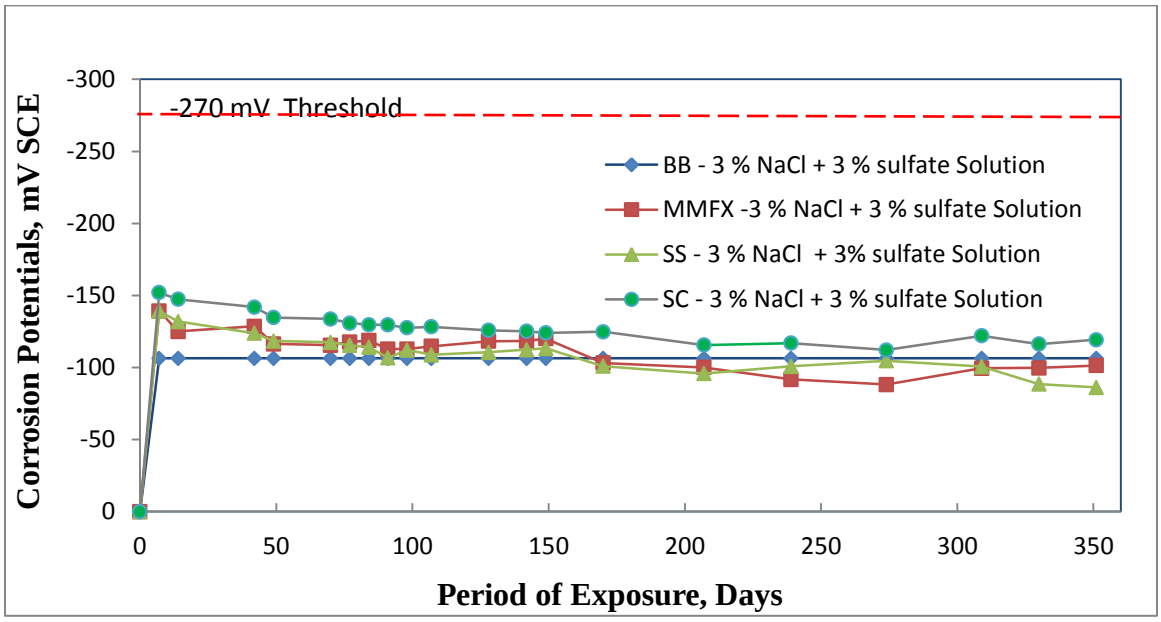


Figure 4.43:Comparison of the Average Corrosion Potential of Steel Specimens Ponded with 3% NaCl and 3% of Sulfate Solution.

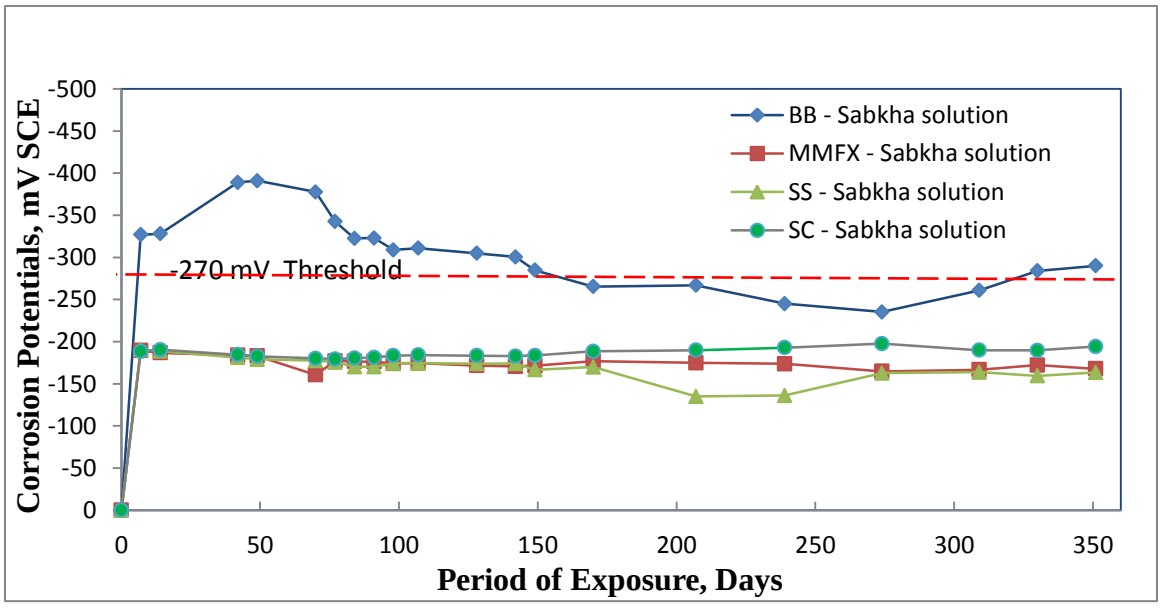


Figure 4.44:Comparison of the Average Corrosion Potential of Steel Specimens Ponded with Sabkha Solution.

### 4.3.5 Chemical Analysis for Free Chloride Concentration

After 19 cyclic exposures conditions, the chloride content at the steel level in ASTM G 109 of the uncracked specimens was measured. Table 4.15 summarizes the chloride content at the bar level for all ASTM G 109 specimens ponded with the sabkha solution. The chloride contents for all the concrete specimens were more than the minimum threshold value of 0.15%. As a result of this high chloride content at the rebar surface of the bar, the black bar was corroded, while MMFX, stainless clad and stainless steel exhibit high corrosion resistance to the sabka solutions.

Table 4.15: Chloride Content at the Bar Level

| Specimen Types | Chloride Concentration (% by Weight of Cement) |
|---|---|
| Black bar | 1.023 |
| MMFX | 1.046 |
| Stainless steel | 1.095 |
| Stainless-Clad | 1.011 |

### 4.3.6 Visual Examination of Steel Bars

At the end of the 12 months exposure period, only the black bar exposed to sabka solution has corroded, so only the concrete specimens ponded with sabkha solution were broken and the anodic steel was visually inspected and photographed.

The inspection of the top bar of the black steel bar in the specimen Figure 4.45a shows that the bar has corroded at the ends of $6^{th}$ wet cycles. Also, marginal general corrosion was noted at the middle of the bar. The condition of the MMFX steel bar, Stainless-Clad steel and Stainless steel bars in the concrete specimens show no corrosion presence as shown in Figures 4.45b, 4.45c and 4.45d after 12 months of exposure.

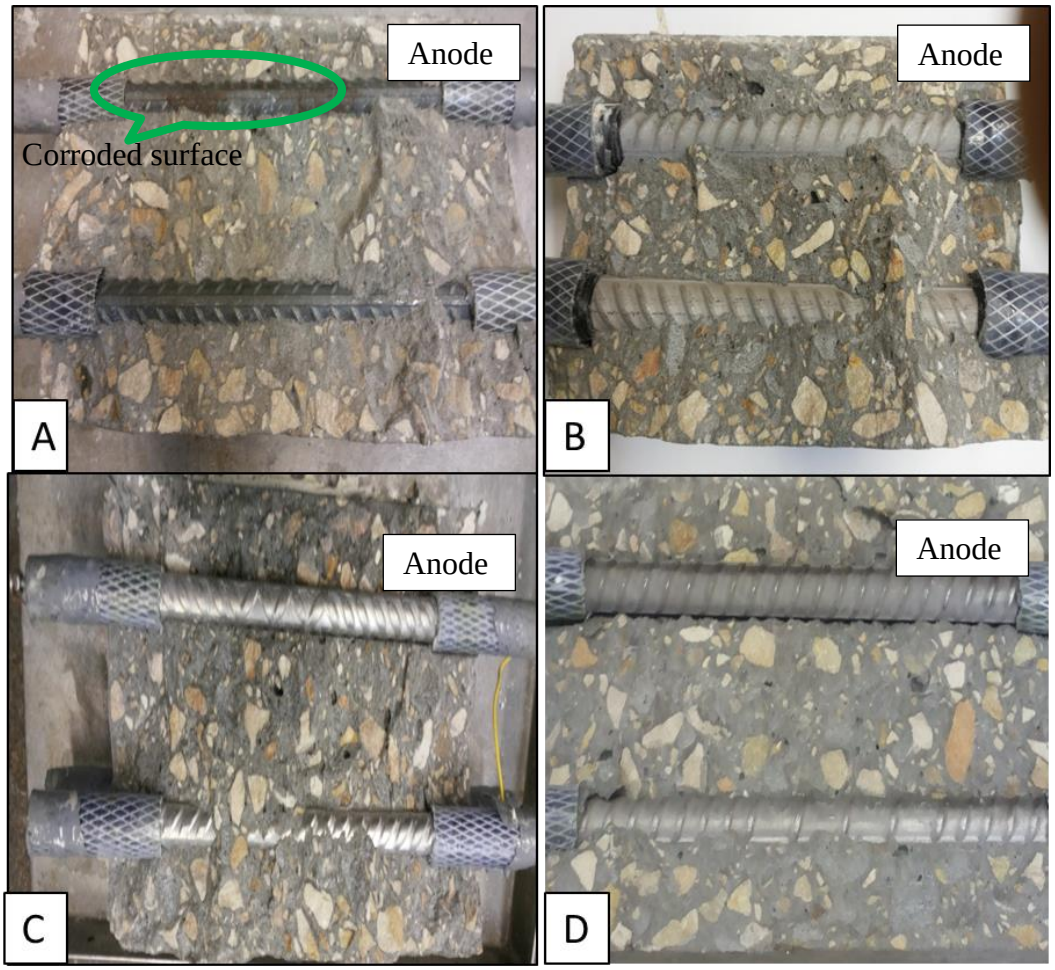


Figure 4.45:Appearance of (A) Black bar (B) Stainless-Clad (C) Stainless Steel (D) MMFX Concrete Specimens after one year of exposure.

# CHAPTER 5

## CONCLUSIONS AND RECOMMENDATIONS

### 5.1 Conclusions

This research was conducted to evaluate the corrosion resistance of selected specialty steel bars. This chapter summarizes and draws conclusions from the results obtained in Chapter 4. Based on the experimental results developed in this investigation, the following conclusions could be drawn:

1. The ultimate tensile strength and hardness of the MMFX bars were the maximum among the specialty steel bars evaluated in this study. These values were 1,200 MPa and 397.6 HV, respectively. The elongation of these bars was the least among the evaluated bars, being 9%. However, this elongation is more than the value required by ASTM A615 that is 8%. The ultimate tensile strength, hardness and elongation of the stainless steel bars was 740 MPa, 296.5 HV and 23% respectively. These values for stainless-clad bars were 680 MPa, 214 HV and 21%, respectively. The ultimate tensile strength, hardness and elongation of the carbon steel bars were 710 MPa, 223 HV and 24%, respectively. The high tensile strength and hardness of MMFX makes it useful for high tensile strength applications.
2. An increase in temperature increased the rate of corrosion of black steel bars while an increase in the temperature had an insignificant effect on the corrosion rate of specialty steel bars. However, the rate of corrosion with an increase in the chloride

concentration in all the steel. However, the corrosion of carbon steel bars, at any temperature, was more than that of the specialty steel bars.

3. An anodic shift in the potentiodynamic curves (PDCs) was noted in all the bars due to an increase in the temperature of the simulated concrete pore solution (SCPS). As expected, the anodic shift leads to an increase in the corrosion current density.
4. General corrosion was noted in the mild steel placed in simulated concrete pore solution (SCPS) contaminated with 2000 ppm chloride and maintained at 25 $^{0}$C. However, pitting corrosion was noted in steel placed in the same SCPS maintained at 55 °C.
5. Potentiodynamic curves (PDCs) for stainless-clad steel placed in simulated concrete pore solution (SCPS) and contaminated with 2000 ppm chloride concentration exhibited little pitting corrosion for the two exposure temperatures. Pitting corrosion was also noted in MMFX and stainless steel bars to SCPS with a chloride concentration of 2,000 ppm. However, Higher the pitting potential for the the stainless clad bars more than that of the MMFX steel bars which is indicative of the fact that the former bars are more corrosion-resistant than the latter one.
6. Reinforcement corrosion was accelerated due to the concomitant presence of chloride and sulphate ions, compared to specimens contaminated with only chloride ions for all the tested steel bars.
7. Among the steels investigated, stainless steel exhibited the highest corrosion resistance, followed by MMFX and stainless steel clad bars.

8. None of the bars embedded in concrete (ASTM G109 test) exhibited any signs of active corrosion for concrete specimen ponded with 3% NaCl, 3% NaCl plus 0.5% sulfate 3% NaCl plus 3% sulphate solutions. This is attributed to the quality and soundness of the concrete used for this work, thus, a much longer period is required for corrosion initiation. However, the black bar in the concrete ponded with sabkha solutions had corroded and a macro current of 12.25 μA was measured after sixth week of wet and dry cycles. The total current in these specimens was 168 coulombs compared to the threshold value of 160 coulombs. Further, the threshold chloride concentration at the rebar level was 1.023% which exceeded the threshold values of 0.15%, by weight of cement. Examination of the bars retrieved from concrete specimens exposed to the sabkha solution indicated the formation of corrosion products on the black bars only. However, corrosion was not observed on stainless steel, MMFX steel and stainless clad steel bars even after one year of ponding with the sabkha solution.

## 5.2 Recommendations

From this research, the corrosion-resistant bars look viable to be utilized in a very aggressive environment, such as the Arabian Gulf, where the design period is expected to be more than 100 years. The solid stainless steel is not cost effective, but the MMFX bars can be used as a substitute. Also, MMFX bar can solve the problem of reinforcement congestions due to its high yield strength. The stainless-clad steel has also shown better corrosion resistance and lower sensitivity to

increase in temperature. Therefore, MMFX and stainless clad bars will be cost-effective for structures to be situated in a very aggressive environment at the long run.

## 5.3 Future Work

In addition to laboratory ASTM G 109 test specimens' results, a long time corrosion monitoring of corrosion resistant steel bars on exposure sites with high concentration of chloride and sulfate ions is recommended. The results of both the laboratory study and the field study can then be compared to determine how well they correlate and determine whether the laboratory procedure effectively simulates the field performance.

# REFERENCES


1. Maslehuddin, M., Rasheeduzzafar, Page, C. L. Al-Mana, A. I., “Influence of Some Parameters Relevant to Arabian Gulf Environment on Reinforcement Corrosion,” Arabian Journal for Science and Engineering: Theme Issue on Corrosion and its Prevention, April 1995, pp. 239-257.
2. Maslehuddin, M., Saricimen, H., Al-Mana, A. I., and Shamim, M., "Performance of Concrete in A High Chloride-Sulfate Environment," American Concrete Institute, Special Publication SP-122, 1990, pp. 469-494.
3. Saricimen, H., Al-Tayyib, A. J., Maslehuddin, M., Shamim, M., "Concrete Deterioration in High Chloride-Sulfate Environment and Repair Strategies," American Concrete Institute, Special Publication, SP-128, 1991, pp. 19-34.
4. D. Darwin, J. Browning, T.V. Nguyen, and C.E. Locke. Mechanical and Corrosion Properties of a High-Strength, High Chromium Reinforcing Steel for Concrete. SD2001-05-F. Lawrence, KS: University of Kansas Center for Research, 2002.
5. Maslehuddin, M., Elleithy, W. M., Al-Amoudi, O. S. B. and Al-Sulaimani, G. J., “Use of Fusion-Bonded Epoxy-Coated Steel Bars: Needed Research,” Proc. 4th Saudi Engineering Conference, 1995, Jeddah, Vol. II, pp. 271-280.
6. Al-Gahtani, A.S. and Maslehuddin, M., Corrosion of fusion-bonded epoxy bonded coated bars in chloride-contaminated plain and silica fume cement concretes exposed to varying temperature, Proceedings, Structural Faults and Repair Conference, Edinburgh, 10-12 June 2008.
7. Al-Amoudi, O. S. B., Maslehuddin, M. and Ibrahim, M., “Long-term performance of FBEC bars in chloride-contaminated concrete,” ACI Materials Journal, v. 101, n. 4, July/August 2004, pp. 303-309.
8. Gerhardus H. Koch, Michiel P.H., Brongers, Neil G. Thompson, Y. Paul Virmani and J.H. Payer. Corrosion Cost and Preventive Strategies in the United State. FHWA-RD-01-156
9. Smith, F.N., and Tullmin, M. Using Stainless Steels as Long-Lasting Rebar Material. Materials Performance, Vol. 38, No. 5, pp. 72-76, 1999.
10. Fontana, M G., Corrosion Engineering, McGraw-Hill Book Company, New York, 1986
11. Jones, Denny A., Principles and Prevention of Corrosion, Macmillan Publishing Company, New York, NY, 1992.

12. Broomfield, John P., Corrosion of Steel in Concrete: Understanding, Investigation and Repair, St. Edmundsbury Press Limited, Bury St. Edmunds, Suffolk, Great Britain, 1997, 238 pp.

13. Hausmann, D. A., "Steel Corrosion in Concrete, How does it Occur," Materials Protection, Nov. 1967, Vol. 6, pp. 19-23.

14. Al-Amoudi, O. S. B., Rasheeduzzafar, Abdul Jauwad, S. N., and Maslehuddin, M., "Corrosion of Reinforcing Steel in Sabkha Environment", King Saud University Journal for Science and Engineering, Vol. 8, 1996, pp. 37-50.

15. Holden W.R., Page C L., and Short N.R., "The Influence of Chloride And Sulfates on Concrete Durability," Corrosion of Reinforcement in Concrete Construction, Crane AP., Editor, Society of Chemical Industry, London, 1983, pp. 143-149.

16. Al-Amoudi, O.S.B. and Maslehuddin, M., "The Effect of Chloride and Sulfate Ions on Reinforcement Corrosion", Cement and Concrete Research, 1993, Vol. 23, No 1, pp. 139-146.

17. Mehta, P.K. and Gerwick, B.C., "Cracking-Corrosion Interaction in Concrete Exposed to Marine Environment," Concrete International, Vol. 4, No 10, October 1982, pp 45-51.

18. Tula, L. and Helene, P., "Contribution to Service Life Prediction of Structures Reinforced with Stainless Steel Reinforcing Bars—Laboratory Approach,"ACI Special Publication 192, 2000, pp. 1053-1070.

19. G. G. Clemena, Final report, Testing of selected metallic reinforcing barsfor extending the service life of future concrete bridges, Virginia Transportation Council, In cooperation with the US Depatrment of Transportation Fedeeral Highway Administration, Charlottesville, Virginia, Dec. 2002, VTRC 03-R7.

20. McDonald, D.B., Pfeifer, D.W., and Sherman, M.R. Corrosion Evaluation of Epoxy-Coated, Metallic-Clad and Solid Metallic Reinforcing Bars in Concrete. Report No. FHWA-RD-98-153. Federal Highway Administration, Washington, D.C., 1998.

21. MMFX Technologies Corporation. 2005. Setting the Standards for the Future.

http://www.mmfxsteel.com.

22. J. L. Smith, Stainless Steel Reinforcing Bars for Concrete, Innovative Technology,

Technical Summary – September 2001.

23. ASTM A615 / A615M-09, Standard Specification for Deformed and Plain Carbon-Steel Bars for Concrete Reinforcement, ASTM International, West Conshohocken, PA, 2009, www.astm.org

24. ASTM A276 / A276M-15, Standard Specification for Stainless Steel Bars and Shapes, ASTM International, West Conshohocken, PA, 2015, www.astm.org.

25. T. Yamaji, T. Hirasaki, R. Takahashi, S. Mizuma, and M. Yamakawa, "Corrosion Study of Stainless Steel Bars in Cracked Concrete, ACI special publication 222, 2004, pp. 115-170.

26. STM A706 / A706M-14, Standard Specification for Deformed and Plain Low-Alloy Steel Bars for Concrete Reinforcement, ASTM International, West Conshohocken, PA, 2014, www.astm.org.

27. Tula, L. and Helene, P., "Contribution to Service Life Prediction of Structures Reinforced with Stainless Steel Reinforcing Bars—Laboratory Approach," ACI Special Publication 192, 2000, pp. 1053-1070.

28. L. Gong, D. Darwin, J.P. Browning, and C.E. Locke, Evaluation of Mechanical and Corrosion Properties of MMFX Reinforcing Steel for Concrete, Rep. No. FHWA-KS-02-8, Kansas Department of Transportation, USA, 2004.

29. J. Jing, Corrosion Resistance of Micro-Composite and Duplex Stainless Steels for Reinforced Concrete Bridge Decks. PhD thesis, University of Kansas, USA, 2006.

30. S. Kahl, Corrosion Resistant Alloy Steel (MMFX) Reinforcing Bar in Bridge Decks, Rep. No. R-1499, Michigan Department of Transportation, USA, 2007.

31. M.F. Hurley, Corrosion Initiation and Propagation Behavior of Corrosion. ResistantConcrete Reinforcing Materials. Doctoral dissertation. University of Virginia, Material Science and Engineering, Charlottesville, 2007

32. D. Darwin, J. Browning, T.V. Nguyen, and C.E. Locke. Mechanical and Corrosion Properties of a High-Strength, High Chromium Reinforcing Steel for Concrete. SD2001-05-F. Lawrence, KS: University of Kansas Center for Research, 2002.

33. McDonald, D.B., Pfeifer, D.W., and Sherman, M.R. Corrosion Evaluation of Epoxy-Coated, Metallic-Clad and Solid Metallic Reinforcing Bars in Concrete. Report No. FHWA-RD-98-153. Federal Highway Administration, Washington, D.C., 1998.

34. NUOVINOX Technical bulletin Stainless steel reinforcing bar with carbon steel centre. Stainless limited Newhall Road Sheffield UK S9 2QL.

35. Stern, M. and A. L. Geary (1957). A theoretical analysis of the slope of the polarization curves, Journal of Electrochemical Society, v. 104, p. 56.

36. Robertson I.N., Newtson C., (2009), “Performance of corrosion inhibitors in concrete exposed to marine environment, ” In: Alexander, M.G., Beushausen, H.-D., Dehn, F., Moyo, P., (eds), Concrete Repair, Rehabilitation and Retrofitting II, Taylor & Francis Group, London, pp 901−906.

37. Gonzalez, A.J., Feliu, S., Andrade, C., and Rodriguez, I., 1991 “On-site Detection of Corrosion of Reinforced Concrete Structures, ” Materials and Structures, Vol. 24, pp. 346-350.

38. Qian, S., and Cusson, D. (2007) “Accelerated Laboratory and Field Investigations of Corrosion Inhibiting Systems For Concrete Bridges,” Northern Area Eastern Conference, Ottawa , Ontario, pp. 1-5.

39. Saleem, M., Shameem, M., Hussain, S. E., and Maslehuddin, M. (1996). “Effect of moisture, chloride and sulphate contamination on the electrical resistivity of Portland cement concrete.” Construction and Building Materials, 10(3), 209–214

40. ASTM C 876-91, “Standard Test Method for Half Cell Potentials of Reinforcing Steel in Concrete,” Annual Book of ASTM Standards, Volume 04.02.

41. Mansfield, F., 1977 “Polarization Resistance Measurements: Experimental Procedure and Evaluation of Data”, Electrochemical Techniques for Corrosion, NACE, Houston, pp. 18-26.

42. ASTM C1152 / C1152M – 04 (2012) e1“Standard Test Method for Acid-Soluble Chloride in Mortar and Concrete,” Annual Book of ASTM Standards, American Society for Testing and Materials, Philadelphia.

43. ASTM G 109 [2007] Standard Test Method for Determining Effects of Chemical Admixtures on Corrosion of Embedded Steel Reinforcement in Concrete Exposed to Chloride Environments. Annual Book of ASTM Standards, American Society for Testing and Materials, Philadelphia.

44. M. Maslehuddin," Corrosion of Steel in Alkeline Media," Bahrain Society of Engineers, 6th Middle East Corrosion Conference, January 1994, Vol.5, pp. 597.

# APPENDIX

## A. Data Interpretation Tables

Table A.1: Interpretation of Half-Cell (Corrosion) Potential Readings (ASTM C 876)

| Half-cell Potential (mV) | Corrosion Activity |
|---|---|
| < -426 | Sever Corrosion |
| > -270 | 90% Probability of Corrosion Occurring |
| -126 to –270 | Corrosion Activity Uncertain |
| < -125 | 90% Probability of No Corrosion Occurring |

Table A.2: Interpretation of Corrosion Rate Data (Scannell, 1997)

| $I_{corr}$ $\mu A/cm^2$ | Corrosion Condition |
|---|---|
| Less than 0.1 | Passive Condition |
| 0.1 to 0.5 | Low to Moderate Corrosion |
| 0.5 to 1.0 | Moderate to High Corrosion |
| Greater than 1.0 | High Corrosion |

Table A.3: Water-Soluble Chloride-Ion Limits in ACI 318-9

| Type of member | Maximum water-soluble chloride ion ($Cl^-$) content in concrete, percent by weight of cement (0.15 %) |
|---|---|
| Prestressed concrete | 0.06 |
| Reinforced concrete exposed to chloride in service | 0.15 |
| Reinforced concrete that will be dry or protected from moisture in service | 1 |
| Other reinforced concrete construction | 0.3 |

# VITAE

## Personal Information


**Name:** **ADESHINA ADEWALE ADEWUMI**

**Marital Status:** Married

**Nationality:** Nigeria

**Date of Birth:** 6th March 1983

**Permanent Address:** 49, Thomas Salako Street, Ogba, Ifako-Ijaye LG. Lagos Nigeria

**Email:** walasco2010@yahoo.com

**Mobile:** +966561729419


## Educational Qualification

- Senior Secondary School Certificate, Lagos, Nigeria, 2001.
- B.Sc. in Civil Engineering, Obafemi Awolowo University, Ile-Ife Nigeria, 2008.
- Received a scholarship from the Ministry of Higher Education to study M.S degree at KFUPM in 2012.
- M.S (Structures & Materials), King Fahd University of Petroleum and Minerals June, 2015, Dhahran Saudia Araiba.

## Publication / Conference Attendance

- Review on self-curing concrete (KFUPM student conference journal, 2012)
- Utilization of Corrosion- Resistant Steel Bars in the Arabian Gulf (KFUPM student conference 2014)
- Corrosion Monitoring Using Electrochemical Noise Technique: a Comprehensive Statistical Analysis (KFUPM student conference 2014)
- Effects of Temperature on the Corrosion Behavior of Carbon Steel and Corrosion-Resistant Steel Bars in Simulated Concrete Pore Solutions (in view)
- Effects of sulfate ions concentration on the Corrosion Behavior of Carbon Steel and Corrosion- Resistant Steel Bars in Simulated Concrete Pore Solutions (in view)
- Estimation of Physical, Mechanical and Hydrological Properties of Pervious Concrete Using Computational Intelligence Approach (In view)